

Quantification of upward brine displacement from saline aquifers and
mechanical effects in geological CO₂ storage

Quantifizierung verdrängter Sole aus salzwasserführenden
Grundwasserleitern und mechanische Auswirkungen bei der
geologischen CO₂-Speicherung

DISSERTATION

zur Erlangung des akademischen Grades

Doctor rerum naturalium

(Dr. rer. nat.)

am Fachbereich Geowissenschaften der Freien Universität Berlin

vorgelegt von

DIPL.-GEOL. ELENA TILLNER

Berlin, 2015

1. Gutachter: **PROF. DR. MICHAEL SCHNEIDER**
Freie Universität Berlin
Fachbereich Geowissenschaften
Institut für Geologische Wissenschaften
Fachrichtung Geochemie, Hydrogeologie, Mineralogie
Arbeitsbereich Hydrogeologie

2. Gutachter: **PROF. DR. DR.-ING. HABIL. MICHAEL KÜHN**
Deutsches GeoForschungsZentrum GFZ, Potsdam
Department 5: Geomorphologie, Hydrologie und
Paläoklimatologie
Sektion 5.3: Hydrogeologie
und

Universität Potsdam
Mathematisch-Naturwissenschaftliche Fakultät
Institut für Erd- und Umweltwissenschaft

Tag der Disputation: 14. Juli 2015

SUMMARY

Carbon Capture and Storage (CCS) is considered as a promising measure to reduce anthropogenic greenhouse gas emissions into the atmosphere. Scientific assessments suggest that deep porous rock formations saturated with brine (saline aquifers) provide the largest storage potential due to their abundance in the Earth's sedimentary basins. However, geological underground storage of CO₂ (carbon dioxide) may also cause serious negative environmental and infrastructural impacts. The far-reaching pressure build-up affects regional fluid flow and may compromise mechanical rock integrity by changes in the recent stress field. Structural failure of reservoir, caprock or adjacent fault zones, accompanied by CO₂ leakage or large-scale displacement of brines are among potential risks associated with CO₂ injection into deeper saline formations. If brine reaches shallower aquifer complexes by upward migration through conductive pathways such as improperly sealed abandoned wells, permeable faults or erosive discontinuities in the overlying rocks, freshwater resources can be endangered by salinization.

The present thesis aims at evaluating the hydraulic and mechanical impacts of industrial-scale CO₂ injection and the resulting pressure increase for a potential saline onshore storage formation in the Middle Buntsandstein sequence of the Northeast German Basin. Here, the main emphasis is to assess the degree and bandwidth of potential shallow aquifer salinization by upward brine migration through permeable regional fault zones at the Beeskow-Birkholz storage site. Thereby, it is important to determine, which geological conditions promote upward brine displacement in geological CO₂ storage, and whether the pressure build-up affects the mechanical integrity of fault zones and/or caprocks. Four geological 3D models with an extent between 1,765 km² and 10,000 km² and different layer structures serve as the basis for this research and are implemented in multi-phase flow and coupled hydro-mechanical simulations. The methodology applied for model set up and data integration varied, depended on the respective focus of investigation. For flow simulations, regional fault zones are described in the models either by real grid elements or by virtual elements that allow for a discrete fault representation without introducing specific grid refinements in the near-fault area. In the mechanical simulations, a plasto-elastic constitutive model for fault zones is applied, using embedded weak planes of corresponding dip angle and dip direction at the respective fault element locations.

Multi-phase flow simulation results show that the magnitude of pressure build-up in the storage formation and pressure development over time determine the intensity and duration of brine flow into overlying aquifers. Salinity in the shallower aquifer increases only locally close to the fault zones, whereby the degree in salinization mainly depends on the lateral boundary conditions, the effective damage zone volume of fault zones, the presence of overlying reservoirs and the initial salinity distribution defined for the simulation scenario. The permeability of fault zones, however, has a comparatively minor impact on shallow aquifer salinization. Short hydraulically conductive fault segments lead to the highest local salinity increase, whereas laterally open boundaries and overlying reservoirs connected to the fault zones significantly diminish the risk of shallow aquifer salinization. Knowledge on the initial

salinity distribution in the fault is essential for salinization assessments, since the displaced brine originates from the upper part of the faults only, and not from greater depths.

Structural failure of fault zones as a consequence of injection-induced pressure build-up and effective stress changes can increase the risk of upward brine migration. To assess the fault slip and dilation tendencies at the respective site, one-way coupled hydro-mechanical simulations were applied in subsequent analysis. A one-way coupling procedure considers the time-dependent pore pressure development obtained from the dynamic flow simulations as input to hydro-mechanical simulations. The hydro-mechanical simulator then calculates potential rock mass failure resulting from stress changes without providing feedback to the flow simulator. In a first approach, the pressure distribution obtained from the flow simulations, was fitted by polynomial functions and integrated into the hydro-mechanical simulator for selected time steps. Simulation results demonstrate that only very few fault elements in the model are affected by shear and tensile rock failure, so that the development of a consistent slip plane along the faults, and thus fault reactivation is consequently expected not to occur at the Beeskow-Birkholz site under the given assumptions. For coupling evaluation, the applied one-way procedure was carried out for an equivalent saline onshore storage site in the Norwegian-Danish Basin close to the city of Vedsted, including a numerical modelling benchmark against the results produced by another well-established modelling group. The application of identical models for this process coupling allows an element-wise implementation of the time-dependant pore pressure distribution from the dynamic flow into the hydro-mechanical simulator. Simulation results show that mechanical impacts are mainly determined by fault conductivity and caprock permeability, which are influencing the spatial pore pressure distribution. A higher permeability of the caprock above the storage formation consequently induces higher vertical uplifts at the ground surface.

In the present thesis, it is shown that the presence of hydraulically conductive faults must not necessarily lead to shallow aquifer salinization, since various factors have been proven to influence the occurrence and degree of salinization under the tested constraints at the respective storage site. The magnitude of pressure increase in the reservoir is the driving factor in upward brine migration through fault zones: larger pressures induce stronger brine displacement, and consequently result in higher salinities in shallow aquifers. The magnitude of pressure build-up in turn, depends on the chosen lateral boundary conditions, the presence of overlying reservoirs and the effective damage zone volume of faults. At Beeskow-Birkholz, shallow aquifer salinization did not occur over large areas and the faults were not affected by structural failure. However, if brine reaches groundwater bodies, the local maximum salinity increase above the salt-freshwater boundary can reach a concentration larger than the limit prescribed by the German Drinking Water Directive.

In summary, numerical models can be well applied to obtain site-specific insights into the fluid flow dynamics in geological CO₂ storage. At the same time, the simulations help to identify the geological conditions with the greatest impact on upward brine migration and provide an initial assessment of the anticipated risks including their extent and significance.

ZUSAMMENFASSUNG

Die Abscheidung und Speicherung von Kohlenstoff (engl. Carbon Capture and Storage, CCS) wird als eine vielversprechende Maßnahme angesehen, die anthropogen verursachten Treibhausgasemissionen in die Atmosphäre zu reduzieren. Wissenschaftliche Schätzungen gehen davon aus, dass poröse und mit Salzwasser gesättigte Gesteinsformationen (saline Aquifere), aufgrund ihrer weiten Verbreitung in den Sedimentbecken der Erde, das größte Speicherpotential bieten. Die Nutzung des Untergrunds für die Speicherung von CO₂ (Kohlenstoffdioxid) kann jedoch schwerwiegende umweltschädliche und infrastrukturelle Auswirkungen haben. Durch die im Allgemeinen sehr weitreichende Druckerhöhung wird die regionale Grundwasserströmung beeinflusst und die mechanische Gesteinsintegrität durch Änderungen im rezenten Spannungsfeld gefährdet. Strukturelles Versagen von Reservoir, abdeckender Barriereschicht, oder nah gelegenen Störungszonen sowie CO₂-Leckage oder großräumige Verdrängung von hoch salinaren Wässern (Sole) werden als potentielle Risiken der CO₂-Speicherung in tiefen salinen Aquiferen angesehen. Erreicht die Sole über hydraulisch durchlässige Migrationspfade, wie möglicherweise unzureichend verschlossene Altbohrungen, permeable Störungen oder erosive Diskontinuitäten im Deckgebirge, flachere Grundwasserleiterkomplexe, können Süßwasserreserven durch Versalzung erheblich beeinträchtigt werden.

In der vorliegenden Dissertation soll daher für eine potentielle saline Speicherformation im Mittleren Buntsandstein des Nordostdeutschen Beckens untersucht werden, welche hydraulischen und mechanischen Auswirkungen eine industriemaßstäbliche CO₂-Speicherung und die damit einhergehende Parendruckerhöhung zur Folge haben kann. Der Schwerpunkt liegt hierbei darauf, den Grad und die Bandbreite einer möglichen Versalzung von überliegenden Aquiferen durch Solemigration über permeable regionale Störungszonen für den Standort Beeskow-Birkholz abzuschätzen. Des Weiteren soll untersucht werden, welche geologischen Gegebenheiten eine aufwärtsgerichtete Solemigration über Störungen begünstigen und wie sich die Druckerhöhung im Speicherhorizont auf die geomechanische Integrität von Störungszonen und/oder Abdecker auswirkt. Vier geologische 3D Modelle, mit einer Ausdehnung zwischen 1.765 km² und 10.000 km² und einem unterschiedlichen Schichtaufbau, bilden die Basis für Mehrphasenfluss- und gekoppelte hydromechanische Simulationen. Modellaufbau und Datenintegration erfolgten in Abhängigkeit des jeweiligen Untersuchungsschwerpunktes unter Anwendung verschiedener Methoden. In den Flussimulationen werden die regionalen Störungszonen in den Modellen entweder über reale Gitterelemente oder über virtuelle Elemente repräsentiert, die eine diskrete Darstellung der Störungen erlauben, ohne das Gitter im Störungsnahbereich zu verfeinern. Für die mechanischen Simulationen werden die Störungszonen in die elastisch-plastischen Modelle als Versagensflächen integriert, die entsprechend der Störungen orientiert sind.

Die Ergebnisse aus den Mehrphasenflusssimulationen zeigen, dass die Intensität und Dauer von Solefluss in überliegende Aquifere bestimmt wird, durch die Stärke des Druckaufbaus in der Speicherformation und der Druckentwicklung über die Zeit. Die Salinität im flachen Aquifer

steigt nur lokal im Nahbereich der Störungen, wobei der Grad der Versalzung im Wesentlichen von den definierten seitlichen Modellrandbedingungen, dem durchflusswirksamen Störungsvolumen, dem Vorhandensein von überliegenden Reservoirn sowie der initialen Salinitätsverteilung abhängt. Die Permeabilität der Störungen hingegen, hat einen vergleichsweise geringen Einfluss auf die Salinität flacherer Aquifere. Kurze hydraulisch durchlässige Störungssegmente bewirken den stärksten lokalen Salinitätsanstieg, wohingegen seitlich offene Modellränder und überliegende Reservoir, die ebenfalls mit den Störungszonen verbunden sind, das Risiko einer Versalzung im flachen Aquifer erheblich mindern. Die initiale Salinitätsverteilung in der Störung ist bei der Beurteilung von Versalzungen ebenfalls von großer Bedeutung, da die verdrängte Sole lediglich aus dem oberen Teil der Störung und nicht aus großen Tiefen stammt.

Strukturelles Versagen von Störungszonen, als Folge des injektionsbedingten Druckanstiegs, würde das Risiko einer Solemigration in überliegende Schichten erhöhen. Um die Tendenz einer Störungsreaktivierung am Speicherstandort zu evaluieren, wurde eine Ein-Weg-Kopplung genutzt. In einer Ein-Weg-Kopplung wird die zeitabhängige Porendruckverteilung aus den Mehrphasenflusssimulationen an den hydromechanischen Simulator übergeben. Der hydromechanische Simulator berechnet als Folge der Spannungsänderung daraufhin mögliches strukturelles Versagen des Gesteins, ohne dass der Mehrphasenflusssimulator Rückinformation erhält. In einem ersten Ansatz, wird die Druckverteilung aus den vorangegangenen Mehrphasenflusssimulationen über Polynomfunktionen angepasst und für ausgewählte Zeitschritte in den hydromechanischen Simulator integriert. Die Simulationsergebnisse zeigen, dass es im Modellgebiet nur sehr vereinzelt zu Scher- und Zugversagen kommt. Die Ausbildung einer konsistenten Gleitfläche entlang der Störungen und folglich eine Störungsreaktivierung, ist unter den getroffenen Annahmen am Standort Beeskow-Birkholz daher eher unwahrscheinlich. Zur Kopplungsevaluierung wurde die vorgestellte Ein-Weg-Kopplung im letzten Teil der Arbeit auch an einem salinen Aquifer einer zweiten potentiellen CO₂-Speicherformation, im Norwegisch-Dänischen Becken, nahe Vedsted, angewandt. Dies schloss eine numerische Benchmark-Studie mit ein, in der die Simulationsergebnisse mit denen einer weiteren Modellierungsgruppe verglichen wurden. Die auf identischen Modellen beruhende Prozesskopplung, ermöglicht eine elementweise Übertragung des berechneten Porendrucks aus dem Mehrphasenflusssimulator an den hydromechanischen Simulator, für ausgewählte Zeitschritte. Die Simulationsergebnisse zeigen, dass eine mechanische Beeinträchtigung des Gesteins von der hydraulischen Durchlässigkeit der Störungszonen sowie der Durchlässigkeit der Deckschichten über der Speicherformation abhängt, da diese die Porendruckverteilung im Reservoir wesentlich beeinflussen. Eine höhere Durchlässigkeit der Deckschicht hat zur Folge, dass sich vertikale Hebungen an der Erdoberfläche verstärken.

In der vorliegenden Arbeit wird gezeigt, dass hydraulisch durchlässige Störungen nicht zwingend zu einer Versalzung oberflächennaher Aquifere führen müssen. Verschiedene Faktoren beeinflussen nachweislich das Auftreten und den Grad einer Versalzung am Untersuchungsstandort. Der Druck in der Speicherformation ist die treibende Kraft der aufwärtsgerichteten Solemigration durch Störungen: in Abhängigkeit der Druckzunahme erhöht sich die Menge der verdrängten Sole in flache Aquifere wodurch der Versalzungsgrad steigt. Die Stärke des Druckaufbaus ist wiederum abhängig von den seitlichen Modellrandbedingungen, dem Vorhandensein von überliegenden Reservoirn und dem durchflusswirksamen

Störungsvolumen. Am Standort Beeskow-Birkholz wurde ein Salinitätsanstieg im flachen Aquifer nur im Nahbereich der Störungen beobachtet, strukturelles Versagen an den Störungen trat nicht auf. Simulationsergebnisse zeigen jedoch, dass die Salzkonzentrationen im Grundwasser den Grenzwert der Deutschen Trinkwasserverordnung im Bereich der Störungen lokal übersteigen können. Zusammenfassend kann festgehalten werden, dass durch die Anwendung von numerischen Modellen standortspezifische Vorhersagen zu den Auswirkungen der geologischen CO₂-Speicherung getroffen werden können. Des Weiteren helfen sie dabei, die geologischen Bedingungen zu identifizieren, die eine aufwärtsgerichtete Solemigration durch Störungen begünstigen. Ferner können numerische Modelle herangezogen werden, um erste Schätzungen hinsichtlich zu erwartender Risiken, deren Ausmaß und Bedeutung vorzunehmen.

ACKNOWLEDGMENTS

The present thesis was partly carried out within the interdisciplinary project brine funded by the German Federal Ministry of Education and Research (grant 03G0758A/B) in the frame of the R&D program GEOTECHNOLOGIEN (GEOTECH-2049), as well as within the SiteChar project funded by the European Union Seventh Framework Programme (FP7/2007-2013) under grant agreement n° 256705. The financial support is very much appreciated.

I want to express my gratitude to the many people who have been supportive over the past years, and without whom this thesis would not have been possible.

My thanks go to Prof. Michael Schneider for accepting to be the first supervisor of this work. He has always been helpful by profusely offering his time and expertise. His constant interest in my studies has motivated me and helped me stay focused on the key issues.

I am very grateful to my second supervisor, Prof. Michael Kühn, for the trust he placed in me during my whole time in his group at the GFZ. His continuous assistance, encouragement and valuable suggestions have hugely contributed to the realization of this work. The great atmosphere in the working group of Section 5.3 is definitely attributable to his friendly and open way of communication, which made me feel comfortable even during the most stressful times.

I owe a very special thanks to Dr.-Ing. Thomas Kempka for the immense support he offered me throughout the last years. I really value his friendly and consistently helpful way of sharing his scientific competency, technical proficiency and profound ideas with me. Without his contribution and lesson, this thesis would not have been possible at all. Thank you!

Many special thanks to Maria Langer and Lina Röhmann for the pleasant and productive work together. I want to thank Benjamin Nakaten for his technical support, as well as his patience as I again did not know what *awk* was trying to tell me. Thanks also to Dr. Fabien Magri for the good cooperation during the brine project. I want to express my gratitude to Dr. Marco De Lucia for the inspiring discussions, which helped me with some important decisions I needed to make. And of course the coffee. Grazie mille! Furthermore, I thank Dr. Natalie Nakaten for being such a dear roommate. Christopher Otto has proved an invaluable motivator and life coach.

Over the last few years I shared a great deal of time and inspiring discussions with many colleagues in Section 5.3, in the former Centre for CO₂ Storage, and in general at GFZ, which I do not have the space to enumerate here. My thanks to all of you!

I want to thank my wonderful family. You did support me to an unbelievable extent, and I am infinitely thankful for that.

Driess, you had my back the whole time, but especially in these last months, you put everything aside to help me. I cannot even begin to tell you how grateful I am.

CONTENTS

SUMMARY	I
ZUSAMMENFASSUNG	III
ACKNOWLEDGMENTS.....	VI
CONTENTS	VII
LIST OF FIGURES	X
LIST OF TABLES.....	XV
LIST OF ABBREVIATIONS AND SYMBOLS	XVI
1 INTRODUCTION.....	1
1.1 THEMATIC OVERVIEW AND THESIS OBJECTIVES	1
1.2 CHAPTER SUMMARY AND SCIENTIFIC CONTRIBUTION.....	3
2 BRINE MIGRATION THROUGH FAULT ZONES: 3D NUMERICAL SIMULATIONS FOR A PROSPECTIVE GERMAN CO₂ STORAGE SITE.....	7
ABSTRACT	7
2.1 INTRODUCTION	7
2.2 STUDY AREA AND SITE GEOLOGY	9
2.3 MODELLING WORKFLOW	12
2.3.1 Geological model.....	12
2.3.2 Fault zone description and applied simulator.....	13
2.4 NUMERICAL MODEL SETUP	15
2.4.1 Grid discretization, parameterization and injection rate	15
2.4.2 Scenario analysis.....	18
2.5 RESULTS.....	19
2.5.1 Scenarios B _o ^o F ₁₋₄ ^{1,000} , B _c ^o F ₁₋₄ ^{1,000} (faults act as conduits) and B _c ^c F ₁₋₄ ⁰ (faults act as barriers).....	19
2.5.2 Scenarios B _c ^o F ₂ ^{1,000} and B _o ^o F ₂ ^{1,000} (Fault 2 acts as a combined conduit-barrier)	24
2.5.3 Scenarios B _c ^o F ₂ ¹⁰⁰ , B _c ^o F ₂ ^{1,000} and B _c ^c F ₂ ^{10,000} (Fault 2 acts as a combined conduit-barrier)	26
2.6 DISCUSSION AND CONCLUSION	30
3 EFFECTIVE DAMAGE ZONE VOLUME OF FAULT ZONES AND INITIAL SALINITY DISTRIBUTION DETERMINE INTENSITY OF SHALLOW AQUIFER SALINIZATION IN GEOLOGICAL UNDERGROUND UTILIZATION	33
ABSTRACT	33
3.1 INTRODUCTION	34
3.2 STUDY AREA	37
3.3 GEOLOGICAL MODEL.....	39

3.3.1 Setup.....	39
3.3.2 Parameterization.....	41
3.3.3 Initial and boundary conditions	41
3.4 SET OF SCENARIOS	42
3.5 RESULTS	44
3.5.1 General outcomes	44
3.5.2 Fault length	47
3.5.2.1 Closed reservoir boundaries	47
3.5.2.2 Open reservoir boundaries	49
3.5.3 Overlying secondary reservoir	50
3.5.3.1 Closed reservoir boundaries	50
3.5.3.2 Open reservoir boundaries	53
3.5.4 Permeability differences between the fault and secondary reservoir	55
3.6 DISCUSSION.....	56
3.7 SUMMARY AND CONCLUSIONS.....	59
4 FAULT REACTIVATION AND GROUND SURFACE UPLIFT ASSESSMENT AT A PROSPECTIVE GERMAN CO₂ STORAGE SITE.....	61
ABSTRACT.....	61
4.1 INTRODUCTION	61
4.2 THE PROSPECTIVE CO ₂ STORAGE SITE – LOCATION AND GEOLOGY.....	62
4.3 PRE-PROCESSING.....	64
4.3.1 Structural geological model.....	64
4.3.2 Gridding process.....	65
4.3.3 Fault model	66
4.3.4 Geomechanical model parameterization.....	66
4.4 GEOMECHANICAL SIMULATIONS.....	67
4.4.1 Initialization.....	67
4.4.2 Simulation	67
4.5 RESULTS AND DISCUSSION	67
4.6 CONCLUSIONS.....	70
5 COUPLED DYNAMIC FLOW AND GEOMECHANICAL SIMULATIONS FOR AN INTEGRATED ASSESSMENT OF CO₂ STORAGE IMPACTS IN A SALINE AQUIFER	71
ABSTRACT.....	71
5.1 INTRODUCTION	71
5.1.1 Study area	71
5.2 COUPLED HYDRO-MECHANICAL SIMULATIONS	73
5.2.1 Structural geological model and parameterization	73
5.2.2 GFZ Potsdam simulation strategy	75
5.2.2.1 Dynamic flow simulations and results	75
5.2.2.2 Geomechanical simulations and results	78
5.2.3 Imperial College London simulation strategy	81
5.2.3.1 Dynamic flow simulations and results	81
5.2.3.2 Geomechanical simulations and results	83

5.3	SUMMARY AND DISCUSSION	86
5.4	CONCLUSIONS	87
6	DISCUSSION AND CONCLUSION	89
	REFERENCES.....	95
	SOFTWARE REFERENCES.....	103
	APPENDIX: PUBLICATIONS OF THE AUTHOR.....	104
1	PAPER (SCI/SCOPUS JOURNALS)	104
2	CHAPTER IN BOOK.....	104
3	CONFERENCE PAPER.....	105
	ERKLÄRUNG	107

LIST OF FIGURES

Figure 1: Outlined rectangle indicates approximate location of the study area Beeskow-Birkholz. Fault trends, contour of salt dome, rivers as well as the outline of the states of Brandenburg and Berlin were derived from STACKEBRANDT AND MANHENKE (2004).	10
Figure 2: 3D geological structural model of the Beeskow-Birkholz site. The Lausitzer Abbruch fault zone is represented by Fault 1, the Fuerstenwalde-Guben fault zone by Faults 2, 3 and 4. Axes show UTM-coordinates (Spatial Reference: EPSG Projection 32633 - WGS84 / UTM zone 33N).....	12
Figure 3: Simplified sketch illustrating the different steps of the virtual element (VE) workflow. Coordinates belonging to the common interface area of neighbouring grid elements are used for the computation of the virtual elements located on both sides of the fault. Different transmissibilities can be assigned to either fault or virtual elements, representing fault core (connection 2) and damage zone (VE 1 and VE 2), respectively.....	13
Figure 4: Applied relative permeabilities and scaled capillary pressures.	16
Figure 5: Pressure evolution at the top of the Detfurth anticline for Scenarios $B_o^o F_{1-4}^{1,000}$, $B_c^o F_{1-4}^{1,000}$ and $B_c^c F_{1-4}^0$	19
Figure 6: Average formation pressures for all investigated scenarios with faults acting as conduits or a combined conduit-barrier.	20
Figure 7: Pressure evolution in the upper aquifers (Muschelkalk and Stuttgart formations) for Scenarios $B_o^o F_{1-4}^{1,000}$ and $B_c^o F_{1-4}^{1,000}$. The observation points are located at the top of each formation close to Fault 2 (western side, central part of the model domain).....	21
Figure 8: Injected vs. displaced mass for all investigated scenarios with faults acting as conduits (average CO ₂ density varies between 602-738 kg/m ³) or a combined conduit-barrier (average CO ₂ density varies between 638-755 kg/m ³).	22
Figure 9: Comparison of relative salt mass change in the four faults for Scenarios $B_o^o F_{1-4}^{1,000}$ and $B_c^o F_{1-4}^{1,000}$	22
Figure 10: Local salinity increase in the uppermost Stuttgart Formation for Scenarios $B_c^o F_{1-4}^{1,000}$ and $B_c^o F_2^{10,000}$. Plotted are net values of the formation.	23
Figure 11: Relative mass change of salt and water in the uppermost Stuttgart Formation for Scenarios $B_o^o F_{1-4}^{1,000}$ and $B_c^o F_{1-4}^{1,000}$	23
Figure 12: Pressure evolution at the top of the Detfurth anticline for Scenarios $B_c^o F_2^{100}$, $B_c^o F_2^{1,000}$, $B_c^o F_2^{10,000}$ and $B_o^o F_2^{1,000}$	24

Figure 13: Pressure evolution in the upper aquifers (Muschelkalk and Stuttgart formations) for Scenarios $B_c^0 F_2^{1,000}$ and $B_o^0 F_2^{1,000}$. The observation points are located at the top of each formation close to Fault 2 (western side, central part of the model domain).....	25
Figure 14: Relative mass change of salt and water in the uppermost Stuttgart Formation for Scenarios $B_c^0 F_2^{1,000}$ and $B_o^0 F_2^{1,000}$	26
Figure 15: Pressure evolution in the upper aquifers (Muschelkalk and Stuttgart formations) for Scenarios $B_c^0 F_2^{100}$, $B_c^0 F_2^{1,000}$ and $B_c^0 F_2^{10,000}$. The observation points are located at the top of each formation close to Fault 2 (western side, central part of the model domain).	27
Figure 16: Comparison of relative salt and water mass change of the Stuttgart Formation for the Scenarios $B_c^0 F_2^{100}$, $B_c^0 F_2^{1,000}$ and $B_c^0 F_2^{10,000}$	27
Figure 17: Extent of the CO ₂ plume in Scenario $B_c^0 F_2^{1,000}$ (Fault 2 DZ permeability 1,000 mD). Axes show UTM-coordinates (Spatial Reference: EPSG Projection 32633 - WGS84 / UTM zone 33N).....	28
Figure 18: Contour map of the study area with outer border of the CO ₂ plume. Shown are the scenarios $B_c^0 F_2^{100}$ (orange), $B_c^0 F_2^{1,000}$ (blue) and $B_c^0 F_2^{10,000}$ (red) as well as Scenario $B_c^c F_{1-4}^0$ (purple). Axes show UTM-coordinates (Spatial Reference: EPSG Projection 32633 - WGS84 / UTM zone 33N).	29
Figure 19: Average salinity increase in the uppermost Stuttgart Formation for all investigated scenarios with faults acting as conduits or a combined conduit-barrier.	30
Figure 20: (a) Dashed rectangle indicates the location of the study area in the State of Brandenburg (Germany), while red lines illustrate the present fault systems. (b) Only the inner faults (black lines), facing to the injection well, were implemented to represent the entire fault zone. Axes show UTM-coordinates (WGS84/UTM zone 33N). Rivers and the outline of the states of Brandenburg and Berlin were derived from TILLNER ET AL. (2013).	38
Figure 21: (a) Stratigraphy of the study area with the active model layers highlighted in red. (b) The geological 3D model with simplified topography comprises up to three layers.....	39
Figure 22: Temporal evolution of brine displacement into the Rupelian basal sands, when all four faults are open, a secondary overlying reservoir exists and reservoir boundaries are closed. The brine mass displaced into the shallow aquifer is equal for all scenarios after 200 years, irrespective whether the fault permeability is higher (solid line), equal (dashed line) or lower (dotted line) to the permeability of the secondary reservoir. Lower fault permeabilities lead to retardation in mass flow only.....	44
Figure 23: An injection-related pattern in fluid flow, as illustrated for Scenario $F_{1-4}^{193\text{km}} B_o$, is observed in all simulations. Within the reservoir, brine is displaced predominantly into parts of the faults lying closer to the injection well. It is the opposite in the shallow aquifer, where flow out of the fault is greater into parts not facing towards the injection.....	45

Figure 24: (a) Profile along Fault 1 ($F_{1-4}^{193\text{km}}$ B_C) shows highest salinities near to the injection well. A decrease in salinization due to a downward flow is observed for the time after the injection period. (b) Cross section normal to Fault 1 illustrates the propagation of the saltwater plume (salinities $> 0.05 \%$), while higher salinities can be observed within the lower element layer. White arrows illustrate schematically the direction of the fluid flow at 20 years and 400 years.....	46
Figure 25: (a) Distribution of the pressure increase within the Detfurth Formation along the highlighted cross section significantly varies depending on the open fault length. Highest pressurization is observed for a short fault ($F_1^{2\text{km}}$ B_C). (b) Pressure development at the base of Fault 1 indicates a substantially faster pressure reduction for greater fault lengths.....	47
Figure 26: (a) Relative mass change in the Rupelian basal sands shows that the mass of brine displaced into the shallow aquifer corresponds to the overall injected fluid mass, if reservoir boundaries are closed. As indicated by the duration of mass flow (black numbers), only a temporal effect on fluid migration occurs. (b) Relative mass change for all lithological units after 330 years (mass flow $< 0.1 \text{ kg/s}$ for all scenarios) illustrates a considerably reduced salinization of the Rupelian basal sands for open reservoir boundaries.	48
Figure 27: (a) Velocity profile within the lower element layer of the Rupelian basal sands shows highest flow velocities out of Fault 1 at the end of injection period. (b) Flow velocities out of Fault 1 increase until the end of the injection period (20 years) and decrease afterwards depending on pressure reduction of the respective scenarios.	49
Figure 28: (a) Cross profile normal to Fault 1 shows, that during the injection period the displaced fluid spreads within the Detfurth and the Muschelkalk. (b) Afterwards, brine is transported out of the respective reservoir due to pressure reduction in both reservoirs. (c) Temporal evolution of the relative mass change shows the resulting retardation in fluid flow into the Rupelian basal sands for Scenario $F_1^{2\text{km}}$ B_C SR _{200mD}	51
Figure 29: Relative mass change of the Rupelian basal sands illustrates the retardation in fluid flow (black numbers) due to the existence of an overlying reservoir, while the overall displaced brine mass into the shallow aquifer is almost identical, when pressure comes to equilibrium.	52
Figure 30: The temporal evolution of the flow velocities out of Fault 1 show a substantial reduction due to lower reservoir pressures for the scenarios considering a secondary overlying reservoir as well as open boundaries.....	53
Figure 31: (a) Temporal evolution of the relative mass change of the Rupelian basal sands shows a lower duration of mass flow for open reservoir boundary conditions. Further a slight backward flow out of the aquifer can be observed. (b) Relative mass change for lithological units at 1,000 years (considering the backflow) illustrates, that salinization in the shallow aquifer is substantially reduced, if reservoir boundaries are open, and further an overlying secondary reservoir exists.....	54

Figure 32: Relative mass change for all lithological units after 1,000 years (considering the backflow) illustrates that if permeability of the fault is lower than of the Muschelkalk Formation ($F_{1-4}^{193\text{km}} B_0 SR_{2000\text{MD}}$) brine is preferentially displaced into the overlying secondary reservoir. Consequently, freshwater salinization in the shallow aquifer is lowest compared to all other scenarios.....	55
Figure 33: (left) Location of the study area Beeskow-Birkholz indicated by dashed rectangle. Main fault zones are shown as well as the anticline structure that presents the prospective CO ₂ storage site (modified after TILLNER ET AL., 2013); (right) All integrated faults displayed in the Petrel software package that build up the fault systems Lausitzer Abbruch, Potsdam, Fuerstenwalde-Guben and Tauer.....	63
Figure 34: (left) 3D geological structural model of the Beeskow site with geological layers and the major fault zones. Fault zone 1 displays the Fuerstenwalde-Guben, fault zone 2 the Lausitzer Abbruch and fault zone 3 the Potsdam fault system (BEUTLER AND STACKEBRANDT, 2012); (right) 3D model generated in the Petrel software package which was subsequently exported into FLAC ^{3D}	65
Figure 35: (left) Geomechanical model displayed in FLAC ^{3D} ; (right) Elements of the mechanical grid that are cut by a fault plane are defined as ubiquitous joints elements.	65
Figure 36: (left) Distribution of vertical displacement after 10 days of CO ₂ injection. The greatest vertical displacement at ground surface is at the injection well location; (right) Distribution of vertical displacement after 20 years of CO ₂ injection. The greatest vertical displacement at ground surface is at the injection well location (vertical exaggeration: 5).	68
Figure 37: Effective stress (σ_e) and pore pressure changes (p_t) are shown for the time steps 0 days, 10 days and 7300 days (20 years) plotted against depth.	69
Figure 38: (top left) The state of the injection formation after 10 days (top right) and 20 years after CO ₂ injection; (bottom left) State of the distributed faults with the injection horizon indicated after 10 days (bottom right) and after 20 years of CO ₂ injection (only shear failure is observed; vertical exaggeration is 5).....	70
Figure 39: The injection well of the prospective CO ₂ storage site is located close to Vedsted in northern Denmark. The dotted rectangle indicates the approximate extension of the structural geological model applied in all simulations. National borders and elevation data were obtained from the DIVA-GIS database (HIJMANS ET AL., 2012). Axes show UTM-coordinates (Spatial Reference: EPSG Projection 32632 - WGS84 / UTM zone 32N).	72
Figure 40: Effective porosity of the Gassum Formation and depth of the formation top. CO ₂ injection occurs at the eastern flank of the central anticline structure bounded by five fault zones.	74
Figure 41: Development of the BHP (bottomhole pressure) and WBP (wellblock pressure) for open and closed faults for an injection period of 40 years and a post-injection period of 10 years.....	76

Figure 42: Pore pressure increase at the top of the storage formation for open (left) and closed faults (right) after 40 years.....	77
Figure 43: Propagation of the gaseous CO ₂ in the upper sand layers of the Gassum Formation after 40 years for open (left) and closed faults (right).....	77
Figure 44: Hydro-mechanical model applied for the hydro-mechanical assessment. Five discrete faults and ten lithological units are implemented. Vertical exaggeration factor is 10.....	78
Figure 45: Vertical displacements at the Gassum Formation top (left) and ground surface (right) after 40 years, assuming hydraulically open faults.....	80
Figure 46: Vertical displacements at the Gassum Formation top (left) and ground surface (right) after 40 years, assuming hydraulically closed faults.....	80
Figure 47: Slip (left) and dilation tendency (right) after 40 years assuming hydraulically open faults. A value of 1 indicates the likely occurrence of slip/dilation, whereas a value of 0 indicates that slip/dilation is unlikely.	81
Figure 48: Development of the BHP (bottomhole pressure) and WBP (wellblock pressure) for hydraulically closed faults.	82
Figure 49: Pore pressure increase in the storage formation (left) and propagation of the CO ₂ -rich phase in the reservoir (right) after 40 years, assuming hydraulically non-conductive faults.....	83
Figure 50: Vertical displacements for the base case scenario after 40 years of simulation.	84
Figure 51: Shear failure assessment (base case) for reservoir (left) and overlying caprock (right) after 40 years.	85
Figure 52: Shear failure assessment (unfavourable case) for reservoir (left) and overlying caprock (right) after 40 years.	85

LIST OF TABLES

Table 1: Vertical grid discretization for the four different reservoirs and their caprocks. Inactive cells are only applied for vertical fault discretization.....	15
Table 2: All calculated scenarios with applied boundary conditions and fault parameterization. Lower aquifers comprise the Middle Bunter formations, upper aquifers the Muschelkalk and Keuper formations.....	18
Table 3: Summary of numerical simulations of brine migration resulting from CO ₂ injection.....	35
Table 4: Vertical grid discretization, depth and hydraulic parameters for the active geological units.....	40
Table 5: Overview about all calculated scenarios, their mean reservoir pressures at the end of injection as well as depth of origin and distribution of the brine displaced into the shallow aquifer.....	43
Table 6: Geomechanical properties assigned to the integrated formations of the geomechanical grid (OUELLET ET AL., 2010; NAGELHOUT AND ROEST, 1997; KOPF, 1965; MOECK ET AL., 2009).	66
Table 7: Downhole pressure for selected geomechanical time steps derived from dynamic flow simulations (TILLNER ET AL., 2013).....	67
Table 8: Mechanical properties derived from KEMPKA ET AL. (2014) (adapted from OUELLET ET AL., 2010; NAGELHOUT AND ROEST, 1997; BELL, 1977) as well as formation depths, densities, pore pressures and vertical stresses. Dilation angle is 0° for all units and 10° for the fault zones.	79
Table 9: Densities and mechanical properties of the lithological units used in the VISAGE based hydro-mechanical model. Properties for the first lithological unit were taken from BELL (1977), while the properties for the remaining units were obtained from GOODMAN (1989).	84

LIST OF ABBREVIATIONS AND SYMBOLS

ABBREVIATIONS

B	lateral reservoir boundary
BC	base case
BHP	bottomhole pressure
CCS	Carbon Capture and Storage
CO ₂	carbon dioxide
DZ	fault damage zone
EPSG	European Petroleum Survey Group
F	fault
FLAC	Fast Lagrangian Analysis of Continua
GeotIS	Geothermal Information System
GEUS	Geological Survey of Denmark and Greenland
GFZ	GeoForschungsZentrum Potsdam
GHG	greenhouse gas
Gt	gigaton
ICL	Imperial College London
IEAGHG	International Energy Agency Greenhouse Gas R&D Programme
IPCC	Intergovernmental Panel on Climate Change
m.a.s.l.	meter above sea level
Mt	megaton
n	number of elements
NE	northeast
NEGGB	Northeast German Basin
NGB	North German Basin
NW	northwest
SE	southeast
SW	southwest
t	time
UC	unfavourable case
UTM	Universal Transverse Mercator
WBP	well block pressure
WGS	World Geodetic System
yr	year
yrs	years
3D	three-dimensional
2D	two-dimensional

SYMBOLS

ρ	density	kg/m^3
p_p, p_t	pore pressure	bar, Pa, MPa
k	permeability	mD, m^2
σ_e	effective stress	Pa
σ_{e_1}	maximum principle effective stress	Pa
σ_{e_2}	intermediate principal effective stress	Pa
σ_{e_3}	minimum principle effective stress	Pa
ν	poisson coefficient	-
S_H	maximal horizontal stress	MPa
S_h	minimum horizontal stress	MPa
S_v	vertical stress	MPa
E	elasticity modulus	GPa
ϕ	friction angle	°
τ_0	cohesion	MPa
T_0	tensile limit	MPa

INDICES

i, x	horizontal x-direction in the Cartesian coordinate system
j, y	horizontal y-direction in the Cartesian coordinate system
k, z	vertical z-direction in the Cartesian coordinate system
x	lower aquifer
y	upper aquifer
k	permeability of fault / reservoir
n	number of active fault zone
o, O	open
c, C	closed
l	fault length

1 INTRODUCTION

1.1 THEMATIC OVERVIEW AND THESIS OBJECTIVES

In 2010, total global greenhouse gas (GHG) emissions into the atmosphere amounted to 49.5 Gt CO₂eq/yr (equivalent carbon dioxide in gigatonnes per year), and thus have almost doubled since 1970 (27 Gt CO₂eq/yr). Thereby, carbon dioxide (CO₂) from fossil fuel combustion and industrial use represents 65 % of the total emissions (32 GtCO₂/yr); (VICTOR ET AL., 2014). Besides measures that improve energy efficiency, the use of less carbon-intensive fuels and renewable energy systems, carbon capture and storage (CCS) in deep geological formations has received increased attention over the past decades as an additional GHG emission mitigation option. According to recent estimates, the CCS technology can contribute to global emission reductions by at least 15 %. The process includes the separation of CO₂ from the flue gas of fossil-fired power plants, its subsequent transportation to suitable geological storage formations and final long-term deposition underground (IPCC, 2005). In addition to depleted oil and gas fields or unmineable coal beds, deep saline (salt-water bearing) aquifers that can be found in all sedimentary basins worldwide, both onshore and offshore, are considered as potential CO₂ storage formations (MICHAEL ET AL., 2010; BENSON AND COLE, 2008; HOLLOWAY, 2005; IPCC, 2005). Due to the wide distribution of the Earth's sedimentary basins, deep saline aquifers have been estimated to provide the largest storage potential with a capacity between 10³ to 10⁴ Gt of CO₂. Injection should take place at depths greater than 800 m to account for a high CO₂ density, and thus high storage efficiency. Further requirements on the storage reservoir comprise a large layer thickness and extent as well as a sufficient formation porosity and permeability. A thick impermeable rock above the formation is essential to minimize CO₂ migration and pressure propagation into overlying units. The absence of leakage pathways for CO₂ and/or formation fluids such as permeable fractures, fault zones or improperly sealed abandoned wells as well as a multi-barrier system of caprocks further increase the safety of the storage site (OELKERS AND COLE, 2008; IPCC, 2005).

Once the CO₂ is injected, various mechanisms can promote its long-term entrapment. Driven by buoyancy, due to density differences between the CO₂ phase and the formation fluid, less dense CO₂ migrates up to the impermeable caprock, where it can be immobilized in structural traps, e.g., below a caprock in an anticline. Residual trapping occurs when a portion of CO₂ is retained in the pore space of the reservoir rock by capillary forces. This mechanism already begins shortly after the injection start and evolves over thousands of years. Two further long-term mechanisms are known as solubility and mineral trapping. Already with beginning of the injection, but mainly in the post-injection phase, CO₂ progressively dissolves in the formation water. Since formation fluids, comprising dissolved CO₂, exhibit a higher density than the initial formation fluids, buoyant driven downward flow occurs, and hence decreases the risk of CO₂ leakage. Reactions between the dissolved CO₂ and the minerals in the geological formation are subsequently expected to result in precipitation of solid carbonates over millions of years, so that CO₂ becomes immobile (E.G. GASDA ET AL., 2011; MACMINN ET AL., 2011; MICHAEL ET AL, 2010; IPCC, 2005; JOHNSON ET AL., 2004).

Several risks may also be associated with CO₂ storage in a saline aquifer, since the high requirements on storage formations mentioned above are rarely fulfilled by geological conditions generally present in the Earth's sedimentary basins. Pore pressure increase may be noticed more than 100 km away from the injection location, if a continuous hydraulic connection throughout the formation exists. Discontinuities in the caprock and/or the presence of fault zones are likely within such large areas, what can facilitate CO₂ leakage and/or upward migration of displaced formation brines (TILLNER ET AL., 2013; BIRKHOLZER ET AL., 2009; PRUESS AND GARCIA, 2001; RUTQVIST AND TSANG, 2001). When considering geological CO₂ storage, the interaction between hydraulic and mechanical processes plays a significant role. Injection-induced pore pressure increase may compromise the integrity of a reservoir, its caprocks and adjacent fault zones due to a simultaneous decrease in effective stresses supported by the rock mass. Shear or tensile failure in the caprock and of the faults as well as vertical displacements at the ground surface are potential consequences. A decrease in effective stresses at a fault can trigger fault slip and dilation, giving rise to new or enhanced hydraulically conductive leakage pathways into overlying formations (E.G. CAPPA AND RUTQVIST, 2011; IEAGHG, 2010; BIRKHOLZER ET AL., 2009; CAPPA, 2009). Due to the fact that fault zones can intersect one or more caprocks, upward brine migration resulting from CO₂ injection may become a serious environmental risk, if brine reaches shallower aquifers and mixes with freshwater (OLDENBURG AND RINALDI, 2011; IPCC, 2005).

Based on the previous explications, two main research objectives are formulated for this thesis:

The **first** objective is to quantify upward brine displacement through permeable regional fault zones resulting from CO₂ injection into a saline onshore storage formation. Thereby, it is aimed to assess the degree and bandwidth of potential shallow aquifer salinization at the prospective site, located at Beeskow-Birkholz in the Northeast German Basin. Furthermore, the geological conditions that promote upward brine migration, resulting from the injection-induced pressure increase have to be determined (Chapter 2 and 3).

The **second** aim is to couple the time-dependent pore pressure development obtained from the flow simulations to mechanical processes in order to assess the potential for fault reactivation by shear or/and tensile failure as well as ground surface uplift at the Beeskow-Birkholz site. For the evaluation of the chosen methodology, these investigations have to be performed for one equivalent storage site including a benchmark against the results produced by another well-established modelling group (Chapter 4 and 5).

The defined research objectives require the construction of one or more 3D structural geological models and their implementation in coupled hydraulic and mechanical simulations. Thereby, the site-specific geological conditions including potentially present complex fault geometries have to be adequately represented. A coupling procedure has to be developed to combine hydraulic and mechanical processes in the simulations at reservoir to regional scale.

1.2 CHAPTER SUMMARY AND SCIENTIFIC CONTRIBUTION

The following sections give a short summary of the investigations carried out within the frame of this cumulative doctoral thesis that consists of three articles published in peer-reviewed journals as well as one article that is submitted for publication in a peer-reviewed journal. Furthermore, the author's contribution to each article is described. All publications are presented in detail in Chapters 2 - 5. In Chapter 6, all results and findings are discussed and a conclusion is given with respect to the thesis objectives.

CHAPTER 2: Brine migration through fault zones: 3D numerical simulations for a prospective German CO₂ storage site

In Chapter 2, the impact of pressure increase and fault permeability on brine displacement processes is determined to assess the degree of potential upper aquifer salinization at the prospective onshore CO₂ storage site Beeskow-Birkholz in Northeast Germany. For that purpose, a 3D regional-scale structural geological model of the investigation area with an extent of 1,765 km² was implemented. The 3D model is parameterized based on available literature and borehole data, and comprises two regional fault zones as well as the targeted storage horizon: the Detfurth sandstone Formation of the Middle Bunter. The injection of 1.7 MtCO₂/yr over 20 years is carried out at the top of an anticline structure in the Detfurth Formation. Different fault leakage scenarios are investigated in numerical simulations using a multi-phase flow simulator. For the discrete description of fault zones, a new workflow was developed and evaluated. It includes the grid transfer from the geological model generated with a pre-processing geological modelling software package to a reservoir simulator and the implementation of fault zones into the model grid as virtual elements to account for fluid flow across and along the discrete fault planes. Different lateral boundary conditions, number of hydraulically conductive faults and fault zone permeabilities are taken into consideration in the individual simulation runs.

As the first author, I implemented the 3D structural geological model, provided assistance in the development of the new workflow including the virtual element concept and its evaluation. I planned and carried out all investigated simulation scenarios and was responsible for result interpretation and visualization. The manuscript was written and revised by me.

The study was published in the International Journal of Greenhouse Gas Control in 2013. Elsevier kindly approved the reuse in this dissertation:

Tillner, E., Kempka, T., Nakaten, B., Kühn, M. (2013): Brine migration through fault zones: 3D numerical simulations for a prospective CO₂ storage site in Northeast Germany. International Journal of Greenhouse Gas Control, 19, p. 689-703. doi: 10.1016/j.ijggc.2013.03.012.

<http://www.sciencedirect.com/science/article/pii/S1750583613001321>

CHAPTER 3: Effective damage zone volume of fault zones and initial salinity distribution determine intensity of shallow aquifer salinization in geological CO₂ storage

In Chapter 3, the focus is to determine the most significant factors controlling upward brine migration through fault zones resulting from geological CO₂ storage at the Beeskow Birkholz site, and to estimate the site-specific bandwidth of potential shallow aquifer salinization. For that purpose, a regional scale 3D model of the study area, with an extent of 10,000 km², was implemented and employed in numerical simulations. In 13 distinct fault leakage scenarios, the impact of different hydraulically conductive fault lengths, lateral boundary conditions as well as the presence of an overlying secondary reservoir on upward brine migration was investigated. The model comprises the Detfurth Formation as the lowermost reservoir, the Muschelkalk Formation as an overlying secondary reservoir, the Rupelian basal sands as the uppermost shallow aquifer as well as four regional fault zones. The original topography of the formation tops and bases was simplified to focus the analysis on clearly identifiable effects related to fault fluid flow. A sharp salt-freshwater interface in the faults, located below the Rupelian basal sands, serves as a tracer boundary to visualize the distribution of saline water within the shallow aquifer. Instead of CO₂, a volume-equivalent mass of 59.76 Mt brine was virtually injected into the Detfurth Formation over 20 years. Thereby, also the long-term response of underground utilization up to thousands of years after the injection stop was taken into account.

Based on the work carried out by TILLNER ET AL. (2013), I provided the input for the scenarios to be investigated and supported their technical implementation. As the second author, I further provided assistance in the interpretation and evaluation of modelling results and was involved in the manuscript preparation and revision as corresponding author. As the first author of this chapter, Maria Langer (GFZ German Research Centre for Geosciences) implemented the 3D geological model, carried out the multi-phase flow simulations and was responsible for result evaluation and illustration. She elaborated the main parts of the manuscript.

This study was submitted for publication in the Hydrology and Earth System Sciences Journal in April 2015. The article is licensed under the terms of the Creative Commons Attribution (CC BY 3.0) License (<http://creativecommons.org/licenses/by/3.0/>), together with an author copyright:

Langer, M., Tillner, E., Kempka, T., Kühn, M. (2015, submitted): Effective damage zone volume and initial salinity distribution determine intensity of shallow aquifer salinization in geological CO₂ storage. *Hydrology and Earth System Sciences*, 12, p. 5703-5748. doi: 10.5194/hessd-12-5703-2015.

<http://www.hydrol-earth-syst-sci-discuss.net/12/5703/2015/hessd-12-5703-2015.html>

CHAPTER 4: Fault reactivation and ground surface uplift assessment at a prospective German CO₂ storage site

In Chapter 4, an assessment of potential hydro-mechanical impacts of pore pressure increase induced by CO₂ injection is undertaken for the Beeskow-Birkholz study area. A 3D structural geological model with an extent of 10,000 km² is implemented in one-way coupled hydro-mechanical simulations to assess ground surface uplift as well as reservoir, caprock and fault

integrity. A one-way coupling considers the time-dependent pore pressure development obtained from the dynamic flow simulations as input to hydro-mechanical simulations. The hydro-mechanical simulator then calculates potential rock mass failure resulting from stress changes without providing feedback to the flow simulator. Thereto, the least favourable scenario with the highest pressure build-up due to reservoir compartmentalization by hydraulically non-conductive fault zones is chosen from the multi-phase flow simulations conducted by TILLNER ET AL. (2013). The pressure distribution in the storage formation prior to CO₂ injection, at the time of the highest pressure build-up after 10 days and at the end of the injection period after 20 years are used as coupling steps and transferred to the hydro-mechanical simulator to calculate the resulting stress changes and potential fault and/or matrix failure.

As the second author, I provided assistance in the implementation of the 3D model, starting from the interpretation of the available data basis, data digitalization and the final model set up. I prepared the multi-phase flow simulation results (TILLNER ET AL., 2013) for application in the one-way hydro-mechanical coupling, which I was also supporting. Further, I was involved in the manuscript preparation and correction. As the first author of this chapter, Lina Röhmann (former GFZ) carried out the 3D model implementation, the one-way coupled hydro-mechanical simulations and result evaluation. She prepared the main manuscript parts and was in charge of manuscript revision.

This article was published in the Energy Procedia Journal in 2013 under the terms of the Creative Commons Attribution-NonCommercial-No Derivatives (CC BY-NC-ND 3.0) License (<http://creativecommons.org/licenses/by-nc-nd/3.0/>). Copyright is retained by the authors:

Röhmann, L., Tillner, E., Magri, F., Kempka, T. (2013): Fault reactivation and ground surface uplift assessment at a prospective German CO₂ storage site. Energy Procedia, 40, p. 437-446. doi: 10.1016/j.egypro.2013.08.050.

<http://www.sciencedirect.com/science/article/pii/S1876610213016445>

CHAPTER 5: Coupled Dynamic Flow and Geomechanical Simulations for an Integrated Assessment of CO₂ Storage Impacts in a Saline Aquifer

In Chapter 5, the mechanical impact of industrial-scale CO₂ storage at a prospective Danish site was investigated. Modelling groups from GFZ Potsdam and Imperial College London carried out one-way coupled 3D hydro-mechanical simulations in a comparative study. The modellers from Imperial College London chose the widely used commercial Schlumberger Eclipse software package for their multi-phase flow simulations and coupled it to the Schlumberger geomechanical simulator VISAGE™. In the modelling strategy followed by GFZ Potsdam, multi-phase flow simulations were carried out using the TOUGH2-MP/ECO2N simulator coupled to the commercial geomechanical simulator FLAC^{3D}. The prospective deep saline onshore CO₂ storage formation is located at the Vedsted site in the Norwegian-Danish Basin. CO₂ injection is carried out at a depth of 1,995 m into the top of an anticline structure of the Gassum Sandstone Formation from the Upper Triassic to Lower Jurassic (2 Mt CO₂/yr over 40 years). Five northwest-southeast trending faults that limit or partly cut through the anticline were treated as either hydraulically conductive or non-conductive for cross-fault flow in the numerical simulations. The

pore pressure distribution obtained from the two reservoir simulators ECLIPSE and TOUGH2-MP at selected time steps served as a coupling parameter for the subsequent calculation of strain changes based on altered effective stresses with VISAGE and FLAC^{3D}.

My contribution to this study, as the first author, was the preparation of the 3D geological structural model obtained from the Geological Survey of Denmark and Greenland (Geological Survey of Denmark and Greenland, GEUS) for flow simulations and the subsequent gridding process. I carried out numerical multi-phase flow simulations for all investigated scenarios using the TOUGH2-MP/ECO2N simulator and prepared the data for the hydro-mechanical coupling. I was further responsible for result evaluation and illustration as well as the preparation and revision of the manuscript.

The study was published in the Energy Procedia Journal in 2014 under the terms of the Creative Commons Attribution-NonCommercial-No Derivatives (CC BY-NC-ND 3.0) License (<http://creativecommons.org/licenses/by-nc-nd/3.0/>). Copyright is retained by the authors:

Tillner, E., Shi, J.-Q., Bacci, G., Nielsen, C.M., Frykman, P., Dalhoff, F., Kempka, T. (2014): Coupled dynamic flow and geomechanical simulations for an integrated assessment of CO₂ storage impacts in a Saline Aquifer. Energy Procedia, 63, p. 2879-2893.
doi: 10.1016/j.egypro.2014.11.311.

<http://www.sciencedirect.com/science/article/pii/S1876610214021262>

Further studies, published or submitted for publication within the time of this doctoral thesis and my own contributions but not integrated here, are listed in the appendix.

2 BRINE MIGRATION THROUGH FAULT ZONES: 3D NUMERICAL SIMULATIONS FOR A PROSPECTIVE GERMAN CO₂ STORAGE SITE

ABSTRACT

Upward brine migration as a result of CO₂ injection into a saline aquifer could endanger freshwater resources, especially in faulted reservoirs. The present study determines the impact of pressure increase and fault permeability on brine displacement processes to assess potential freshwater salinization. For that purpose, different fault leakage scenarios were carried out by numerical modelling of a prospective storage site in Northeast Germany using a newly developed workflow that includes the grid transfer from the geological model generated with the applied pre-processing software Petrel to the reservoir simulator TOUGH2 and the implementation of virtual elements for the discrete description of fault zones. The results show that compartmentalization due to closed boundaries and faults cause the highest pressurization within the storage formation. Closed boundaries generally lead to higher brine migration rates especially if a number of permeable faults are present, whereas the permeability of fault zones only has a minor impact and does not influence salinization of shallower aquifers significantly. Although the salinity in shallower aquifers increases more sharply in the vicinity of the faults, with an average salinity increase by a maximum of 0.24 %, the risk of freshwater salinization is estimated as low under the given circumstances for the potential site at Beeskow-Birkholz.

2.1 INTRODUCTION

Carbon Capture and Storage (CCS) has become a promising technology for reducing anthropogenic greenhouse gas emissions into the atmosphere. Besides depleted oil and gas fields, deep porous rock formations saturated with brine (saline aquifers) offer the largest storage potential and can be found in all sedimentary basins worldwide (HOLLOWAY, 2005; IPCC, 2005). However, geological storage of CO₂ also bears several risks such as structural failure, CO₂ leakage or large-scale displacement of resident brines as a consequence of a generally far-reaching pressure build-up (IEAGHG, 2010). Considering brine migration, salinization of freshwater resources may become a potential environmental impact, since pressurization may force the displaced brine to flow upward into potable groundwater if conductive pathways such as improperly sealed abandoned wells, permeable faults or fractures are present (OLDENBURG AND RINALDI, 2011; IPCC, 2005).

Several studies have already focused on brine displacement and freshwater salinization as a result of industrial-scale CO₂ injection into a saline aquifer. For example, BIRKHOLZER ET AL. (2009) investigated the impact of pressure build-up in a synthetic multi-layered groundwater system during CO₂ injection and concluded that especially large-scale pressure changes have to be considered with regard to upward brine migration into freshwater aquifers. Low permeability

seals may also allow for considerable brine leakage out of a storage formation vertically upward and/or downward. Nevertheless, it is considered as extremely unlikely that vertical interlayer pressure propagation through a multi-barrier system of caprocks significantly affects shallow aquifers. However, the simulation study of BIRKHOLZER ET AL. (2009) did not consider direct high-permeability conduits between the deep saline storage formation and shallower aquifers. There is general agreement that the degree of pressure build-up and brine displacement strongly depends on the lateral flow boundaries of the storage formation that may either act as a limiting factor to fluid movement and pressure dissipation or as the opposite (IEAGHG, 2010). CAVANAGH AND WILDGUST (2011) demonstrate that pressurization and brine displacement therefore need to be addressed at a regional scale with geologically accurate boundary conditions. NICOT (2008) studied the far-field impact on shallow groundwater by up-dip displacement of brines in the Gulf Coast region by two different injection scenarios and showed that induced water-level rises are of the same order of magnitude as seasonal and inter-annual variations. CHABORA AND BENSON (2009) investigated the pressure changes in permeable zones overlying CO₂ storage reservoirs and the associated brine migration through the sealing caprock by means of a detection factor correlating the hydrologic properties of the storage reservoir and seal to the magnitude of expected pressure build-up. According to the authors pressure changes of 0.1 bar are likely to be detectable. LEMIEUX (2011) conducted a systematic literature review to summarize the current knowledge on potential impacts of geological CO₂ storage in deep saline aquifers on shallow groundwater resources, including studies investigating both the near- and far-field impact. The author LEMIEUX (2011) points out that many numerical models are based on strong simplifications and assumptions due to insufficient data. More laboratory measurements and field experiments as well as site-specific numerical investigations are needed to capture what will actually happen in the field.

While further investigations have recently focused more specifically on quantifying and analysing the risks of CO₂ and/or brine migration via open or abandoned wells as potential leakage pathways (E.G. BIRKHOLZER ET AL., 2011; CELIA ET AL. 2011; BACHU AND BENNION, 2009), studies on brine migration through permeable fault zones are to our knowledge relatively rare and were only carried out for synthetic models. Site-specific investigations do not exist so far with regard to this issue. OLDENBURG AND RINALDI (2011) set up an idealized two-dimensional model consisting of a vertical conductive pathway representing a well or permeable fault and investigated how pressure-driven brine migration induced by pressurization during CO₂ injection impacts shallow reservoirs. Their simulations show that depending on pressure and salinity gradients brine displacement is either an establishment of a new hydrostatic equilibrium or sustained upward flux, if the dense brine is allowed to spread laterally in the upper aquifer. PRUESS (2011, 2005A) showed that if fluids leak from a geologic storage reservoir along an idealized fault zone, leakage behaviour is influenced by the interaction between multiphase flow and heat transfer, and hence variations in flow rates may occur. WALTER ET AL. (2012) focus on risk assessment and quantification of freshwater salinization resulting from upward brine migration in the frame of a CO₂ storage operation, taking into account the probability of its occurrence. Different simulations were carried out, including models consisting of a vertical permeable fault. The authors conclude that saltwater intrusion into potable groundwater caused by CO₂ storage operations occurs most likely locally and not over large areas, if multi-barrier caprocks are present.

Nevertheless, freshwater salinization or near-surface brine migration is certainly not only a potential problem of CO₂ storage, but may also have a geogenic origin. There exist, for instance, different regions in the Northeast German Basin (NEGGB), where saltwater reaches the shallow aquifer system (GRUBE ET AL., 2000). MAGRI ET AL. (2008 AND 2005) performed thermohaline simulations to assess the transport mechanisms of saline water in the NEGGB indicating that an interaction of hydrostatic and thermally induced forces (mixed convection) is the main cause for surface occurrences of saltwater in these regions. In the deeper aquifers highly saline waters forming close to deep salt diapirs are forced to migrate upward by thermohaline convection and with regional topography-driven groundwater flow, whereas shallow salt dissolution is the major cause for gravitational convection in the deeper aquifers. With regard to future risk assessment for potential CO₂ storage sites it will be required to be able to distinguish clearly between geogenic processes and the storage process. Therefore, future large scale onshore CCS projects also need to assess quantitatively the risk of salinization of shallow freshwater aquifers due to brine displacement from the CO₂ storage reservoir. Taking into account the available knowledge described above, this study moves a step further with its focus on discrete faults as leakage pathways addressed at regional-scale for a prospective site in Northeast Germany based on available geological and structural data. So far, CO₂ and/or brine leakages from storage complexes were studied only with regard to caprocks or wells as potential pathways in real 3D geological setups (see above). Reason for that is the fact that the implementation of fault zones into a reservoir model as they appear in nature with fault-dip, curvature and displacement by using discrete grid cells following the discrete fault geometry would greatly increase the number of elements and complexity of the models and is therefore computationally challenging. The approach described here is based on a newly developed workflow which includes the grid transfer from the applied pre-processing software package Petrel (SCHLUMBERGER, 2010A) to the reservoir simulator TOUGH2-MP (ZHANG ET AL., 2008) and the implementation of virtual elements for the discrete description of fault zones. The virtual elements reduce the complexity of the discretization process, and furthermore make visualization of the results straight forward. The present study analyses the impact of fault permeability on upward brine migration due to the pressure elevation in the storage complex as a result of CO₂ injection. Various leakage scenarios were tested with the expectation that increasing pressure levels in the reservoir and larger permeabilities of the fault zones as leakage pathways will govern the degree of salinization in shallower aquifers.

2.2 STUDY AREA AND SITE GEOLOGY

The study area Beeskow-Birkholz is located in the NEGGB, approximately 80 km southeast of Berlin and part of a Mesozoic anticline structure overlaying an Upper Permian (Zechstein) salt dome. The asymmetric anticline is of approximately 20 km length and 5 km width and characterized by a NW-SE oriented longitudinal axis that runs sub-parallel to two major regional fault zones, namely the Lausitzer Abbruch and the Fuerstenwalde-Guben fault zone (Figure 1).

Tectonic movements in the early Cretaceous during the Alpine orogeny have caused a reactivation of many ancient variscan basement faults in the NEGGB. Tectonic expansion until the Upper Cretaceous and a subsequent phase of compressional deformation from the beginning of

the Upper Cretaceous have generated complex fault systems such as the Fuerstenwalde-Guben fault zone that consists of several individual faults characterized by a combination of different dip-slip movements. The Lausitzer Abbruch fault zone is a normal fault dipping northeast and characterized by a total length of 170 km and displacements of up to 1,000 m (BEUTLER AND STACKEBRANDT, 2012; STACKEBRANDT, 1998; KATZUNG AND EHMKE, 1993). Salt tectonic movements of the Upper Permian Zechstein driven by the tectonic deformation during the Alpine orogeny and continued sedimentary loading have caused an uplift and erosion of the overlying Middle and Upper Mesozoic sediments in the study area (STACKEBRANDT AND MANHENKE, 2004).

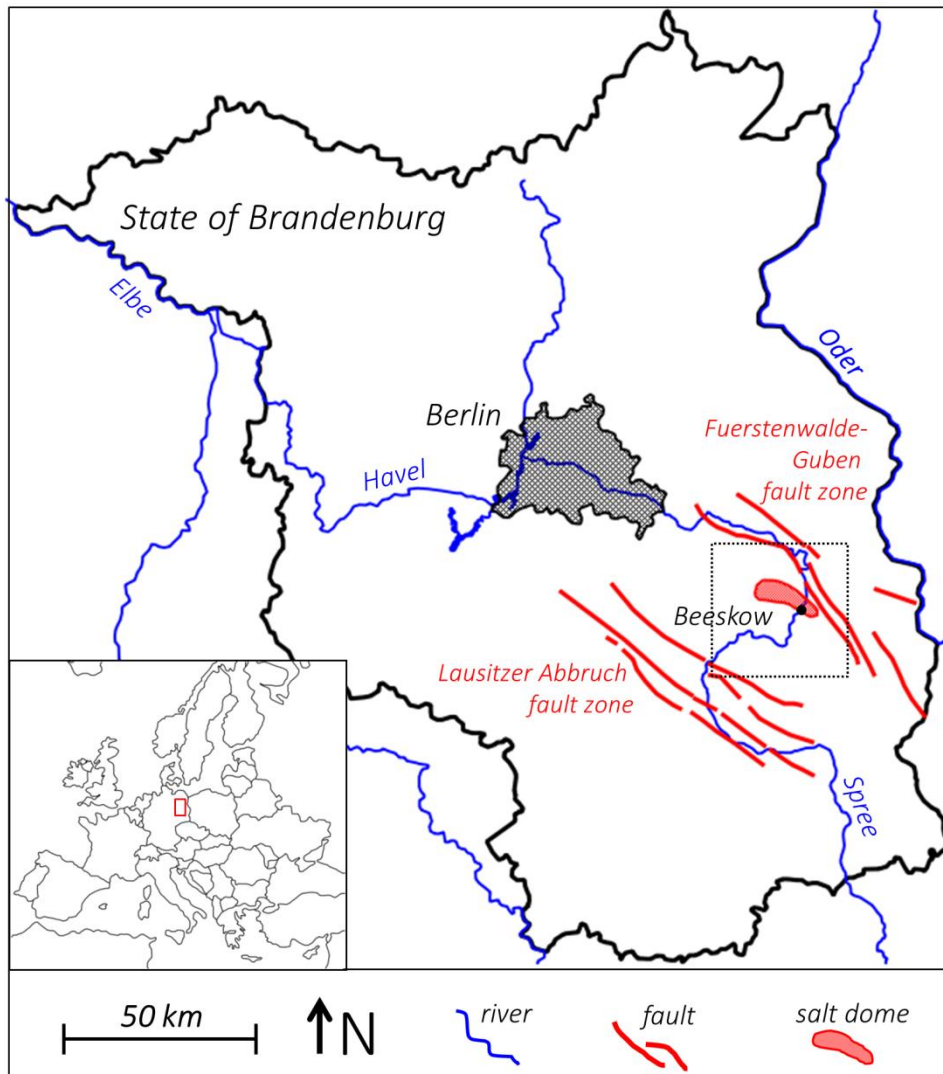


Figure 1: Outlined rectangle indicates approximate location of the study area Beeskow-Birkholz. Fault trends, contour of salt dome, rivers as well as the outline of the states of Brandenburg and Berlin were derived from STACKEBRANDT AND MANHENKE (2004).

The top of the Zechstein salt dome is located at a depth of approximately 1,550 m. Cretaceous and Jurassic rocks were most likely not deposited in the central part of the anticline and are missing. Therefore, the unconsolidated rocks dating from Tertiary to Quaternary are in direct contact with the Upper Triassic Keuper formations. At margins of the anticline, Jurassic

sediments are still present, whereas Cretaceous formations only exist locally in very small areas. Potential reservoir rocks comprise several sandstone formations of the Middle Bunter, namely the Volpriehausen, Detfurth and Hardegsen Formation with a thickness varying from 8 m to 23 m. The limestones of the Lower Muschelkalk (Middle Triassic) and the Stuttgart sandstone formation of the Middle Keuper (Upper Triassic) form two further suitable reservoir rocks within the stratigraphic sequence of the study area. These permeable formations are saltwater-bearing aquifers of different salinity levels and sealed by a multi-barrier system of caprocks of the Upper Bunter, the Middle and Upper Muschelkalk and the Lower Keuper, mainly made up of mudstones and anhydrites. The Rupelian clay situated in depths between 150 m to 200 m and characterized by an average thickness of 80 m forms the main regional barrier that separates the deep Triassic salt-water bearing sandstone aquifers from the upper freshwater aquifers of Upper Tertiary and Quaternary age. The rock consists, as the name implies, mainly of mudstone and was deposited in large parts of northern and northeastern Germany due to subsidence of the NEGB and marine transgression during the early Tertiary. However, processes related to the quaternary glaciation have locally caused a partly deep-reaching erosion of the Rupelian clay that may allow for a connection between the deep saline aquifers and shallow freshwaters. Upward rising brine could mix with potable groundwater resources and endanger freshwater supply (STACKEBRANDT AND MANHENKE, 2004).

2.3 MODELLING WORKFLOW

2.3.1 GEOLOGICAL MODEL

In a first step, a static geological 3D model with an areal size of 42 km x 42 km and a thickness of 766 m was developed using the software package Petrel (Figure 2).

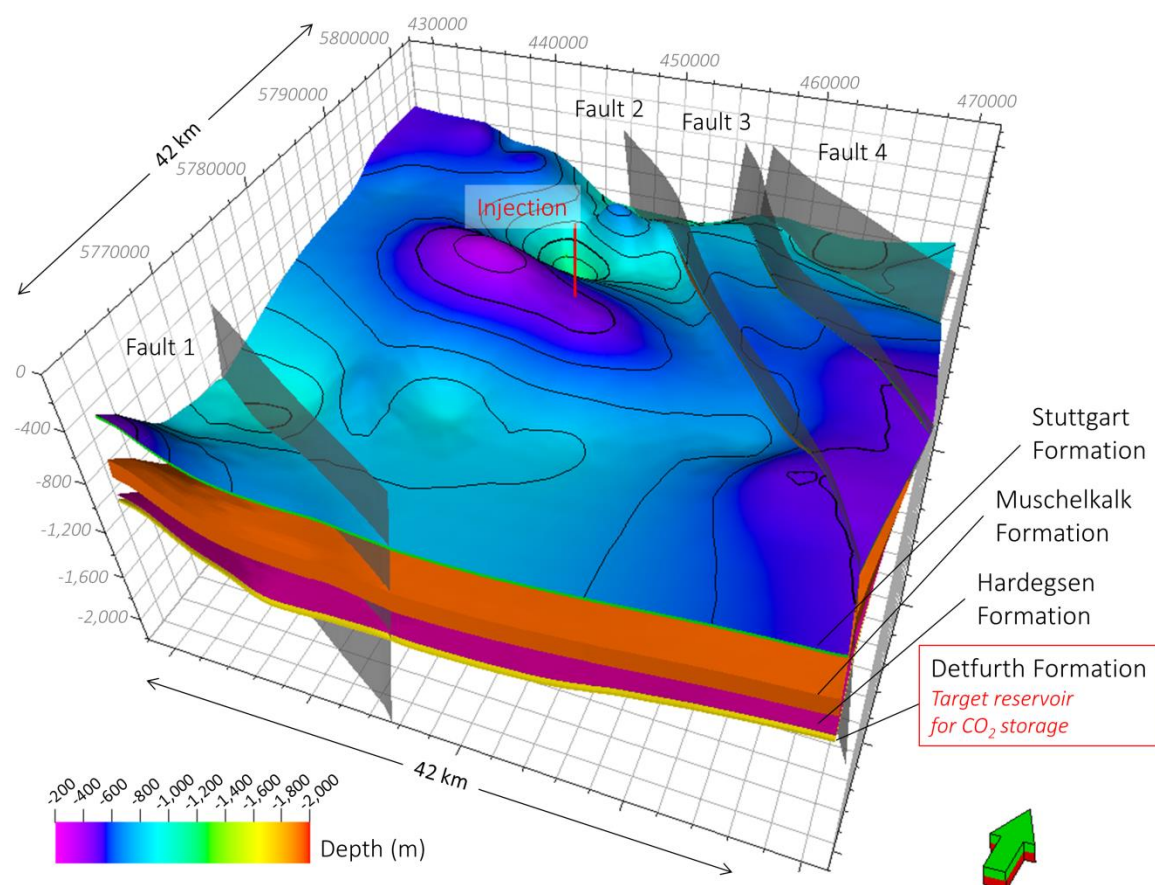


Figure 2: 3D geological structural model of the Beeskow-Birkholz site. The Lausitzer Abbruch fault zone is represented by Fault 1, the Fuerstenwalde-Guben fault zone by Faults 2, 3 and 4. Axes show UTM-coordinates (Spatial Reference: EPSG Projection 32633 - WGS84 / UTM zone 33N).

For that purpose, depth and thickness maps from the Geological Atlas of the State Brandenburg (STACKEBRANDT AND MANHENKE, 2004) as well as data from previous gas exploration campaigns carried out during the late 1970s (former German Democratic Republic, unpublished data), such as borehole data were used to digitize stratigraphic contour lines and major fault lines. Well data of three deep wells penetrating the Zechstein (Rotliegend) was further taken for a depth adjustment and thickness correction of the different lithologies and model calibration. In total, four different horizons and one major fault plane of the Lausitzer Abbruch fault zone (in the following *Fault 1*) located south-west as well as three major fault planes of the Fuerstenwalde-Guben fault zone (in the following *Fault 2, 3, 4*) located north-east of the anticline have been integrated into the 3D geological model. Both fault zones are characterized by mean displacement values of approximately 25 m. The vertical displacement along the four fault

planes was derived from the across-fault juxtaposition of the various horizons incorporated into the model and ranges between a few meters up to 60 m (Lausitzer Abbruch fault zone) and 130 m (Fuerstenwalde-Guben fault zone). The stratigraphic layers of the 3D geological model comprise from bottom to top, two sandstone formations of the Middle Bunter, namely the Detfurth and Hardegsen Formation followed by the limestones of the Lower Muschelkalk and another sandstone formation of the Middle Keuper (Stuttgart Formation), in a depth of 340 m (top of anticline). The target formation for CO₂ injection in the present study is the lowermost formation of the 3D geological model, the Detfurth Formation situated at a depth of about 1,080 m (top of anticline) and characterized by a thickness of 23 m. The thicknesses of the impermeable intermediate caprocks vary between 35 m to 320 m.

2.3.2 FAULT ZONE DESCRIPTION AND APPLIED SIMULATOR

A structured hexahedral grid generated on the 3D geological model with Petrel was applied for reservoir flow simulations. For this purpose, a workflow was developed including the grid transfer from Petrel to the reservoir simulator TOUGH2-MP and the discrete integration of faults into the reservoir-scale dynamic model by a concept taking into account variable fault geometries without modification of the initial gridding scheme. Faults are implemented as virtual elements that follow the discrete fault geometry and allow for arbitrary fault parameterization, thickness, and inter-connectivity (Figure 3).

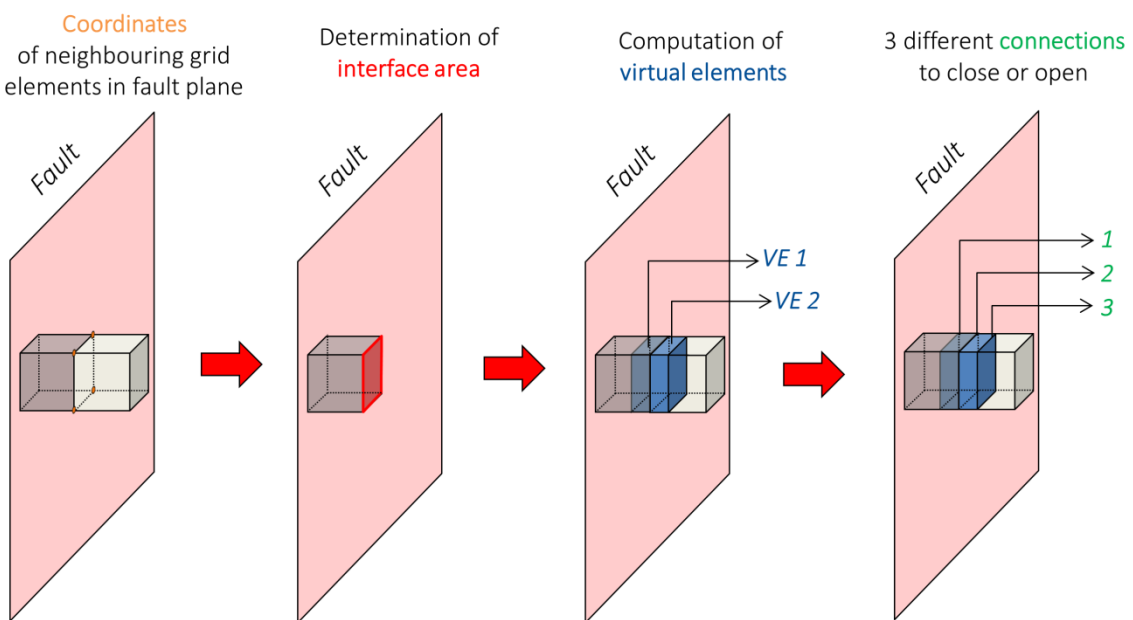


Figure 3: Simplified sketch illustrating the different steps of the virtual element (VE) workflow. Coordinates belonging to the common interface area of neighbouring grid elements are used for the computation of the virtual elements located on both sides of the fault. Different transmissibilities can be assigned to either fault or virtual elements, representing fault core (connection 2) and damage zone (VE 1 and VE 2), respectively.

The term ‘virtual elements’ was chosen since these multiple discrete grid cells do not exist in the 3D geological model generated with Petrel but are incorporated into the grid, while transferring it into the reservoir simulator TOUGH2. This approach further offers the possibility to describe each fault zone separately and calculate mass flow of displaced brine through the faults. Individual flow-related petrophysical properties can be assigned to either the fault core or generally low-permeability and/or the virtual elements at both sides of the fault representing the outer damage zone of relatively high permeability. A further advantage of this method is that also large displacements along the faults still allow for upward or/and along/cross-fault brine migration, since the discrete grid blocks describing the fault zones (virtual elements) connect the permeable formations, independently of whether the offset to either side of the fault is very large or not. The workflow starts with reading the initial reservoir model structured hexahedral grid constructed in Petrel and storing it in an adapted data structure representing element identification numbers (IDs), coordinates, centres and volumes of the virtual elements, further needed in the input files of the reservoir simulator TOUGH2.

The virtual elements are generated as follows: Neighbouring real grid elements located on both sides along each fault plane of the geological model are characterized by a common interface area, related to four coordinates in the plane (Figure 3). The shape of the interface area directly corresponds to the size and shape of the neighbouring grid elements and arrangement of the four coordinates. For the generation of the virtual elements the interface is shifted by the chosen element width in positive and negative direction from the fault zone, starting from the interface centre. Thus, the eight coordinates of the virtual elements, now located left and right from the fault plane are known and volumes can be calculated according to GRANDY (1997). Fault inter-connections are calculated considering element coordinates based on the method of GREINER AND HORMANN (1998) and stored in an adapted data structure representing each fault as a separate grid (local grid refinement). Further information required to carry out a simulation run in TOUGH2, such as virtual element connection distances as well as interfacing areas to other lateral and horizontal neighbouring elements, is directly written in the simulator input files. Each fault inter-connection is now represented by two virtual elements leading to irregular and winding fault structures and the development of an unstructured grid inside the initially structured one. Therefore, the connections along a fault are ordered from the starting point neglecting the initial i, j, k-ordering in the reservoir model grid. A winding counter was implemented to track fault geometry changes to assign proper virtual element connections. In total, three different inter-connections can be treated as either open or closed for flow for each fault, namely the two connections between the real grid elements and the virtual elements representing the damage zone located left and right from the fault core (connection 1 and 3, Figure 3), as well as the connection between the virtual elements themselves, representing the fault core (connection 2, Figure 3). An impermeable fault core, for instance, that acts as a barrier to fluid flow and prevents flow across the fault can be implemented by removing the connection between the two virtual elements in the simulator input files.

2.4 NUMERICAL MODEL SETUP

2.4.1 GRID DISCRETIZATION, PARAMETERIZATION AND INJECTION RATE

The model with an areal size of about 42 km x 42 km and a thickness of 766 m was discretized into a total number of 1,572,760 elements ($n_i=140$, $n_j=137$, $n_k=82$) by using a uniform lateral grid size of 300 m x 300 m. The vertical discretization of the grid elements varies depending on the different formations (Table 1). The grid elements that describe the intermediate caprocks overlaying the Detfurth, Hardegsen and Muschelkalk formations are defined as impermeable, and therefore inactive in the reservoir flow simulations (in total 690,480 inactive elements). Nevertheless, the inactive caprocks needed to have a certain vertical discretization since the computation of virtual elements describing the fault zones directly corresponds to the nodal point coordinates of the elements along the faults (Table 1). Fault 1 is represented by 15,580, Fault 2 by 32,636, Fault 3 by 23,452 and Fault 4 by 14,268 virtual elements resulting in a total number of active real and virtual elements of 968,216. This number varies depending on the different scenarios that have been performed due to varying fault definitions (see Section 2.4.2).

Table 1: Vertical grid discretization for the four different reservoirs and their caprocks. Inactive cells are only applied for vertical fault discretization.

Layer	Total thickness (m)	Number of elements	Element thickness (m)	Status
Stuttgart Formation	20	5	4	active
<i>Caprock 3</i>	320	16	20	<i>inactive</i>
Muschelkalk Formation	140	14	10	active
<i>Caprock 2</i>	220	10	22	<i>inactive</i>
Hardegsen Formation	8	4	2	active
<i>Caprock 1</i>	35	10	3.5	<i>inactive</i>
Detfurth Formation	23	23	1	active

The finest resolution with a vertical height of 1 m was chosen for the Detfurth Formation to account for buoyancy effects. The porosity and permeability distribution is modelled as homogenous and the values derived from the borehole data vary from 17 % and 400 mD (Millidarcy) in the Detfurth Formation, 16 % and 300 mD in the Hardegsen Formation, 20 % and 200 mD in the Muschelkalk Formation to 25 % and 100 mD in the Stuttgart Formation. Previous studies at Beeskow-Birkholz investigated the influence of caprock permeabilities on the salt concentration in formations above the reservoir by means of simplified numerical models. The results have shown that a significant salinization of shallower aquifers of the model was only achieved for caprock permeability values of 1 mD and above (KÜHN ET AL., 2011). The intermediate caprocks are assumed to have permeabilities below 1 mD, and thus were defined as impermeable in all simulations. Permeability anisotropy was not assigned. The calculation of relative permeabilities was performed based on experimental data from the Stuttgart Formation (Middle Keuper) of the Ketzin pilot site (KEMPKA AND KÜHN, 2013) located in the State of

Brandenburg, approximately 20 km northwest of Potsdam, since it currently provides the most confident data on storage related parameters for relevant sandstone formations in Germany (Figure 4). Capillary pressures were calculated according to VAN GENUCHTEN (1980) and upscaled from the existing laboratory data according to LEVERETT (1941). A rock grain density of $2,600 \text{ g/m}^3$ and pore compressibility of $7.2 \times 10^{-10} \text{ 1/Pa}$ were assigned to all four formations. Brine and CO₂ densities are calculated in TOUGH2-MP/ECO2N for each grid block during the simulation. Density variations with fluid pressure are furthermore taken into account for calculating the compressibility of CO₂ and brine (for a more detailed information on the implementation the reader is referred to ZHANG ET AL., 2008; PRUESS, 2005B). The average brine densities in the study area prior to injection vary between $1,116 \text{ kg/m}^3$ (Stuttgart Formation), $1,169 \text{ kg/m}^3$ (Muschelkalk Formation) and $1,174 \text{ kg/m}^3$ (Hardegsen and Detfurth formations) and do not increase significantly until the end of CO₂ injection (< 0.06 %).

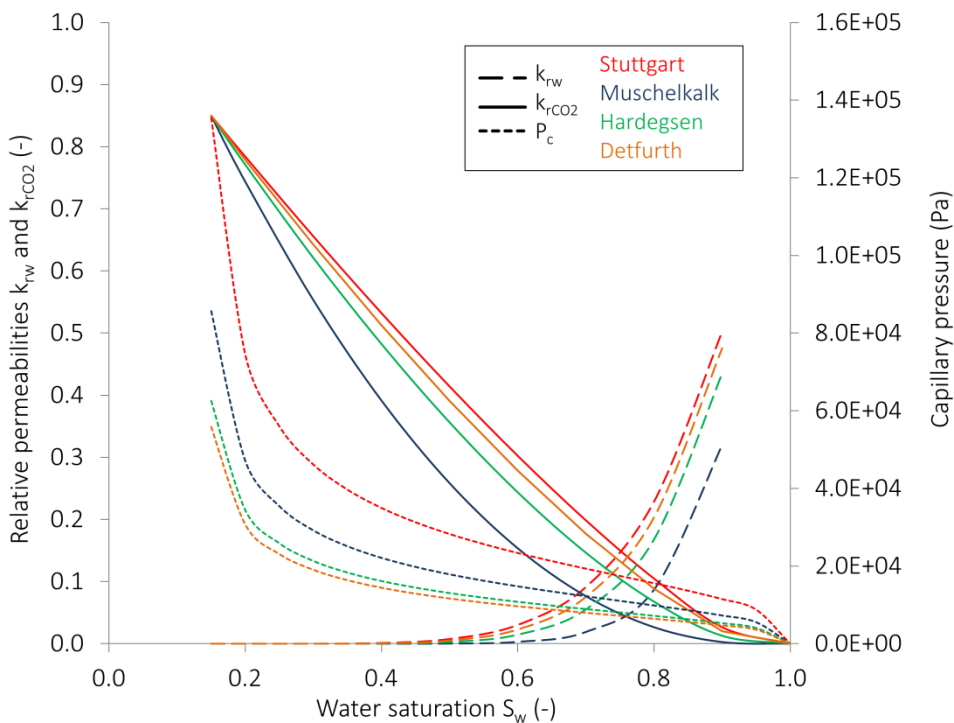


Figure 4: Applied relative permeabilities and scaled capillary pressures.

The temperature was calculated using a geothermal gradient of approximately $30 \text{ }^\circ\text{C/km}$ resulting in an average reservoir temperature of $50 \text{ }^\circ\text{C}$ in the Detfurth Formation that corresponds to the data from the exploration campaigns. During the simulation runs, the temperature remains unchanged in time and space. A hydrostatic pressure regime was selected, leading to an initial pressure of approximately 102 bar in the Detfurth Formation at the top of the anticline in a depth of 1,080 m. The salinity increases with depth from beneath the Rupelian clay with 50,000 mg/kg (units are milligrams of salt per kg of solution) by 220,000 mg/kg per km (in accordance to TESMER ET AL., 2007), with a minimum salinity of 9 % (90,000 mg/kg) at the top of the anticline in the Stuttgart Formation to a maximum allowable salinity of 25 % (250,000 mg/kg) starting at a depth of approximately 1,070 m as it was observed by borehole measurements. This results in an average salinity of 17 % in the Stuttgart Formation

(170,000 mg/kg), 24 % in the Muschelkalk Formation (240,000 mg/kg) and 25 % in both the Hardegsen and Detfurth Formation (250,000 mg/kg). The lateral boundaries were either defined as hydraulically open or closed depending on the different scenarios performed. A laterally open ‘Dirichlet’ boundary representing an infinite aquifer was achieved by multiplying the boundary element volume by a factor of 100 to avoid pressure effects by closed boundaries.

Due to the lack of field based data for fault characterization, estimates and assumptions with respect to fault architecture and lithology had to be made. Fault zones of the upper crust are lithologically heterogeneous and structurally anisotropic volumes that may either act as conduits, barriers or combined conduit-barriers to enhance or impede fluid flow (CAINE ET AL., 1996). In the frame of this study, all three types of fault zone behaviour were investigated (see also Section 2.4.2). For reasons of simplicity and as a first step, uniform fault architecture without any spatial or temporal variations in permeability and porosity was assumed. For the cross-fault barrier scenario, assuming high percentage of impermeable rocks from the fault core, no connection exists between the real grid elements and the virtual elements, representing the damage zone, to prevent flow perpendicular to the fault plane but still allow for flow along it. Thus, the reservoir is structurally compartmentalized by the faults. In the combined conduit-barrier case, fault zones are assumed to consist of a single high-strain core continuous throughout the fault plane providing an cross-fault barrier to flow surrounded by a permeable damage zone representing the along/up-fault conduit (FAULKNER ET AL., 2010; CAINE ET AL., 1996, CHESTER AND LOGAN, 1986). In these simulations, there exists no connection between the virtual elements themselves, representing the fault core. In the third case, all connections were left open to simulate fault zones as conduits that allow for both upward and along or cross-fault flow. A uniform porosity of 23 % and high permeabilities varying between 1,000 -10,000 mD were used in all scenarios with open faults (conduit- and combined conduit-barrier-system) and assigned to the damage zone (both virtual elements). The growth of damage zones and their scaling with fault displacement has been investigated by various authors (E.G. SAVAGE AND BRODSKY, 2011; FAULKNER ET AL., 2010; MITCHELL AND FAULKNER, 2009; VERMILYE AND SCHOLZ, 1998). Fault displacements that vary between 10 m – 1,000 m, for instance, may result in damage zone widths of 10 m up to at least hundred meters. Based on this positive correlation described by the authors mentioned above, a damage zone width of 20 m that corresponds to the mean vertical displacement of 25 m along both fault zones in the study area was estimated and assigned to all four discrete faults in the model, represented by two virtual elements at both sides of the fault with 10 m thickness each.

The 3D geological model as described above including the Middle Bunter, Muschelkalk and Keuper formations was applied to assess brine migration through the four major faults triggered by an annual injection rate of 1.7 million tons of CO₂ over a time span of 20 years. CO₂ injection occurs directly at the top of the anticline into the Detfurth Formation via a vertical injection well with a constant rate of 53.9 kg/s. Previous models showed that CO₂ injectivity was significantly reduced by salt precipitation in the near-well area reducing the pore volume in the near-well area by up to 15 %. Therefore, about 655,000 tons of brine per year were injected simultaneously with the CO₂ to avoid formation dry-out and resulting salt precipitation in the near-well area. Identical CO₂ and brine injection rates apply to all investigated scenarios.

2.4.2 SCENARIO ANALYSIS

To assess upward brine flow through the four permeable faults induced by CO₂ injection into the Detfurth Formation, seven different scenarios have been computed taking into account different fault damage zone (in the following DZ) permeabilities and boundary conditions (Table 2). Abbreviations for distinct scenario names are as follows:

$$\text{Scenario} = B_x^y F_n^k$$

where B denotes lateral boundaries that may either be open [o], or closed [c] in the lower [x] and/or upper aquifers [y]. F denotes fault, whereas n is the number of addressed faults and k the respective fault DZ permeability in Millidarcy (mD). Note that lower aquifers comprise the Middle Bunter formations, upper aquifers the Muschelkalk and Keuper formations.

Table 2: All calculated scenarios with applied boundary conditions and fault parameterization. Lower aquifers comprise the Middle Bunter formations, upper aquifers the Muschelkalk and Keuper formations.

Scenario	Boundaries	Fault behavior	Open faults	Permeability DZ	Porosity DZ
$B_o^o F_{1-4}^{1,000}$	open				
$B_c^o F_{1-4}^{1,000}$	open: <i>upper aquifers</i> closed: <i>lower aquifers</i>	conduit	Fault 1, 2, 3, 4	1,000 mD	23 %
$B_c^c F_{1-4}^0$	closed	barrier	-	-	-
$B_c^o F_2^{100}$	open: <i>upper aquifers</i> closed: <i>lower aquifers</i>			100 mD	
$B_c^o F_2^{1,000}$	open: <i>upper aquifers</i> closed: <i>lower aquifers</i>	combined conduit-barrier	Fault 2	1,000 mD	23 %
$B_o^o F_2^{1,000}$	open	barrier		1,000 mD	
$B_c^o F_2^{10,000}$	open: <i>upper aquifers</i> closed: <i>lower aquifers</i>			10,000 mD	

Scenario $B_o^o F_{1-4}^{1,000}$ is the base case with laterally open boundaries in all formations and open faults in horizontal and vertical direction with DZ permeabilities of 1,000 mD. Scenario $B_c^o F_{1-4}^{1,000}$ is a modification of Scenario $B_o^o F_{1-4}^{1,000}$ with regard to brine migration. The boundaries in the Middle Bunter formations (Defurth and Hardegsen formations) are closed, whereas a boundary element volume multiplier (factor 100) was used to simulate a laterally open aquifer in the Muschelkalk and Stuttgart formations and to allow for a pressure gradient development forcing brine to migrate upward along the permeable faults (faults act as conduits in both scenarios). Scenario $B_c^c F_{1-4}^0$ is a modification of Scenario $B_o^o F_{1-4}^{1,000}$ with all faults and boundaries closed to quantify changes in resulting pressure (faults act as barriers).

In Scenario $B_c^o F_2^{1,000}$, this idea was expanded by assuming that all faults are closed (impermeable damage zone and fault core; Fault 1,3,4 act as barriers) except Fault 2 representing the only conductive pathway with a DZ permeability of 1,000 mD for the upward migration of displaced brine. Given that flow is only possible along Fault 2 and upwards, a higher pressure build-up due to compartmentalization affects brine migration. To investigate the

influence of fault permeability on brine migration, values of 100 mD and 10,000 mD were assigned to the DZ of Fault 2 in Scenario $B_c^0 F_2^{100}$ and $B_c^0 F_2^{10,000}$, respectively. In Scenario $B_o^0 F_2^{1,000}$, again only Fault 2 acts as a conduit for flow along the fault plane and in vertical direction (DZ permeability of 1,000 mD, no cross-flow), whereas in this case a laterally open boundary in all formations was chosen to point out the differences in pressure build-up and brine migration compared to Scenario $B_c^0 F_2^{1,000}$ (Fault 1,3,4 act as barriers, Fault 2 acts as a combined conduit-barrier).

2.5 RESULTS

2.5.1 SCENARIOS $B_o^0 F_{1-4}^{1,000}$, $B_c^0 F_{1-4}^{1,000}$ (FAULTS ACT AS CONDUITS) AND $B_c^c F_{1-4}^0$ (FAULTS ACT AS BARRIERS)

For the Scenarios $B_o^0 F_{1-4}^{1,000}$ and $B_c^0 F_{1-4}^{1,000}$ a maximum pressure of 197 bar after 20 days of injection developed at the top of the anticline in the Detfurth Formation, starting from an initial pressure of 102 bar (Figure 5).

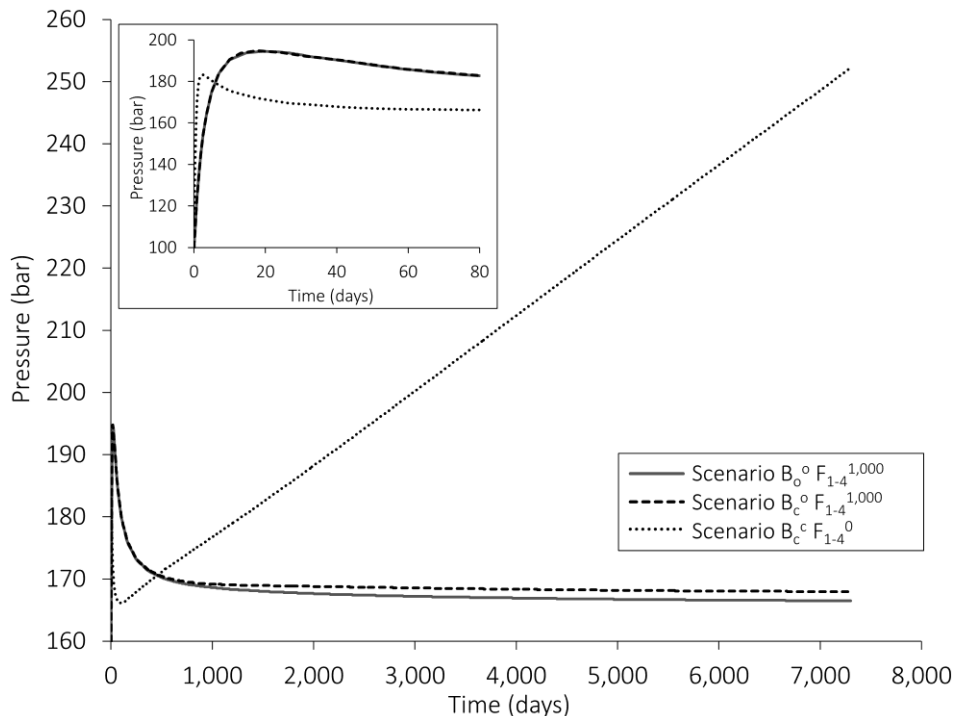


Figure 5: Pressure evolution at the top of the Detfurth anticline for Scenarios $B_o^0 F_{1-4}^{1,000}$, $B_c^0 F_{1-4}^{1,000}$ and $B_c^c F_{1-4}^0$.

Pressure subsequently decreases until the end of injection, whereas the pressure dissipation rate in Scenario $B_c^0 F_{1-4}^{1,000}$ with closed boundaries in the lower Middle Bunter aquifers is lower compared to Scenario $B_o^0 F_{1-4}^{1,000}$ with laterally open boundaries in all formations. This results in a lower pressure after 20 years of injection with 168 bar for Scenario $B_o^0 F_{1-4}^{1,000}$ and 170 bar for Scenario $B_c^0 F_{1-4}^{1,000}$ (increase by a factor of 1.65 and 1.67, respectively). In Scenario $B_c^c F_{1-4}^0$

pressure increases faster in the first days of injection up to a first peak of 185 bar after already 2.5 days (Figure 5). Pressure subsequently decreases and starts to increase again after 100 days of injection to a maximum of 254 bar after 20 years (increase by a factor of 2.5).

According to the gas storage industry in Germany, a pressure increase by a factor of 1.68 above the initial pressure is the average allowed limit (SEDLACEK, 1999). However, staying below the fracture pressure of the reservoir rock or the caprock was not enforced in the model due to the fact that all models were supposed to run with the same injection regime. The pressure developments at the top of the anticline coincide with the development of the average pressure in the Detfurth Formation, which increases from 144 to 152 bar in Scenario $B_o^0 F_{1-4}^{1,000}$, to 154 bar in Scenario $B_c^0 F_{1-4}^{1,000}$ and to 242 bar in Scenario $B_c^c F_{1-4}^0$ until the end of injection after 20 years (Figure 6).

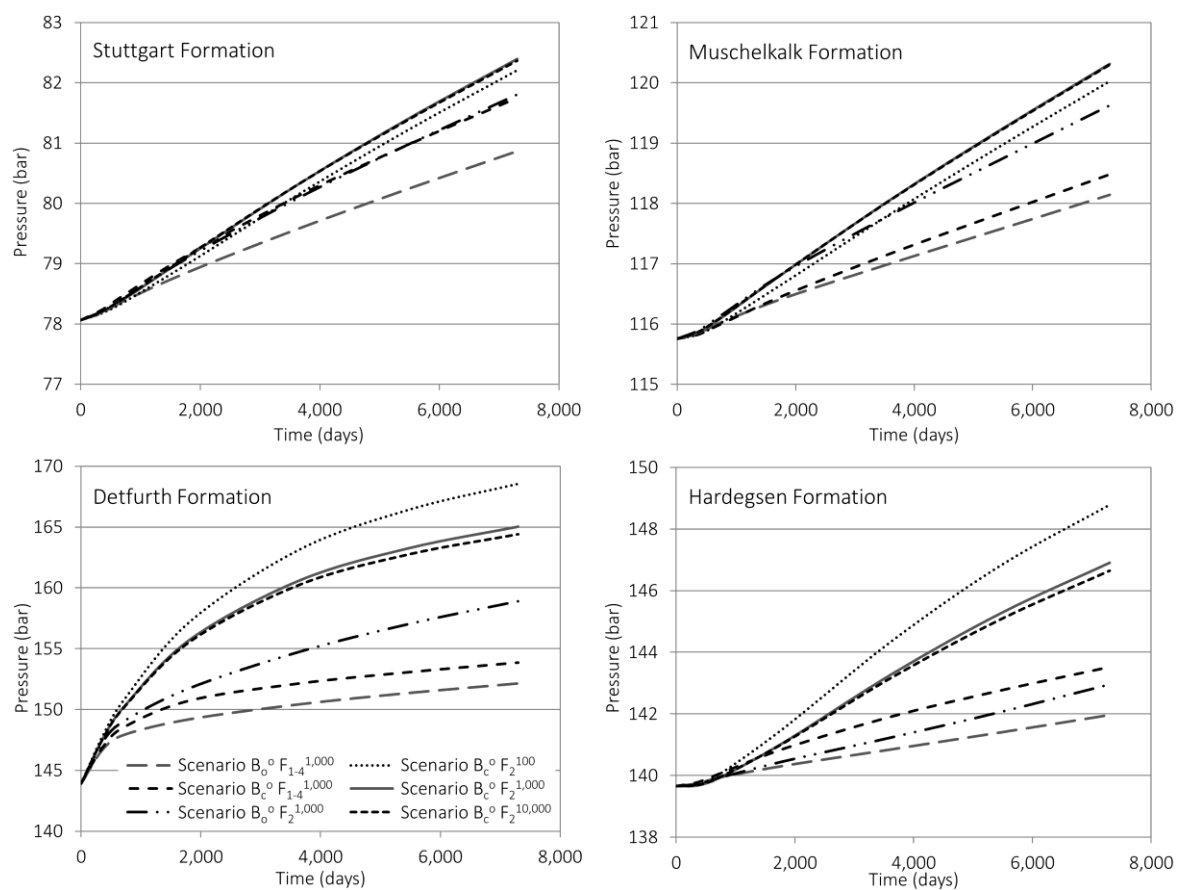


Figure 6: Average formation pressures for all investigated scenarios with faults acting as conduits or a combined conduit-barrier.

Figure 7 compares the pressure evolution in the upper aquifers (Muschelkalk and Stuttgart formations) of Scenarios $B_o^0 F_{1-4}^{1,000}$ and $B_c^0 F_{1-4}^{1,000}$. For that purpose, two observation points at 1,005 m (Muschelkalk Formation) and 670 m depth (Stuttgart Formation) at the central western part of Fault 2 were determined. In the first 1,000 days of injection, no significant differences in pressure development can be observed for both Scenarios and formations. Subsequently, pressure also rises steeper (both formations) in Scenario $B_c^0 F_{1-4}^{1,000}$ with closed boundaries in

the lower Middle Bunter aquifers. This results in a pressure difference of 0.65 bar (Stuttgart Formation) and 0.8 bar (Muschelkalk Formation) between the investigated scenarios at the end of injection. The average formation pressures for both aquifers (Figure 6) also reflect this development.

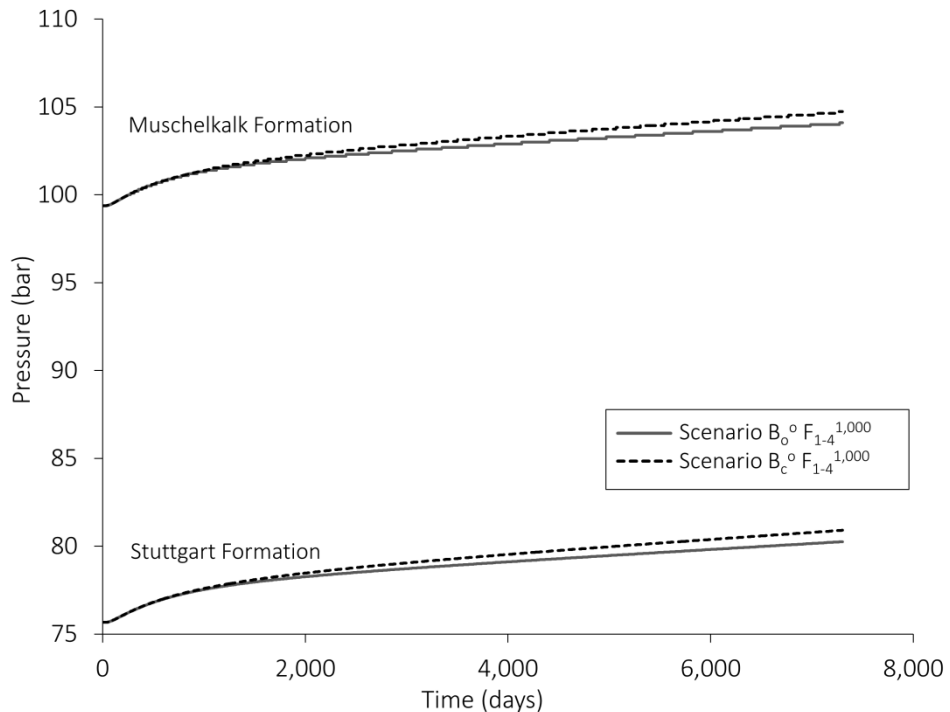


Figure 7: Pressure evolution in the upper aquifers (Muschelkalk and Stuttgart formations) for Scenarios $B_o^0 F_{1-4}^{1,000}$ and $B_c^0 F_{1-4}^{1,000}$. The observation points are located at the top of each formation close to Fault 2 (western side, central part of the model domain).

In Scenario $B_o^0 F_{1-4}^{1,000}$ considering laterally open boundaries in all four formations, the amount of water and salt in the Detfurth formation displaced towards boundaries and via the four faults is 50 Mt H₂O and 17.5 Mt NaCl, and thus slightly higher compared to Scenario $B_c^0 F_{1-4}^{1,000}$ (49 Mt H₂O, 17.1 Mt NaCl; Figure 8). However, in this scenario the complete amount of water and salt displaced out of the Detfurth Formation is migrating into the overlying formations via the four faults. Because salinity varies across the model in vertical direction, mass balancing is clearer and nonambiguous if water and salt are considered separately, even though the salt is transported with the water. The relative salt mass change within the four open faults is up to 0.6 % higher taking into account closed boundaries for the Middle Bunter formations (Scenario $B_c^0 F_{1-4}^{1,000}$) after 20 years of injection. Salt mass increases mainly in Fault 2 and Fault 3 by 0.78 Mt and 0.55 Mt (Scenario $B_c^0 F_{1-4}^{1,000}$) and 0.46 Mt and 0.33 Mt (Scenario $B_o^0 F_{1-4}^{1,000}$, Figure 9). For Scenario $B_o^0 F_{1-4}^{1,000}$ this equals an increase in salinity levels of the major Fault 2 by 0.68 % (1,600 mg/kg) whereas the salinity of Fault 2 increases by 1.2 % (2,700 mg/kg) in Scenario $B_c^0 F_{1-4}^{1,000}$.

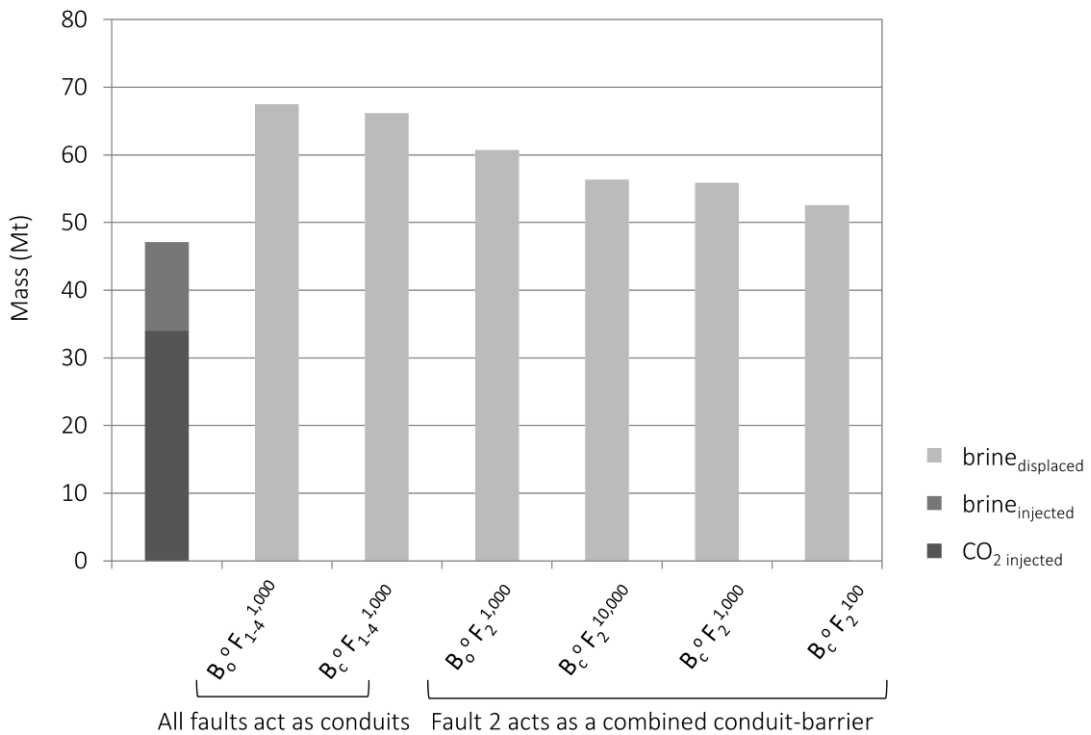


Figure 8: Injected vs. displaced mass for all investigated scenarios with faults acting as conduits (average CO_2 density varies between $602\text{-}738 \text{ kg/m}^3$) or a combined conduit-barrier (average CO_2 density varies between $638\text{-}755 \text{ kg/m}^3$).

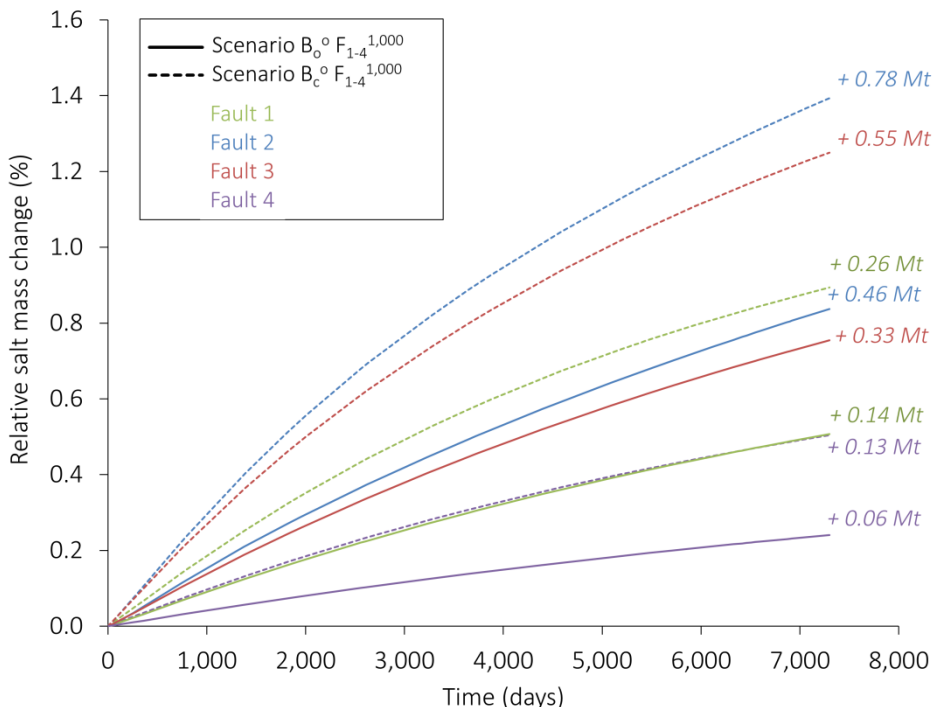


Figure 9: Comparison of relative salt mass change in the four faults for Scenarios $B_o^o F_{1-4}^{1,000}$ and $B_c^o F_{1-4}^{1,000}$.

Figure 10 shows that a maximum salinity increase up to 47,000 mg/kg can be observed in the Stuttgart Formation close to the four major fault planes for Scenario $B_c^o F_{1-4}^{1,000}$ and after 20 years of CO₂ injection with the greatest increase close to Fault 2 and 3. However, due to dilution the average salinity of the entire Stuttgart Formation increases only by 0.24 % (407 mg/kg) in Scenario $B_c^o F_{1-4}^{1,000}$ and by 0.17 % (290 mg/kg) in Scenario $B_o^o F_{1-4}^{1,000}$ due to higher relative salt mass than water mass changes at the end of injection (Figure 11).

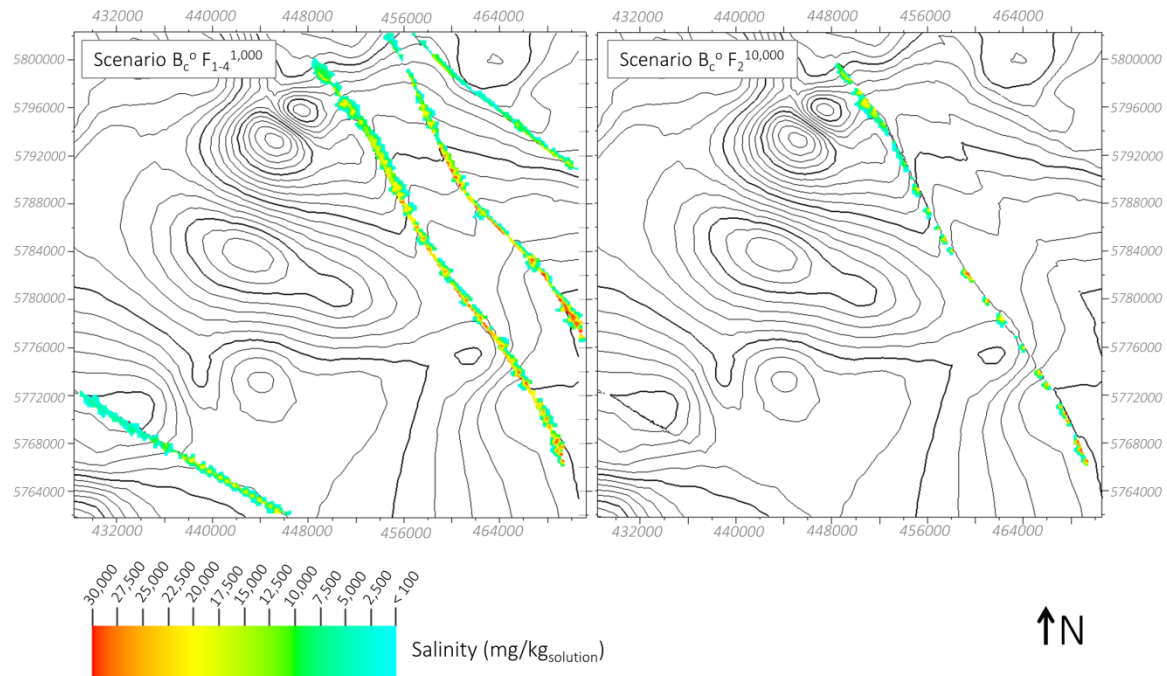


Figure 10: Local salinity increase in the uppermost Stuttgart Formation for Scenarios $B_c^o F_{1-4}^{1,000}$ and $B_c^o F_2^{10,000}$. Plotted are net values of the formation.

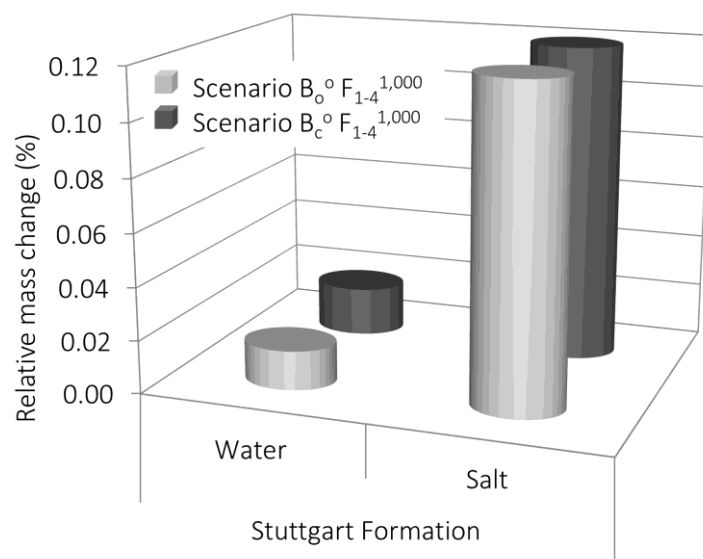


Figure 11: Relative mass change of salt and water in the uppermost Stuttgart Formation for Scenarios $B_o^o F_{1-4}^{1,000}$ and $B_c^o F_{1-4}^{1,000}$.

Shape and size of the CO₂ plume are very similar for Scenarios B_o⁰F₁₋₄^{1,000} and B_c⁰F₁₋₄^{1,000}. It expands in NW-SE direction according to the orientation of the anticline with a length of approximately 18.7 km and width of 5 km. At the end of simulation time (20 years), about 4 % of the injected CO₂ is dissolved in the formation water. The CO₂ plume in the investigated Scenario B_c⁰F₁₋₄⁰ with closed faults and boundaries (average CO₂ density: 724-795 kg/m³) is considerably smaller showing a length of 17 km and a width of 4.2 km. In none of the cases, CO₂ reaches the fault zones.

2.5.2 SCENARIOS B_c⁰F₂^{1,000} AND B_o⁰F₂^{1,000} (FAULT 2 ACTS AS A COMBINED CONDUIT-BARRIER)

A comparison between Scenario B_c⁰F₂^{1,000}, where only Fault 2 acts as a combined conduit-barrier for flow and Scenario B_o⁰F₂^{1,000} with identical fault properties but laterally open boundaries in all formations shows a maximum pressure peak of 197 bar at the top of the anticline for both scenarios after 20 days of injection (Figure 12). Pressure subsequently dissipates and starts to increase again after about 2 years of injection indicating a steeper increase in Scenario B_c⁰F₂^{1,000} up to a pressure of 180 bar at the end of injection compared to 174 bar in Scenario B_o⁰F₂^{1,000} (increase by a factor of 1.76 and 1.71, respectively). The average pressure in the Dettfurth rises steeper in Scenario B_c⁰F₂^{1,000} up to 165 bar until the end of injection (159 bar, Scenario B_o⁰F₂^{1,000}).

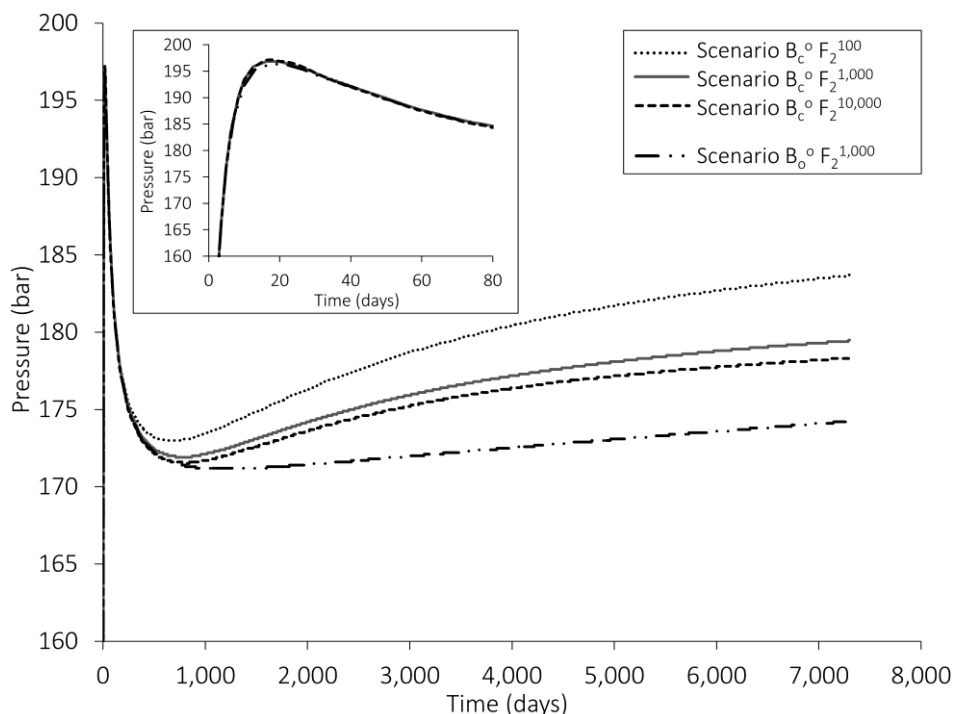


Figure 12: Pressure evolution at the top of the Dettfurth anticline for Scenarios B_c⁰F₂¹⁰⁰, B_c⁰F₂^{1,000}, B_c⁰F₂^{10,000} and B_o⁰F₂^{1,000}.

A comparison of pressure evolution in the upper aquifers (Muschelkalk and Stuttgart formations) between Scenario $B_c^0 F_2^{1,000}$ and $B_o^0 F_2^{1,000}$ was undertaken (Figure 13). The observation points are identical to those described in Section 5.1. After 1,000 days of injection the pressure in both formations shows also a steeper increase in Scenario $B_c^0 F_2^{1,000}$ with closed boundaries in the lower Middle Bunter aquifers. For both formations, a pressure difference of 2 bar between the investigated scenarios at the end of injection is observed. This results in a pressure of 89.8 bar in the Stuttgart Formation for Scenario $B_c^0 F_2^{1,000}$ (87.8 bar, Scenario $B_o^0 F_2^{1,000}$) and a pressure of 113.1 bar in the Muschelkalk Formation (111.1 bar, Scenario $B_o^0 F_2^{1,000}$). However, the difference in the average formation pressure until the end of injection is with 0.6 bar for both formations slightly lower (Figure 6).

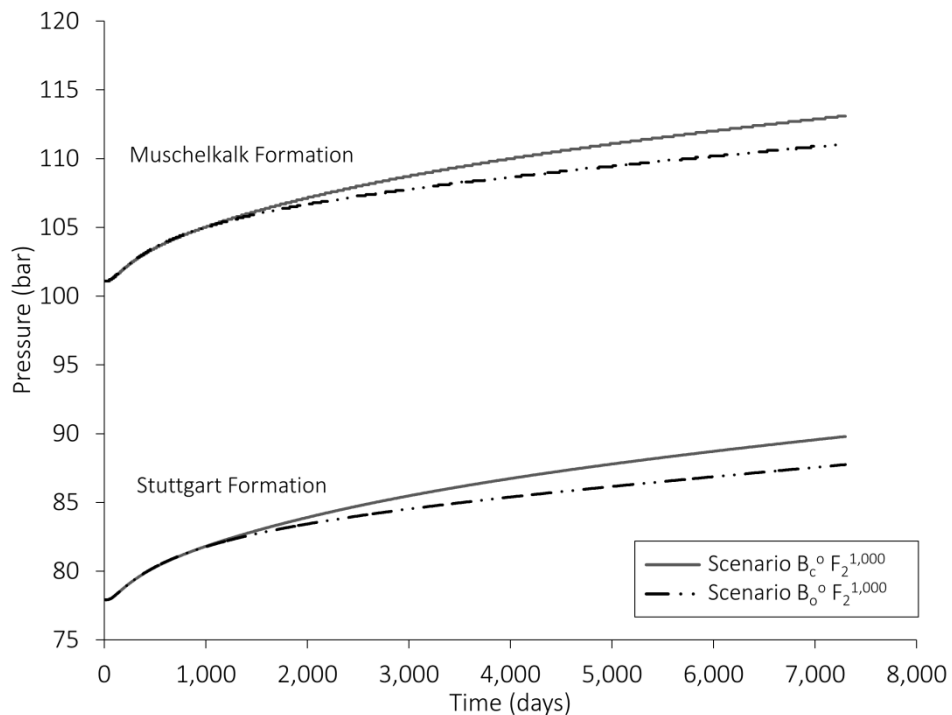


Figure 13: Pressure evolution in the upper aquifers (Muschelkalk and Stuttgart formations) for Scenarios $B_c^0 F_2^{1,000}$ and $B_o^0 F_2^{1,000}$. The observation points are located at the top of each formation close to Fault 2 (western side, central part of the model domain).

In Scenario $B_o^0 F_2^{1,000}$ about 45.5 Mt H₂O (15.2 Mt NaCl) are displaced into Fault 2 and the lower open boundaries whereas in Scenario $B_c^0 F_2^{1,000}$ about 41.9 Mt H₂O (13.9 Mt NaCl) are displaced out of the Detfurth Formation into Fault 2 and the overlying formations and not also into the lower boundaries (Figure 8). The salinity in Fault 2 therefore increases by 1.7 % (3,840 mg/kg) in Scenario $B_c^0 F_2^{1,000}$ and 0.34 % (765 mg/kg) in Scenario $B_o^0 F_2^{1,000}$. Figure 14 shows that salt and water mass in the upper aquifers have also increased comparing Scenario $B_c^0 F_2^{1,000}$ (6.2 Mt NaCl and 21.4 Mt H₂O) and Scenario $B_o^0 F_2^{1,000}$ (5.4 Mt NaCl and 17.1 Mt H₂O). Locally, in the vicinity of Fault 2, the salinity in the Stuttgart Formation increases by up to 43,000 mg/kg (Scenario $B_c^0 F_2^{1,000}$) and 41,000 mg/kg (Scenario $B_o^0 F_2^{1,000}$) whereas the average salinity of the Stuttgart Formation increases by 0.04 % in both scenarios resulting in a total amount of 75 mg/kg for Scenario $B_c^0 F_2^{1,000}$ and 61 mg/kg for Scenario $B_o^0 F_2^{1,000}$ until the end of injection.

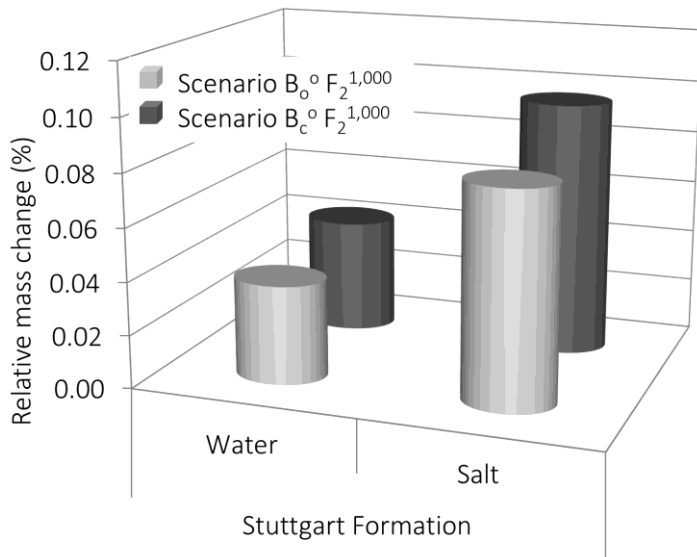


Figure 14: Relative mass change of salt and water in the uppermost Stuttgart Formation for Scenarios $B_c^0 F_2^{1,000}$ and $B_o^0 F_2^{1,000}$.

2.5.3 SCENARIOS $B_c^0 F_2^{100}$, $B_c^0 F_2^{1,000}$ AND $B_c^0 F_2^{10,000}$ (FAULT 2 ACTS AS A COMBINED CONDUIT-BARRIER)

These three scenarios were performed to investigate the impact of fault DZ permeability on upward brine migration. The DZ permeability values of Fault 2 were varied with 100 mD ($B_c^0 F_2^{100}$), 1,000 mD ($B_c^0 F_2^{1,000}$) and 10,000 mD ($B_c^0 F_2^{10,000}$). For all scenarios a maximum pressure of 197 bar after 20 days of injection developed at the top of the anticline, starting from an initial pressure of 102 bar (Figure 12). Pressure subsequently decreases in all scenarios with the sharpest decrease in Scenario $B_c^0 F_2^{10,000}$, followed by Scenario $B_c^0 F_2^{1,000}$ and Scenario $B_c^0 F_2^{100}$. After 800 days of injection pressure starts to increase again with the sharpest increase in Scenario $B_c^0 F_2^{100}$. Pressure at the top of the Detfurth anticline estimates 184 bar in Scenario $B_c^0 F_2^{100}$ (increase by a factor of 1.8), 180 bar in Scenario $B_c^0 F_2^{1,000}$ (increase by a factor of 1.76) and 178 bar in Scenario $B_c^0 F_2^{10,000}$ (increase by a factor of 1.75). This pressure development at the injector coincides with the average pressure of the formation with the sharpest increase for Scenario $B_c^0 F_2^{100}$ after an injection period of 20 years (Figure 6). The highest pressure response in the upper aquifers (Muschelkalk and Stuttgart Formation) after 20 years of injection can be observed in Scenario $B_c^0 F_2^{1,000}$ and the lowest in Scenario $B_c^0 F_2^{100}$ resulting in a pressure difference of 0.7 bar (Figure 15) and even less considering the average formation pressure (Figure 6).

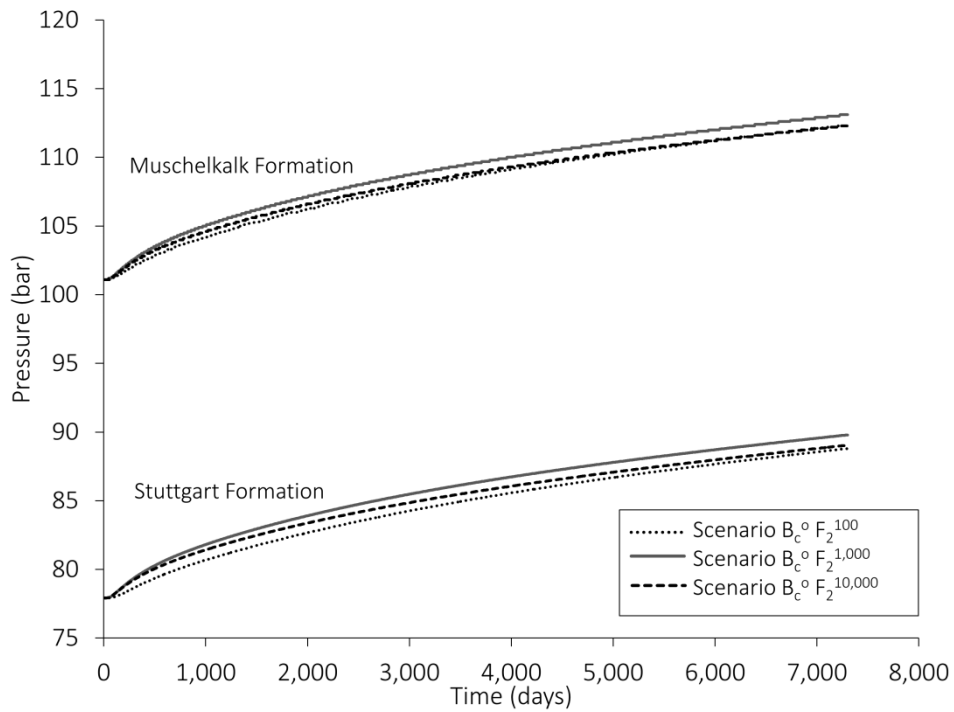


Figure 15: Pressure evolution in the upper aquifers (Muschelkalk and Stuttgart formations) for Scenarios $B_c^\circ F_2^{100}$, $B_c^\circ F_2^{1,000}$ and $B_c^\circ F_2^{10,000}$. The observation points are located at the top of each formation close to Fault 2 (western side, central part of the model domain).

The amount of water and salt that is displaced out of the Detfurth Formation into Fault 2 is 39.4 Mt H₂O and 13.1 Mt NaCl for Scenario $B_c^\circ F_2^{100}$, 41.9 Mt H₂O and 13.9 Mt NaCl for Scenario $B_c^\circ F_2^{1,000}$ and about 42.3 Mt H₂O and 14.1 Mt NaCl for Scenario $B_c^\circ F_2^{10,000}$, respectively (Figure 8). While salt and water mass have not changed significantly within the Hardegsen (< 0.01 %) and Muschelkalk formations (< 0.004 %), the average salinity in the Stuttgart Formation increased by 0.02 % (34 mg/kg) in Scenario $B_c^\circ F_2^{100}$, 0.04 % (75 mg/kg) in Scenario $B_c^\circ F_2^{1,000}$ and 0.06 % (96 mg/kg) in Scenario $B_c^\circ F_2^{10,000}$ due to higher relative salt mass than water mass changes at end of injection (Figure 16).

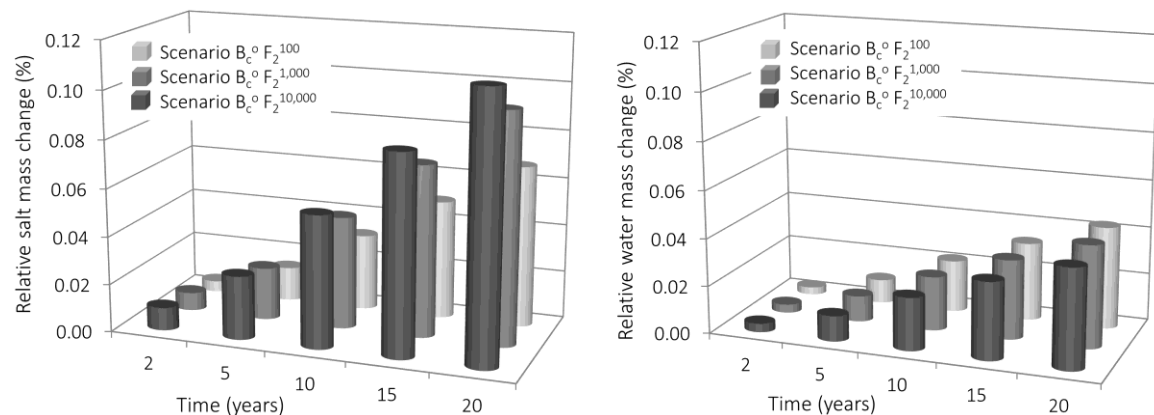


Figure 16: Comparison of relative salt and water mass change of the Stuttgart Formation for the Scenarios $B_c^\circ F_2^{100}$, $B_c^\circ F_2^{1,000}$ and $B_c^\circ F_2^{10,000}$.

The highest local salinity increase in the uppermost Stuttgart Formation of up to 50,000 mg/kg can also be observed in Scenario $B_c^0 F_2^{10,000}$ with the highest fault DZ permeability and is limited to the vicinity of the fault (Figure 10).

The extent of the CO₂ plume is shown in Figure 17. It expands in NW-SE direction according to the orientation of the anticline with a length of approximately 17.5 km and width of 4.9 km in Scenario $B_c^0 F_2^{100}$. In Scenario $B_c^0 F_2^{1,000}$ and $B_c^0 F_2^{10,000}$ the plume expands more towards Fault 2 and has a larger extent with about 300 m and 900 m, respectively (Figure 18). At the end of simulation time (20 years) about 4 % of the injected CO₂ are dissolved in the formation water. As mentioned earlier, in no case the CO₂ reaches any of the fault zones in the area.

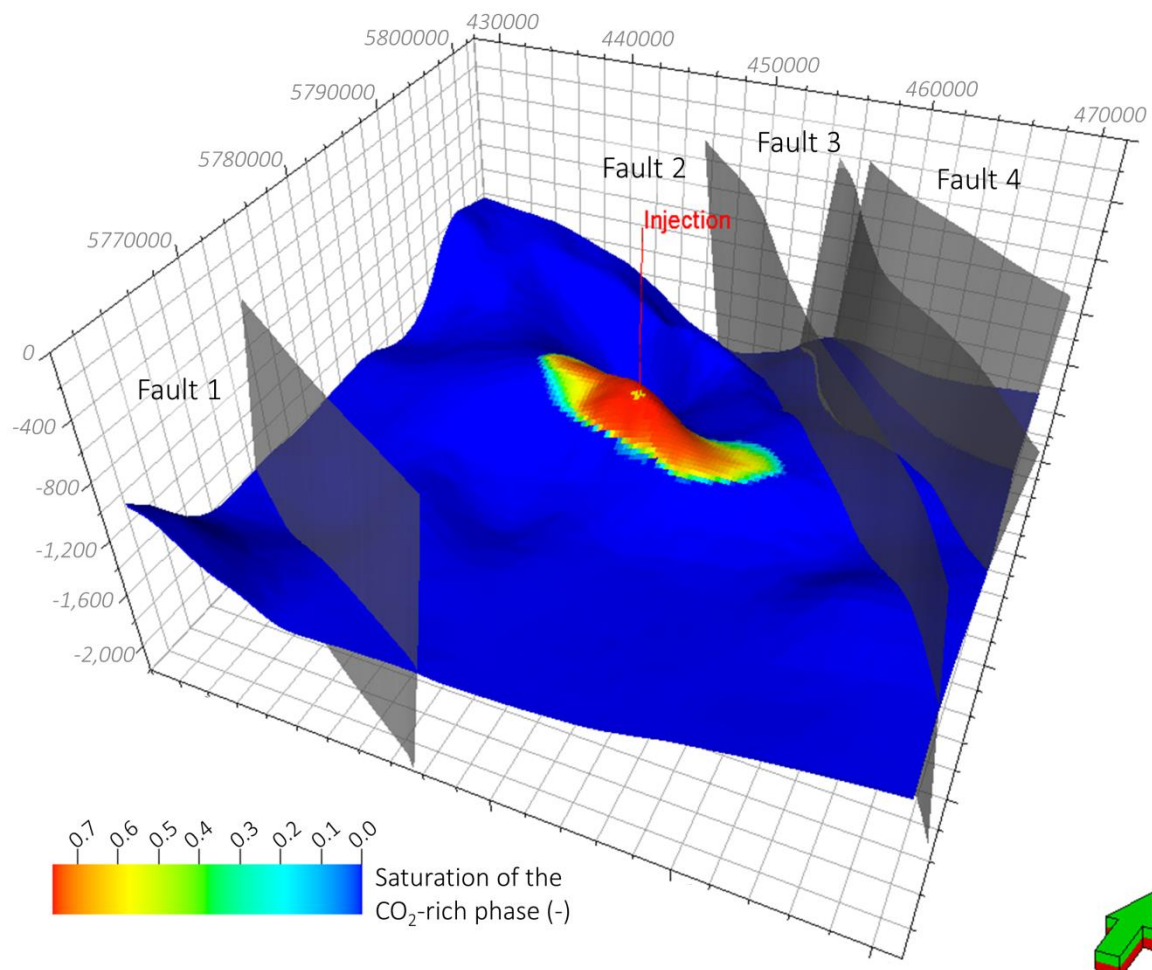


Figure 17: Extent of the CO₂ plume in Scenario $B_c^0 F_2^{1,000}$ (Fault 2 DZ permeability 1,000 mD). Axes show UTM-coordinates (Spatial Reference: EPSG Projection 32633 - WGS84 / UTM zone 33N).

In Scenario $B_c^0 F_{1-4}^0$ with closed boundaries and closed faults, the highest pressurization with a relative pressure increase at the top of the Detfurth anticline (injector location) by a factor of 2.5 and an average formation pressure increase by a factor of 1.7 after 20 years of injection was observed. A comparison of Scenario $B_c^0 F_2^{1,000}$ and $B_o^0 F_2^{1,000}$ has shown that the average pressure build-up in the overlying aquifers is up to 0.6 bar higher (2 bar higher close to Fault 2) with closed boundaries in the lower aquifers. The highest pressure dissipation and decelerated pressure increase at the beginning of CO₂ injection was observed for Scenario $B_o^0 F_{1-4}^{1,000}$ (all faults act as conduits) and $B_o^0 F_2^{1,000}$ (Fault 2 acts as a combined conduit-barrier) with laterally

open boundaries in all formations. Open boundaries and faults that act as conduits allowing for flow along/across the fault and upwards (Scenario $B_c^o F_{1-4}^{1,000}$) also lead to the laterally largest CO₂ plume, whereas the smallest plume can be observed in Scenario $B_c^c F_{1-4}^0$ (closed boundaries, faults act as barriers to upward and cross-flow). Scenarios $B_c^o F_2^{100}$, $B_c^o F_2^{1,000}$ and $B_c^o F_2^{10,000}$ have shown that higher fault DZ permeability forces the CO₂ plume to extend more towards the fault. Four open faults and closed boundaries in the lower aquifers allow for the highest amount of brine that is displaced towards the faults into the overlying formations whereas lower fault DZ permeabilities lead to lower displacement rates.

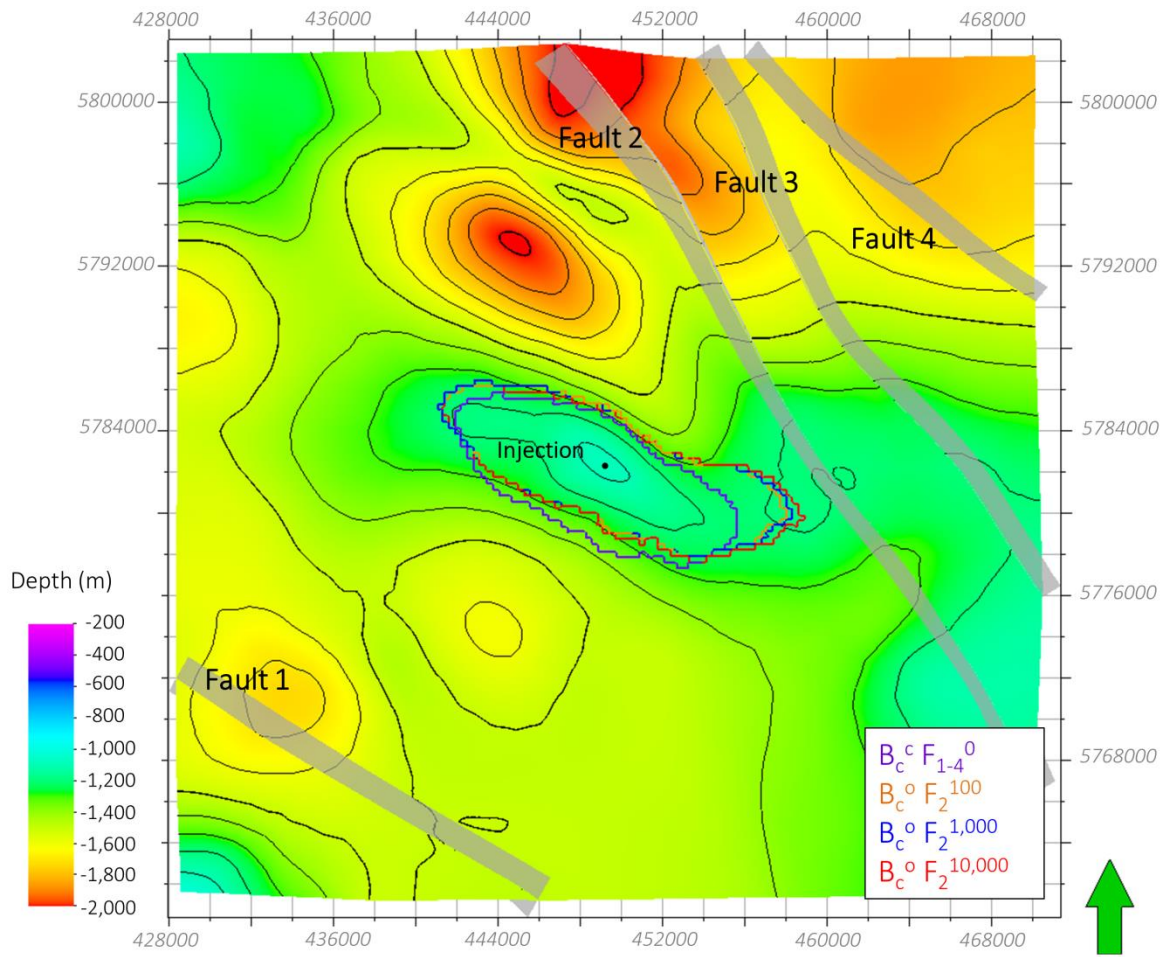


Figure 18: Contour map of the study area with outer border of the CO₂ plume. Shown are the scenarios $B_c^o F_2^{100}$ (orange), $B_c^o F_2^{1,000}$ (blue) and $B_c^o F_2^{10,000}$ (red) as well as Scenario $B_c^c F_{1-4}^0$ (purple). Axes show UTM-coordinates (Spatial Reference: EPSG Projection 32633 - WGS84 / UTM zone 33N).

The highest average salinity increase in the uppermost Stuttgart Formation can be observed in Scenario $B_c^o F_{1-4}^{1,000}$ with closed boundaries in the two lower aquifers (Detfurth and Hardgesen Formation) and open boundaries in the uppermost aquifers (Muschelkalk and Stuttgart Formation) as well as four open faults (DZ permeability of 1,000 mD). While the salinity did not change significantly in the Hardegse and Muschelkalk formations (< 0.02 %) the average salinity in the Stuttgart Formation increased by 0.24 % (407 mg/kg).

Scenarios $B_c^o F_2^{100}$, $B_c^o F_2^{1,000}$ and $B_c^o F_2^{10,000}$ show that fault permeability has a minor influence on brine migration considering the average salinity changes of the upper aquifers. In Scenario $B_c^o F_2^{100}$ the salinity increases in the Stuttgart Formation by 0.02 % (34 mg/kg), in Scenario $B_c^o F_2^{1,000}$ by 0.04 % (75 mg/kg) and in Scenario $B_c^o F_2^{10,000}$ by 0.06 % (96 mg/kg) until the end of the simulation time (Figure 19). In the vicinity of Fault 2 the salinity increases by up to 50,000 mg/kg in Scenario $B_c^o F_2^{10,000}$ and by up to 47,000 mg/kg close to all four faults in Scenario $B_c^o F_{1-4}^{1,000}$.

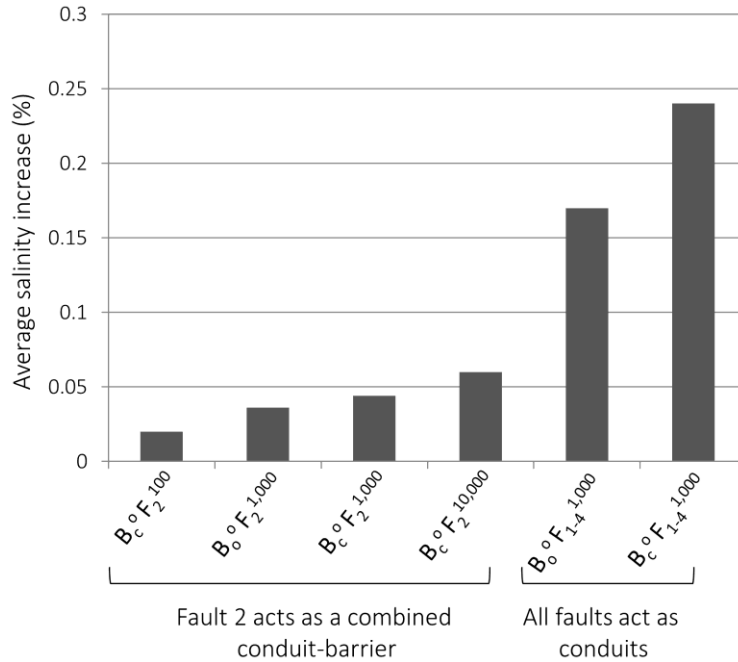


Figure 19: Average salinity increase in the uppermost Stuttgart Formation for all investigated scenarios with faults acting as conduits or a combined conduit-barrier.

2.6 DISCUSSION AND CONCLUSION

In this study it is shown that regional-scale 3D models based on structural data of a prospective CO₂ storage site in Northeast Germany can be applied and computed for quantitative assessment with regard to pressure increase and brine migration into shallower aquifers by a newly developed workflow and the implementation of faults zones as virtual elements. Modelling results show that compartmentalization due to closed boundaries and faults that act as barriers to upward and cross-flow, cause the highest pressurization in the storage formation that goes along with the steepest pressure build-up and a relative increase by a factor of 2.5 (injector location) and 1.6 (average formation pressure) after 20 years of injection. Closed boundaries in the lower aquifers and low fault DZ permeability still allow for a relative pressure increase by a factor of 1.8 (at the top of the anticline) and 1.2 (average formation pressure), respectively. Taking into account the allowed limit of pressure increases in the gas storage industry in Germany of factor 1.68 above the initial pressure (relative pressure increase of 68 %) as reported by SEDLACEK (1999) only the cases with open or partly open lateral boundaries and all

four fault zones permeable are eligible within the time as of about 3 years. If only one fault zone is permeable, it needs to have a very high DZ permeability ($> 1,000 \text{ mD}$) to allow for a long-term pressure release below the limiting factor 1.68. In the short term of days all models almost reach a pressure increase by a factor of up to two in the reservoir. However, pressure build-up in the storage formation could be mitigated in all scenarios except the one with closed boundaries and faults that act as barriers to upward and cross-flow by splitting the injection rate on at least two injectors instead of one. In any case, the pressure increase in aquifers above the storage reservoir is lower by orders of magnitude. The pressure build-up in the overlying aquifers is up to two bar higher with closed boundaries in the lower aquifers. Laterally open boundaries and highly permeable faults lead to the strongest pressure dissipation and decelerate the pressure increase at the beginning of CO_2 injection. Compartmentalization and increased pressure build-up further lead to considerably smaller CO_2 plumes with an almost 1.7 km smaller extent compared to those that develop when laterally open boundaries are applied. At lower reservoir pressures, resulting from higher fault DZ permeabilities the CO_2 plume occupies a larger volume and causes the entire plume to be larger due to the CO_2 PVT properties (e.g. compressibility). Topography effects (CO_2 plume propagates preferentially along the orientation of the anticline) and higher flow rates into the fault at higher fault DZ permeabilities also cause the CO_2 plume to come up almost 1 km closer to the fault. It is important to note that in no case the CO_2 reaches any of the fault zones.

Larger pressure build-up due to closed boundaries generally leads to stronger brine displacement and higher salinities in the fault zones and the higher aquifers. In particular, closed boundaries in the two lower aquifers (Detfurth and Hardgegsen Formation) and open boundaries in the uppermost aquifers (Muschelkalk and Stuttgart Formation) as well as four open faults (DZ permeability of 1,000 mD) showed highest amounts of upward brine migration. While the average salinity did not change significantly in the Hardegsen and Muschelkalk formations ($< 0.02 \%$) the average salinity in the Stuttgart Formation increased by 0.24 % (407 mg/kg) at the end of injection. Laterally open boundaries in all formations and four open faults (DZ permeability of 1,000 mD) cause a salinity increase in the uppermost Stuttgart Formation by at least 0.17 % (290 mg/kg) after 20 years. Closed boundaries in the lower aquifers and only one major fault open allowing for flow along the fault and upwards show less salinity changes in the uppermost aquifers. Also fault DZ permeability has been found to have only a minor influence on salinization and can be neglected. With a fault DZ permeability of 100 mD, salinity increases in the Stuttgart Formation by 0.02 % (34 mg/kg), with a fault DZ permeability of 1,000 mD by 0.04 % (75 mg/kg) and by 0.06 % (96 mg/kg) with a fault DZ permeability of 10,000 mD after 20 years of CO_2 injection. However, the salinity within the fault itself increases stronger, by 1.7 % (3,840 mg/kg), if it is the only open fault allowing for upward directed flow or flow parallel to the fault zone (combined conduit-barrier; no cross-flow) compared to an increase of 1.2 % (2,700 mg/kg) when all faults act as conduits for cross-flow and upward directed flow. Therefore, the salinity also increases stronger in the vicinity of the faults in the uppermost formation by up to 50,000 mg/kg if only one fault allows for upward directed flow or flow parallel to the fault zone (combined conduit-barrier; no cross-flow) and a little less by up to 47,000 mg/kg but with a greater local expansion when all faults act as conduits for cross-flow and upward directed flow. However, subsequent dilution leads to the comparably low average salinity increase.

In general, it can be concluded that only the overpressure within the storage complex governs brine migration, whereas unexpectedly the DZ permeability of the fault zone does not significantly influence salinization of upper aquifers. The shallower one gets in the multi-barrier system the lower are pressure increases and salinization by orders of magnitude. Nevertheless, under the given circumstances, freshwater salinization is small and taking into account that two further caprocks also seal the Stuttgart Formation with a total thickness of 200 m brine migration is unlikely under the tested constraints. Nevertheless, faults were assumed permeable throughout the entire length, which presumably is an over-simplification of nature and is therefore probably not as realistic as more heterogeneous scenarios. However, definitive internal structures of fault zones are not known and cannot be detected. Consequently, we need to study a range of parameters between certain end-members and due to that reason, we started here with the implementation of one possible fault-end-member. Further research is underway to extend the assumptions made by the implementation of heterogeneous fault zones with spatial variations in porosity and permeability and related non-uniform architecture. A few transmissible vertical pipes within mostly impermeable fault zones (representing a certain heterogeneous structure), connecting the different permeable formations might for instance result in an earlier and higher salinization of the upper aquifers than the overall transmissible case and will therefore be subject of further investigations. To investigate the evolution of brine migration after the end of injection and the possibility of a brine-backflow from the upper aquifers further simulations including a post-injection phase shall also be performed in the future. An increased injection rate as well as longer injection times is also recommended to be taken into account for further investigations.

Finally, the next studies will also aim at coupling the model discussed here with a shallow multi-layer aquifer model that includes freshwater to investigate processes triggering and mitigating brine migration at a regional- to basin-scale. Therefore, the reservoir model as described in this study will be extended to assess large-scale brine displacement and potential freshwater salinization especially with regard to high-risk areas such as erosional thinouts in the Rupelian clay.

3 EFFECTIVE DAMAGE ZONE VOLUME OF FAULT ZONES AND INITIAL SALINITY DISTRIBUTION DETERMINE INTENSITY OF SHALLOW AQUIFER SALINIZATION IN GEOLOGICAL UNDERGROUND UTILIZATION

ABSTRACT

Injection of fluids into deep saline aquifers causes a pore pressure increase in the storage formation, and thus displacement of resident brines. Via hydraulically conductive faults, brine may migrate upwards into shallower aquifers, and lead to unwanted salinization of potable groundwater resources. In the present study, we investigated different scenarios for a prospective storage site close to the city of Beeskow in the Northeast German Basin by using a 3D regional scale model ($100 \text{ km} \times 100 \text{ km} \times 1.34 \text{ km}$) that includes four ambient fault zones. The focus was on assessing the impact of fault length and the effect of an overlying secondary reservoir as well as model boundary conditions on the potential salinization of shallow groundwater resources. We employed numerical simulations of brine injection as a representative fluid using the simulator TOUGH2-MP.

Our simulation results demonstrate that pressure build-up within the reservoir determines the intensity and duration of fluid flow through the faults, and hence salinization of shallower aquifers. Application of different boundary conditions proved that these have a crucial impact on reservoir fluid displacement. If reservoir boundaries are closed, the fluid migrated upwards into the shallow aquifer, corresponds to the overall injected fluid mass. In that case, a short hydraulically conductive fault length and the presence of an overlying secondary reservoir leads only to retardation in brine displacement up to a factor of five and three, respectively. If the reservoir boundaries are open, salinization is considerably reduced: In the presence of a secondary reservoir, 33 % of equivalent brine mass migrates into the shallow aquifer, if all four faults are hydraulically open over their entire length, whereas the displaced equivalent brine mass is only 12 % for a single fault of two kilometres length. Taking into account the considered geological boundary conditions, the brine originates in maximum from the upper 4 m to 298 m of the investigated faults. Hence, the initial salt-freshwater interface present in the fault is of high relevance for the resulting shallow aquifer salinization.

The present study demonstrates that the existence of hydraulically conductive faults is not necessarily an exclusion criterion for potential injection sites, because salinization of shallower aquifers strongly depends on initial salinity distribution, location of hydraulically conductive faults and their length as well as geological boundary conditions. These constraints are location specific, and need to be explored thoroughly in advance of any field activity. They provide the basis for scenario analyses and a reliable risk assessment.

3.1 INTRODUCTION

Carbon Capture and Storage (CCS) can contribute to the reduction of global anthropogenic carbon dioxide emissions. Different geological underground formations have been suggested as target storage sites, whereby deep saline aquifers provide the worldwide largest storage potential as part of the earth's widely distributed sedimentary basins (IPCC, 2005). Due to their extent and storage capacity, shallow aquifers in sedimentary basins comprise also considerable freshwater resources, which are of great importance for regional water supply. However, brine displacement due to the elevated pore pressure in the storage formation is one potential risk of CO₂ storage in saline aquifers. Saline fluids could reach shallower freshwater aquifers through different migration pathways, and significantly impair groundwater quality. Especially fault zones are of particular importance, as they form potential weakness zones within the host rock, and might act as large-scale permeable conduits penetrating several caprocks.

Displacement of brine and potential freshwater salinization as a result of CO₂ storage has been investigated in several studies. Table 3 summarizes the initial conditions and essential results of numerical simulations concerning this issue. The models applied are either synthetic (OLDENBURG AND RINALDI, 2011; BIRKHOLZER ET AL., 2011; BIRKHOLZER ET AL., 2009) or refer to a certain study area (TILLNER ET AL., 2013; ZOUH ET AL., 2010; YAMAMOTO ET AL., 2009; NICOT, 2008). Several studies examine pressure perturbation and resulting brine migration in a multi-barrier system without considering vertical conduits. It was shown that pressure build-up can be observed in a distance of more than 100 km from the injection zone (BIRKHOLZER ET AL., 2009). Thereby, the choice of initial conditions and petrophysical parameters have a crucial impact on the pressure development, as demonstrated by two independent studies considering industrial-scale CO₂ injection in the Illinois Basin (PERSON ET AL., 2010; ZHOU ET AL., 2010). After PERSON ET AL. (2010), the pressure perturbation is limited to a distance of about 25 km from the injection location for a total injection rate of 80 Mt CO₂/yr, whereas ZHOU ET AL. (2010) simulated a pressure build-up as far as 300 km from the injection area (100 Mt CO₂/yr).

However, upward brine migration only occurs if pressure perturbation in the reservoir is large enough to overcome the weight of the fluid column in a vertical conduit. It further depends on magnitude of pressure increase, and whether brine is allowed to spread laterally in the upper aquifer, if a steady-state is reached or continuous flow develops (OLDENBURG UND RINALDI, 2011; BIRKHOLZER ET AL., 2011). Especially faults can represent vertical conduits, which may have an essential influence on groundwater flow and brine migration due to their extent and distribution in the Earth's upper crust. Nevertheless, a meaningful implementation of complex geological structures into a sufficiently discretised model grid is very difficult, especially at regional scale. TILLNER ET AL. (2013) investigated the influence of permeable faults on brine displacement referring to a real study area. The authors simulated upward brine migration through complex fault systems depending on reservoir compartmentalisation and fault permeability, whereby faults were implemented by the virtual element approach (NAKATEN ET AL., 2013). The results of TILLNER ET AL. (2013) indicate that the degree of pressurization is the driving mechanism for brine migration, while permeability of fault zones does not influence salinization of shallower aquifers significantly.

Table 3: Summary of numerical simulations of brine migration resulting from CO₂ injection

Authors	Study area and model extend	Reservoir boundaries	Simulator	Injection rate and duration	Injected fluid	Objectives	Results
Birkholzer et al., 2009	<ul style="list-style-type: none"> synthetic 125,000 km² (radial symmetric) 	open	TOUGH2/ECO2N	1.52 Mt/yr over 30 years	CO ₂	Pressure build-up and brine migration in the reservoir and through low permeable caprocks	<ul style="list-style-type: none"> Considerable pressure build-up in a distance of > 100 km from injection zone Vertical brine migration through a sequence of seals extremely unlikely
Birkholzer et al., 2011	<ul style="list-style-type: none"> synthetic 12 km² (radial symmetric) 	closed	TOUGH2/EOS7	Simulated by pressure build-up	-	Brine migration up a leaking wellbore	<ul style="list-style-type: none"> Continuous flow only occurs if pressure perturbation in the reservoir is large enough to overcome the increased weight of the fluid column
Nicot, 2008	<ul style="list-style-type: none"> Gulf Coast, USA 80,000 km² 	closed	MODFLOW96	50 Mt/yr and 250 Mt/yr over 50 years	Water	Pressure build-up and migration of brine in the reservoir and through low permeable caprocks	<ul style="list-style-type: none"> Average water table rise is in the same order of magnitude as seasonal and inter-annual variations
Oldenburg and Rinaldi, 2011	<ul style="list-style-type: none"> synthetic 1 km (2D) 	closed	TOUGH2/EOS7	Simulated by pressure build-up	-	Brine displacement in shallower aquifers through a vertical conduit (borehole or fault)	<ul style="list-style-type: none"> Depending on brine density and pressure gradient fluid migrates upward until a new static steady-state equilibrium is reached or a sustained flow develops, if the brine is allowed to spread laterally.
Tillner et al., 2013	<ul style="list-style-type: none"> North German Basin 1,764 km² 	closed and open	TOUGH2-MP/ ECO2N	1.7 Mt/yr over 20 years	CO ₂	Brine migration through faults dependent on reservoir compartmentalisation and fault permeability	<ul style="list-style-type: none"> Degree of pressurization is the driving mechanism for brine migration Permeability of fault zones does not influence salinization of shallower aquifers significantly

Authors	Study area and model extend	Reservoir boundaries	Simulator	Injection rate and duration	Injected fluid	Objectives	Results
Yamamoto et al., 2009	<ul style="list-style-type: none"> • Bay of Tokyo, Japan • 4,200 km² 	open	TOUGH2-MP/ECO2N	10 Mt/yr over 100 years	CO ₂	Pressure build-up and brine migration in the reservoir and through low permeable caprocks	<ul style="list-style-type: none"> • Pressure build-up of a few bars can occur in the shallow confined aquifers over extensive regions
Zhou et al., 2010	<ul style="list-style-type: none"> • Illinois basin, USA • 241,000 km² 	open	TOUGH2/ECO2N	100 Mt/yr over 50 years	CO ₂	Pressure build-up and CO ₂ /brine migration in the reservoir and through low permeable caprocks	<ul style="list-style-type: none"> • Pressure build-up of 1 bar and 0.1 bar can be expected as far as 150 km and 300 km from the injection area, respectively • pressure increase of 35 bar at injection does not affect caprock integrity
This study	<ul style="list-style-type: none"> • North German Basin • 10,000 km² 	closed and open	TOUGH2-MP/ECO2N	1.7 Mt/yr over 20 years	Water	Brine migration through fault zones depending on different geological conditions	<ul style="list-style-type: none"> • Boundary conditions, fault length and existence of an overlying secondary reservoir affect pressure development in the reservoir and thereby freshwater salinization

Their investigations focused on the prospective storage site Beeskow-Birkholz (in the following only referred to as Beeskow) in Northeast Germany, which is also considered in this work.

Here, we present a regional scale 3D model with a simplified geometry, neglecting topographic variations while the four considered fault zones are implemented with their complex arrangement and curvature. Hence, the presumed simplifications should avoid numerical artefacts, and serve for improved comprehensibility of the relevant processes. In different leakage scenarios the effect of fault lengths, boundary conditions, and the presence of an overlying secondary reservoir on upward brine displacement as a result of fluid injection were assessed. The goal of this study was to deepen the general understanding of the underlying processes, as well as to characterize the impact of all investigated parameters to obtain site-specific findings on potential freshwater salinization.

3.2 STUDY AREA

The prospective CO₂ storage site is located 80 km southeast of Berlin in the Northeast German Basin (NEGGB), which is part of the Southern Permian Basin (Figure 20a). According to the estimated storage capacity, it was planned to inject 34 Mt CO₂ over a period of 20 years (1.7 Mt CO₂/yr) into a Mesozoic anticline structure at Beeskow (VATTENFALL, 2009). Several sandstone formations of the Middle Buntsandstein, such as the Volpriehausen, Detfurth, and Hardegsen formations form potential reservoir rocks (Figure 21a). They consist of basal sandstones and an alternating sequence of mudstones with sandy and silty layers (VATTENFALL, 2010). The Detfurth Formation is characterized by the highest effective thickness of 23 m, and was therefore chosen as target storage horizon for CO₂ injection. Porous and fractured sediments of the lower Muschelkalk (Middle Triassic) represent a secondary suitable reservoir. A multi-barrier system of different caprocks from the Upper Buntsandstein, the Middle and Upper Muschelkalk, as well as the Lower Keuper seals the Detfurth Formation and the overlying secondary reservoirs. The Rupelian clay (Oligocene, Upper Tertiary) forms a regional barrier between freshwater-bearing glacial sediments (Upper Tertiary and Quaternary) and the underlying saline aquifers. It is located at a depth between 150 m and 200 m (STACKEBRANDT, 1998). Basal sandstones of the Rupelian with a thickness varying between 2.5 m and 30 m are widespread, and mark the beginning of saltwater-bearing aquifers (GRUBE ET AL., 2000). During the latest three Pleistocene glacial phases, advances of the Scandinavian ice sheets locally formed deep-reaching erosion channels within the Rupelian clay. Hence, a hydraulic connection between deep saline aquifers and freshwater-bearing sediments exists in some parts of the area. Depending on the pressure potential, saline water could rise and mix with potable groundwater resources. As shown by KEMPKA ET AL. (2015), salt concentrations in the Quaternary deposits and fillings of the erosion channels can locally be larger than 10 g/kg.

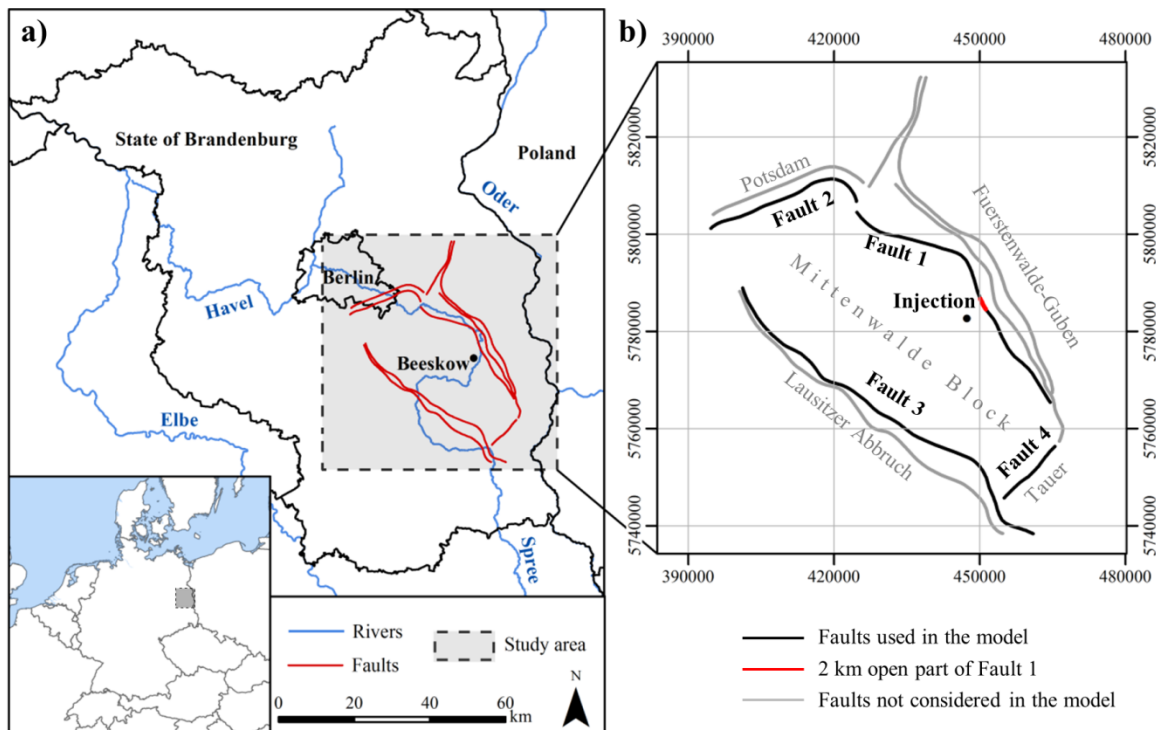


Figure 20: (a) Dashed rectangle indicates the location of the study area in the State of Brandenburg (Germany), while red lines illustrate the present fault systems. (b) Only the inner faults (black lines), facing to the injection well, were implemented to represent the entire fault zone. Axes show UTM-coordinates (WGS84/UTM zone 33N). Rivers and the outline of the states of Brandenburg and Berlin were derived from TILLNER ET AL. (2013).

The fault system of the study area consists of four regional fault zones comprising several individual faults. It divides the sedimentary cover of the study area into a regional block structure (Mittenwalde Block; Figure 20b). The Lausitzer Abbruch and the Fuerstenwalde-Guben fault zones with NW-SE orientation, as well as the Tauer and the Potsdam fault zones striking NE-SW, enclose this compartment. All faults are normal faults with a steep inclination (between 67.8° and 74.3° in average). However, the Fuerstenwalde-Guben fault zone consists of several individual faults also characterized by reverse components of dip-slip. It has a total length of 120 km, and is characterized by an offset of a few hundred metres (HOTZAN UND VOSS, 2013). The Lausitzer Abbruch fault zone dips NE, and shows displacements up to 1,000 m (BEUTLER AND STACKEBRANDT, 2012). This complex system was formed during the Variscan orogeny, whereby many faults were reactivated during the Alpine orogeny (STACKEBRANDT, 1998).

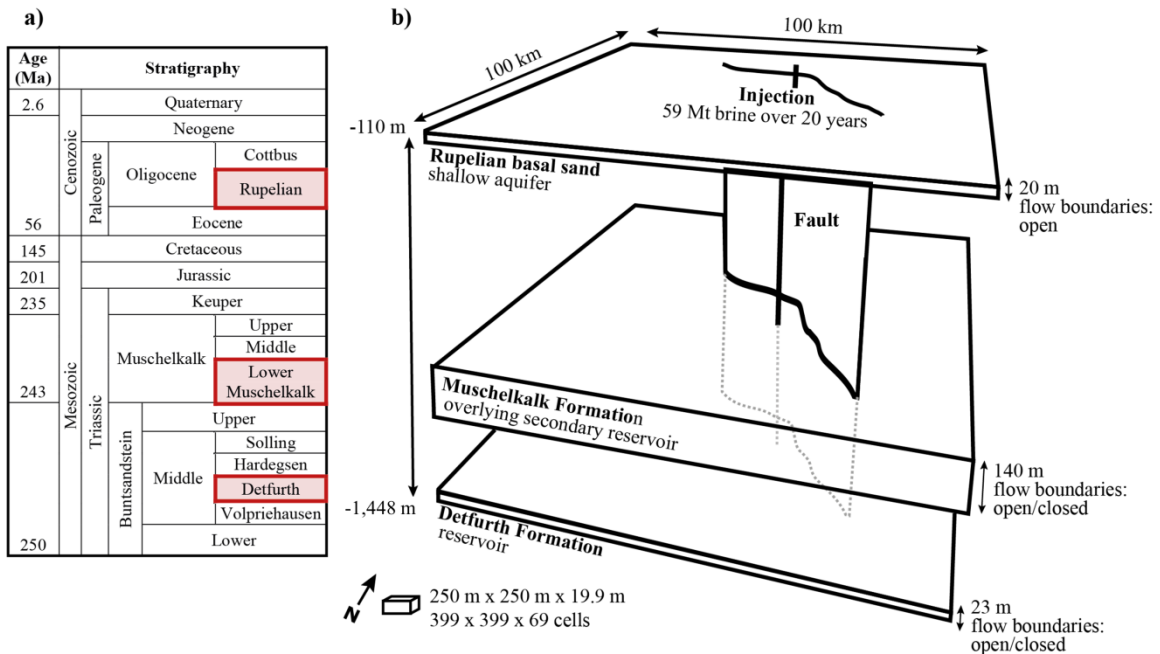


Figure 21: (a) Stratigraphy of the study area with the active model layers highlighted in red. (b) The geological 3D model with simplified topography comprises up to three layers.

3.3 GEOLOGICAL MODEL

We used the Petrel software package (SCHLUMBERGER, 2011) for the 3D geological model construction and the subsequent gridding process, and the reservoir simulator TOUGH2-MP/ECO2N for 3D multi-component flow simulations (ZHANG ET AL., 2008; PRUESS, 2005B). All simulations were conducted on a high performance computing system with 256 cores. Finally, results were imported back into Petrel for visualization purposes.

3.3.1 SETUP

The implementation of the 3D geological model refers to the structural and geological characteristics of the study area as described above. It has a horizontal extent of 100 km × 100 km and a vertical thickness of 1,340 m. Figure 21b shows the geological model with a regular lateral grid resolution of 250 m × 250 m. The vertical discretisation depends on the different model layers, and ranges between 10 m and 19.9 m (Table 4). The model consists of up to three layers: the Rupelian basal sands as the uppermost shallow aquifer, the Muschelkalk Formation as an overlying secondary reservoir and the Detfurth Formation as lowermost reservoir. The Rupelian basal sands are 20 m thick and located at a depth of 110 m (GRUBE ET AL., 2000). The Lower Muschelkalk Formation is at 1,025 m depth and has a thickness of 140 m, while the reservoir is at 1,425 m depth with a thickness of 23 m (TILLNER ET AL., 2013). The model is limited to the saline groundwater complex up to the Rupelian clay (situated above the Rupelian basal sands and not considered in the present model) as regional seal between salt and freshwater.

Table 4: Vertical grid discretization, depth and hydraulic parameters for the active geological units.

Unit	k (mD)	Φ (%)	thickness (m)	depth (m)	element layers	vertical resolution (m)
Rupelian basal sands	1,000	20	20	-110 to -130	2	10
Muschelkalk Formation	200	20	140	-1,025 to -1,165	7	19.9
Detfurth Formation	400	17	23	-1,425 to -1,448	2	11.5
Faults	700	18.5			50	19.9

In a previous study, KÜHN ET AL. (2011) investigated the influence of caprock permeabilities on shallower aquifer salinization at the prospective storage site Beeskow. Their results showed that for caprock permeabilities equal or lower than 10^{-17} m^2 no increase in salt concentration in formations above the reservoir has to be expected. In the present study, we assumed that the caprocks have lower permeabilities and therefore defined them as impermeable for fluid flow in all simulations, so that only the faults provide a hydraulic connection between the shallow aquifer and the reservoir. Thus, the elements of the faults as well as the different reservoir layers were “active” in our simulations, whereby the elements representing the caprocks were not considered. Depending on the different scenarios performed (varying fault length; with or without overlying secondary reservoir), the model consists of 635,508 to 1,811,473 active elements.

Within our model only the inner faults, which enclose the Mittenwalde Block were implemented as a representation of the entire fault zone (Figure 20b). Thereby, fault related parameters were assigned to the elements located at the respective vertical fault plane. The fault element width of 250 m corresponds to the overall lateral grid resolution. This element width is relatively large but still realistic, since all regional fault zones consist of several individual faults and show considerable displacements. In general, fault offset is linked to the width of the damage zone (WIBBERLEY ET AL., 2008; FAULKNER ET AL. 2010; MITCHEL AND FAULKNER, 2009). For example, faults with displacements between 10 m and 1,000 m can have damage zone widths between tens and hundreds of metres. However, there exists no simple relationship, since the width of the damage zone is highly dependent on lithology, pressure, temperature, and strain rate during shear and potentially tensile deformation (SHIPTON ET AL., 2006). Due to the relatively steep inclination of all faults and to maintain maximum grid regularity, the dip angle was neglected in the present model and all faults were assumed to be strictly vertical. In the following, the Fuerstenwalde-Guben fault zone is addressed as Fault 1. The Potsdam, the Lausitzer Abbruch and the Tauer fault zones are referred to as Faults 2, 3 and 4, respectively (Figure 20b).

The applied geological model was considered in the numerical simulations by simplifying the original topography of the formation tops and bases to focus the analysis on clearly identifiable effects of fault fluid flow.

3.3.2 PARAMETERIZATION

All lithological units were parameterized according to TILLNER ET AL. (2013) and VATTFALL (2009), with values derived from borehole data and literature and modelled as homogenous and isotropic. The Detfurth Formation has a permeability of 400 mD, while the overlying secondary reservoir (Muschelkalk Formation) is characterized by a permeability of 200 mD (Table 4). Porosity and permeability of the Rupelian basal sands were chosen according to TESCH ET AL. (1987). Fault permeability was assumed higher than that of the host rock, because of fault-parallel permeability enhancement of the damage zone due to the presence of a fracture network (CAINE ET AL., 1996; JOURDE ET AL., 2002). Thus, hydraulic properties of the faults were chosen to be in between of those of the Rupelian basal sands and the Detfurth Formation to allow for analysis of different time-dependent flow patterns (Table 4). Because faults have a smaller offset at their boundaries, and consequently a less distinct damage zone, it was presumed that permeability declines in these areas. This was implemented into the model by using permeability multipliers in the respective elements. The permeability declines linearly towards the ends of the fault, applied to the first 15 % of its length. A lateral barrier for groundwater flow due to a low permeable fault core was not considered.

3.3.3 INITIAL AND BOUNDARY CONDITIONS

In all investigated scenarios, Dirichlet boundary conditions were applied to the Rupelian basal sands. These were implemented by volume multipliers of 10^{10} at the boundary elements of each layer, so that the aquifer has quasi-infinite extension. The boundaries of the Detfurth and the Muschelkalk formations are either open (boundary element volume multiplication by 10^5) or closed (no boundary element volume multiplication), depending on the investigated scenario. For the temperature distribution, a constant geothermal gradient of 30 °C/km was used, starting from 15 °C at the model top. All simulations were performed at isothermal conditions resulting in a constant initial temperature in time and space. Studies suggest that the salinity in the Rupelian basal sands is between 0.8 % and 3.8 % (TESCH ET AL., 1987), and increases with depth until full saturation in the Triassic layers (HANNEMANN AND SCHIRRMEISTER, 1998). However, in the present models the transition between freshwater and brine was defined to be abrupt. Here, the Rupelian basal sands contain freshwater (zero salinity), whereas a salinity of 25 % was assigned to all underlying units. These conditions were chosen, as they lead to the maximum possible salinization in the uppermost aquifer, and thus represent the most unfavourable scenario for shallow aquifers under the given assumptions. Furthermore, a sharp salt-freshwater interface serves as a tracer boundary to visualize the distribution of saline water within the shallow aquifer. All simulations were performed at hydrostatic pressure conditions. Considering the density of brine, pressure at the top of the Detfurth Formation at 1,425 m depth is approximately 165 bar.

At the Beeskow storage site, it was planned to inject 34 Mt of CO₂ over a time span of 20 years into the Mesozoic anticline structure (TILLNER ET AL., 2013). Instead of CO₂, the equivalent volume of brine was injected into the storage formation in the present study, because we assume that there is no substantial impact on resulting brine migration whether CO₂ or water is injected. Furthermore, with such a model we investigate injection-related brine displacement, and keep the findings transferable to various other types of subsurface storage. Considering a reservoir

pressure of approximately 165 bar at the top of the Detfurth Formation and a temperature of 58 °C, the resulting CO₂ density is 668.5 kg/m³ (SPAN AND WAGNER, 1996). Brine density is 1,175 kg/m³, taking into account the salinity of 25 %. Thus, a volume equivalent mass of 59.76 Mt brine was injected into the storage formation, corresponding to a rate of 94.6 kg/s.

Fluid compressibility is considered in TOUGH2-MP/ECO2N by the use of its density changes, while brine densities are calculated for each element during the simulation. Pore compressibility causes a higher storage coefficient in the formations when pressure increases. Since our simulations should show the greatest possible effect on brine displacement, pore compressibility was neglected. Diffusion was also not considered, because it has an irrelevant effect within our model due to the chosen grid discretization and the long timespan it would require to observe substantial effects. If one takes into account a lateral element size of 250 m × 250 m, a fluid diffusion coefficient of 2×10^{-9} m²/s and a sharp freshwater-saltwater interface in the fault, it would take about 1 million years for the salinity front to propagate into a neighbouring element.

3.4 SET OF SCENARIOS

In total, 13 scenarios were selected to investigate the conditions for upward brine flow through the faults. Besides fault lengths, boundary conditions were varied and a potentially overlying secondary reservoir was considered. Scenarios are identified by the following abbreviations:

$$\text{Scenario} = F_n^l B_{O/C} SR_k$$

Where F denotes fault with the coefficients l indicating the total fault length and n the number of active faults. Further, the lateral boundary conditions (B) of both reservoirs can be either open (O) or closed (C). SR denotes that an overlying secondary reservoir exists and k specifies the permeability of that reservoir. All simulated scenarios with their varying initial and boundary conditions are summarized in Table 5.

The base cases consist of two layers, while three different fault lengths were considered. Either all four fault zones with a total length of 193 km were assumed to be permeable, or Fault 1 was defined to be hydraulically conductive with a length of 60 km. In the third case, only a length of 2 kilometres in the central part of Fault 1 was presumed to be open for fluid flow (Figure 20b). All other parts of the faults were supposed to be impermeable, and therefore consist of inactive elements. These settings represent three different baseline examples, which should distinctly show differences for a better understanding of the relevant processes, and particularly define the possible spectrum of brine displacement. Further scenarios considered the three different fault lengths described above as well as the Muschelkalk Formation as an overlying secondary reservoir, since multi-barrier systems should preferably be chosen as potential CO₂ injection sites to minimize the risk of leakage. For all these cases, scenarios with both open and closed reservoir boundaries were examined to illustrate the entire range of a potential freshwater salinization depending on the given geological constraints.

Table 5: Overview about all calculated scenarios, their mean reservoir pressures at the end of injection as well as depth of origin and distribution of the brine displaced into the shallow aquifer.

	Scenario	Duration of mass flow into the shallow aquifer*	Mean Δp in the Detfurth Formation (bar) [†]	Lateral distance affected by salinity increase (km) [#]		Upper part of the fault, where brine originates from (m) [#]	
				Max.	Min.	Max.	Min.
Closed reservoir boundaries	2 layers	$F_1^{2km} B_C$	330	19.4	6.1	-	298
		$F_1^{60km} B_C$	115	8.2	2.4	1.5	32
		$F_{1-4}^{193km} B_C$	66	4.6	2.4	1.2	30
	3 layers	$F_1^{2km} B_C SR_{200mD}$	1,050	15.9	6.1	-	265
		$F_1^{60km} B_C SR_{200mD}$	390	5.2	2.4	2	20
		$F_{1-4}^{193km} B_C SR_{200mD}$	225	2.9	2	1.5	19
Open reservoir boundaries	2 layers	$F_1^{2km} B_O$	31	3.5	4	-	108
		$F_1^{60km} B_O$	31	2.2	2.2	0.95	29
		$F_{1-4}^{193km} B_O$	42	2.1	2.2	0.95	28
	3 layers	$F_1^{2km} B_O SR_{200mD}$	31	3.2	2.8	-	59
		$F_1^{60km} B_O SR_{200mD}$	40	1.6	1.7	0.95	17
		$F_{1-4}^{193km} B_O SR_{200mD}$	45	1.3	1.7	0.95	17
		$F_{1-4}^{193km} B_O SR_{2000mD}$	23	0.6	1.1	0.35	4
							> 1

*total mass flow > 0.1 kg s⁻¹

[†]t = 20 years

[#]t = end of mass flow

Different fault permeabilities were not considered because previous simulations carried out with closed reservoir boundaries have primarily shown only a temporal effect of fault permeability without any significant change in salinization. The mass of brine displaced into the shallow aquifer was the same in any case irrespective whether the fault permeability was higher, equal or lower than the permeability of the secondary reservoir (Figure 22). A retardation in mass flow into the shallow aquifer by a factor of two was observed only for a fault permeability of 10 mD compared to the base case (700 mD), if all four faults were assumed to be hydraulically conductive. However, one simulation was applied in the present study to investigate the impact of permeability differences between reservoir and faults on upward brine migration taking into account open boundary conditions. In Scenario $F_{1-4}^{193km} B_O SR_{200mD}$, the permeability of the Muschelkalk Formation was increased by one order of magnitude to 2,000 mD, so that in contrast to all other scenarios, the permeability of the secondary reservoir is higher than the fault permeability.

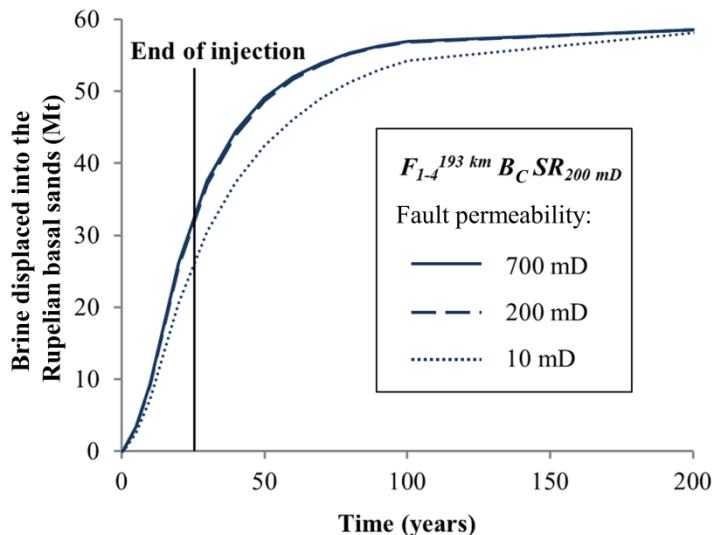


Figure 22: Temporal evolution of brine displacement into the Rupelian basal sands, when all four faults are open, a secondary overlying reservoir exists and reservoir boundaries are closed. The brine mass displaced into the shallow aquifer is equal for all scenarios after 200 years, irrespective whether the fault permeability is higher (solid line), equal (dashed line) or lower (dotted line) to the permeability of the secondary reservoir. Lower fault permeabilities lead to retardation in mass flow only.

3.5 RESULTS

3.5.1 GENERAL OUTCOMES

Some general outcomes are valid for all simulations. These results are presented first for a better understanding of the system. Figure 23 shows the mass flow in kg/s as an example for Scenario $F_{1-4}^{193km} B_O$ after 20 years, corresponding to the end of the injection period. At this time, reservoir pressures have reached their maximum, and thus effects on upward brine flow are most noticeable. An injection-related pattern in pressure distribution and fluid flow can be observed. Starting from the injection location, brine is displaced radially within the reservoir,

and hence predominantly into parts of the faults close to the point of injection. Along the undulating Fault 3, which is located approximately 30 km away from the injection well, mass flow into parts facing towards the injection can be more than two times higher than into parts of the fault not facing the injection well (Figure 23). However, the opposite case is noticeable in the shallow aquifer, where flow out of the fault into parts of the aquifer facing away from the injection (lower pressures) is greater than into parts facing it (higher pressures). Hence, a redistribution of fluid flow occurs along the fault. Moreover, an asymmetric flow out of Fault 1 was observed within the Rupelian basal sands. Again, a higher mass flow out of the fault occurs into parts of the aquifer not facing the injection well since brine is displaced away from the point of highest pressurization. Consequently, salinities are higher normal to the fault in areas further away from the injection. This flow behaviour is valid for all scenarios and varies only in its intensity depending on pressure build-up and reduction.

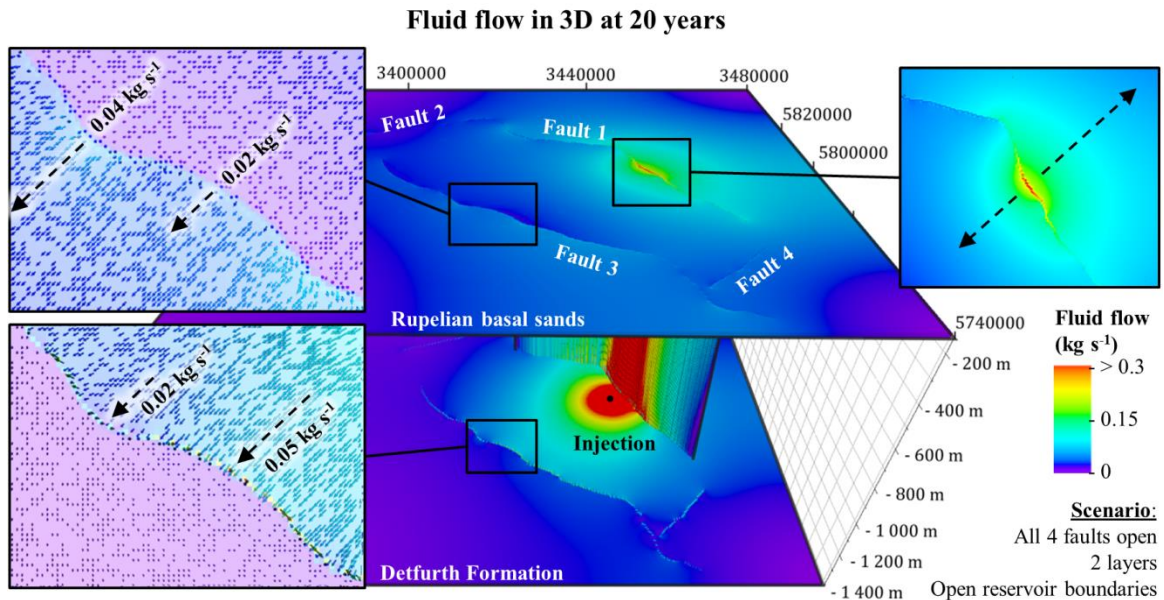


Figure 23: An injection-related pattern in fluid flow, as illustrated for Scenario $F_{1-4}^{193\text{km}} B_0$, is observed in all simulations. Within the reservoir, brine is displaced predominantly into parts of the faults lying closer to the injection well. It is the opposite in the shallow aquifer, where flow out of the fault is greater into parts not facing towards the injection.

Duration and intensity of fluid flow determines the spatial distribution of displaced saltwater. Maximum mass flow was observed along Fault 1 close to the injection decreasing towards the lateral boundaries of the fault. This pattern is reflected in the salinization of the freshwater aquifer, as shown in Figure 24a as an example for Scenario $F_{1-4}^{193\text{km}} B_C$. A maximum salinity of 23 % is reached within the lower element layer of the shallow aquifer at the end of the injection period, whereas salinity varies only by 5 % to 10 % at the fault edges. Brine migrates upwards through the fault as a result of the injection, and then spreads laterally within the Rupelian basal sands (Figure 24b). Salinity levels are generally highest within the lower element layer, indicating that the denser saline water preferably spreads along the base of the aquifer. For the given Scenario $F_{1-4}^{193\text{km}} B_C$, the saltwater plume width in the Rupelian basal sands reaches a maximum

of 2.4 km normal to the central part of Fault 1 and 1.2 km normal to the fault ends (Table 5). For the determination of the lateral distance affected by salinization, only salinities, which exceed 0.05 %, were considered. Due to the reduced brine displacement after the injection stop, a downward flow was observed. The more dense saline water accumulates at the base of the shallow aquifer. Moreover, a slight backflow into the fault occurs due to the increased weight of the water column as a result of the vertical brine displacement. Consequently, the salinity at the top element of the fault decreases by 1.5 % to 23.5 % after a simulated time of 400 years (Figure 24b), and the mass of brine within the fault slightly decreases due to the higher amount of freshwater, what can be observed in the relative mass change within the fault.

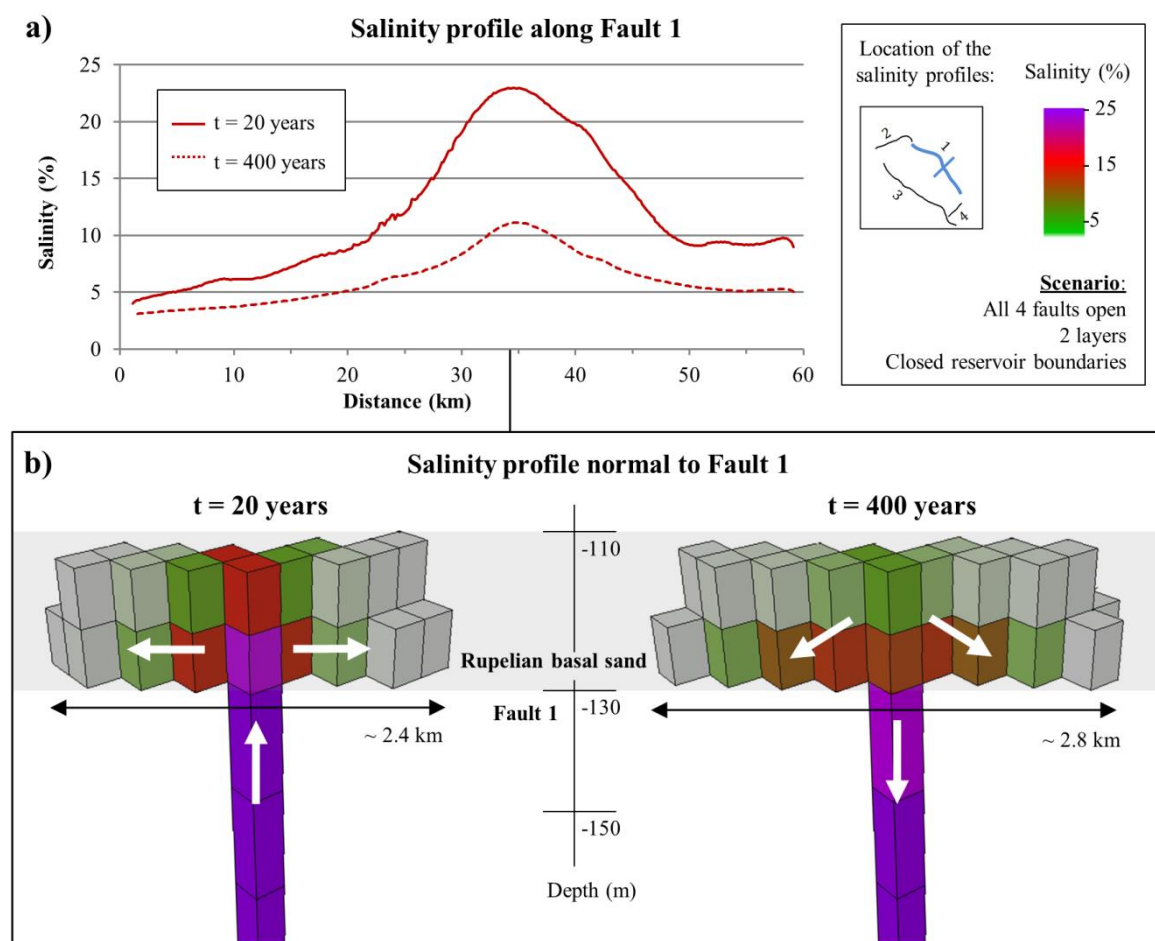


Figure 24: (a) Profile along Fault 1 ($F_{1-4}^{193\text{km}} B_C$) shows highest salinities near to the injection well. A decrease in salinization due to a downward flow is observed for the time after the injection period. (b) Cross section normal to Fault 1 illustrates the propagation of the saltwater plume (salinities $> 0.05 \%$), while higher salinities can be observed within the lower element layer. White arrows illustrate schematically the direction of the fluid flow at 20 years and 400 years.

Moreover, the maximum origin depth of the brine displaced into the shallow aquifer was estimated by calculating the fluid flow velocity at the top of the fault. The displaced brine derives from distinctly greater depths close to the injection than at the fault edges (Table 5), e.g. Scenario $F_{1-4}^{193\text{km}} B_C$ shows that close to the injection well, the displaced saline water mainly originates from the upper 30 m of the fault, whereas brine migrates from the upper 3 m at the

fault edges only. In all simulations, displaced brine leading to a salinization of the shallow aquifer is displaced only from the upper part of the fault and not originating from the reservoir.

3.5.2 FAULT LENGTH

3.5.2.1 CLOSED RESERVOIR BOUNDARIES

Figure 25a shows the distribution of the pressure increase within the upper element layer of the Detfurth Formation for different fault lengths and closed reservoir boundaries. We found the maximum pressure build-up at the injection point to be 89.9 bar for Scenario $F_1^{2km} B_C$, while pressure drops were observed in the surrounding of the faults. As expected, the highest pressure increase within the entire Detfurth Formation was encountered by implementing a hydraulic conductive fault segment with a length of two kilometres only. The pressure increases by 19.4 bar on average until the end of injection period in Scenario $F_1^{2km} B_C$, but only by 4.6 bar when all four faults are open for fluid flow (Table 5).

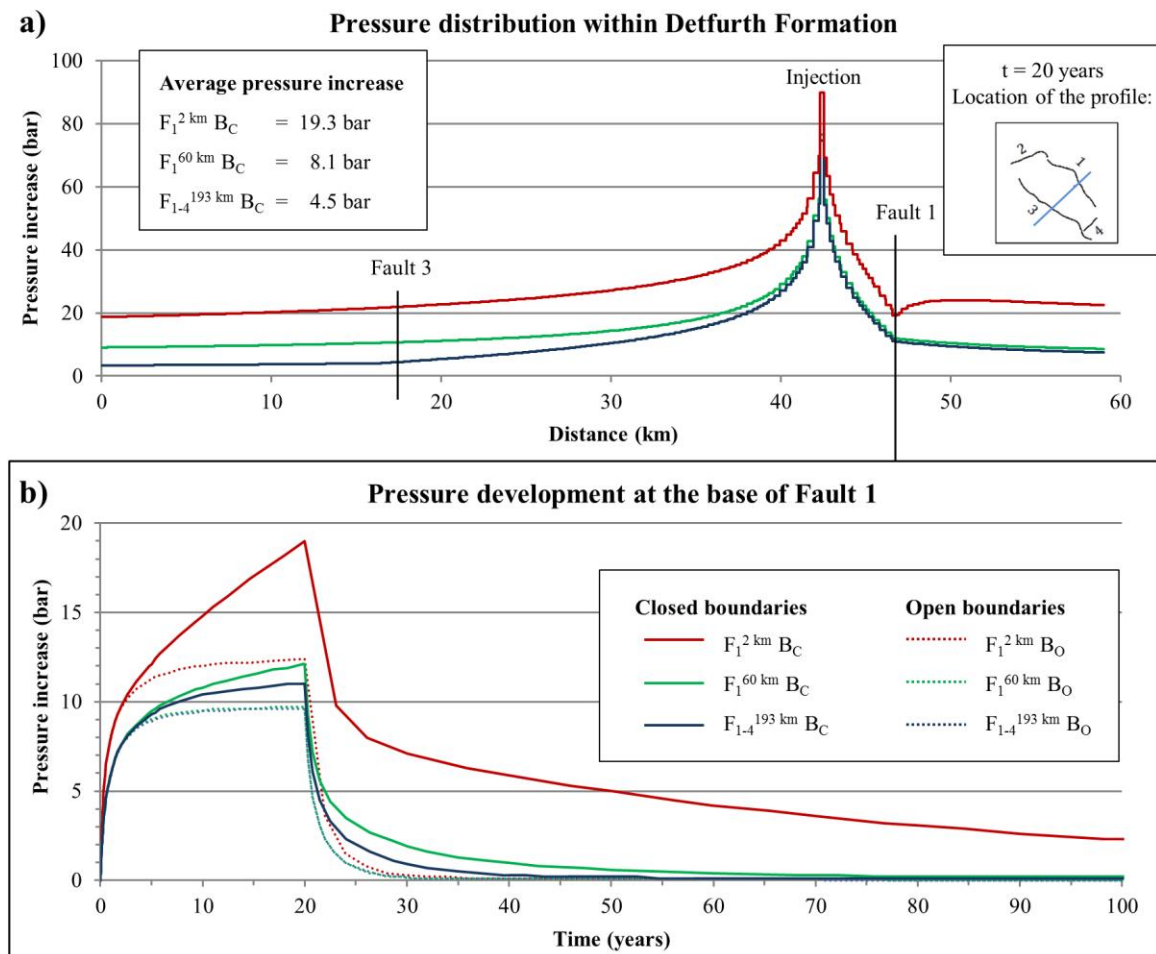


Figure 25: (a) Distribution of the pressure increase within the Detfurth Formation along the highlighted cross section significantly varies depending on the open fault length. Highest pressurization is observed for a short fault ($F_1^{2km} B_C$). (b) Pressure development at the base of Fault 1 indicates a substantially faster pressure reduction for greater fault lengths.

The differences in pressurization of ca. 1.0 bar at the base of Fault 1 between scenarios $F_1^{60\text{km}} B_C$ and $F_{1-4}^{193\text{km}} B_C$ are low compared to the significant differences in total fault length. The pressure development at the base of Fault 1 shows that pressure increases until the injection stops after 20 years (Figure 25b). In the following, the reduction of pressure is considerably faster, the greater the fault length. If all four faults are open (Scenario $F_{1-4}^{193\text{km}} B_C$), fluid flow into the shallow aquifer lasts for about 66 years, and is approximately five times faster than in Scenario $F_1^{2\text{km}} B_C$ (Table 5). For result evaluation, only a cumulative mass flow into the Rupelian basal sands above 0.1 kg/s was taken into account. To retrace and visualize the exchange of fluids between the different units, the relative mass change as a function of time was determined for the different geological units. Figure 26a illustrates that if the reservoir boundaries are closed, the mass of brine displaced into the shallow aquifer corresponds to the overall injected fluid mass. In this case, the open fault length has only a temporal effect on fluid migration.

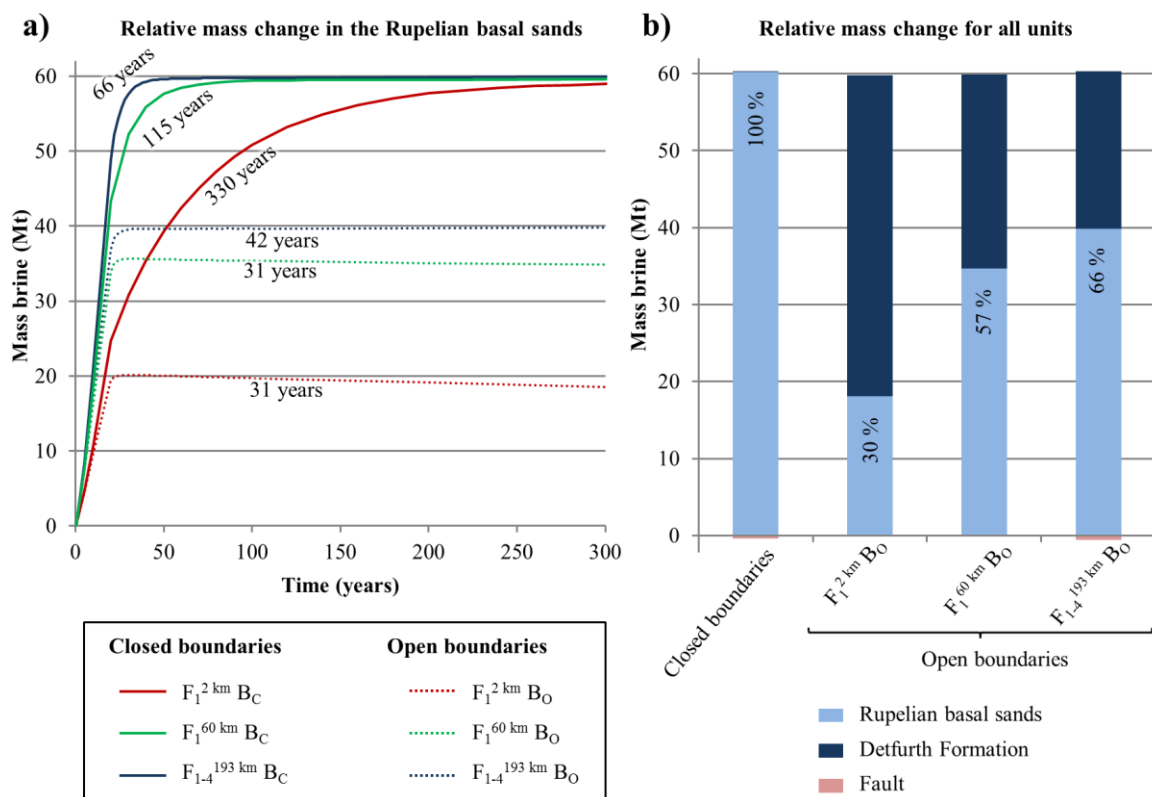


Figure 26: (a) Relative mass change in the Rupelian basal sands shows that the mass of brine displaced into the shallow aquifer corresponds to the overall injected fluid mass, if reservoir boundaries are closed. As indicated by the duration of mass flow (black numbers), only a temporal effect on fluid migration occurs. (b) Relative mass change for all lithological units after 330 years (mass flow < 0.1 kg/s for all scenarios) illustrates a considerably reduced salinization of the Rupelian basal sands for open reservoir boundaries.

A higher pressure build-up within the reservoir generally results in higher flow velocities out of the faults. Figure 27 shows the velocity profile through the lower element layer of the Rupelian basal sands. At the end of injection period, flow velocity out of the fault can be up to 29 m/yr (9.2×10^{-7} m/s) for a high pressure build-up due to a short fault length of two kilometres ($F_1^{2\text{km}} B_C$), while in scenarios $F_1^{60\text{km}} B_C$ and $F_{1-4}^{193\text{km}} B_C$ flow velocities range between 6.3 m/yr and

5.8 m/yr (1.8×10^{-7} m/s), respectively. Peaks in the velocity profile around the fault refer to the difference in fluid density between the displaced brine and residual freshwater within the aquifer. Maximum flow velocities were observed around Fault 1, which is located closest to the injection point. Further, velocity increases at the top of all other faults however, not as significantly as observed for Fault 1 (e.g. Fault 3, Figure 27a). Flow velocities reach a maximum after 20 years. Subsequent to the injection stop, pressure reduction, and lower brine displacement are accompanied by decreasing flow velocities (Figure 27b).

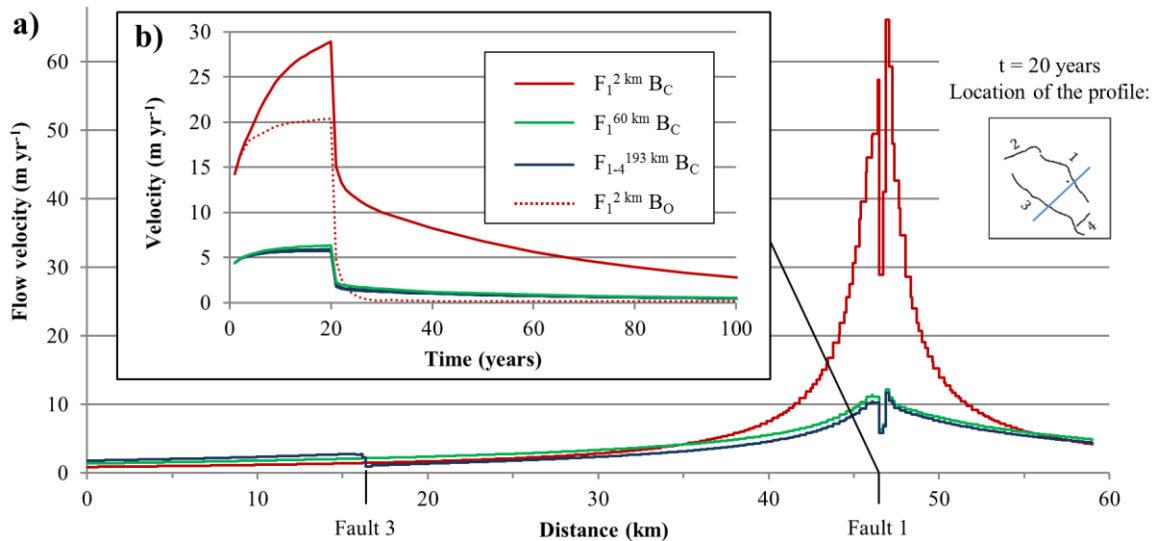


Figure 27: (a) Velocity profile within the lower element layer of the Rupelian basal sands shows highest flow velocities out of Fault 1 at the end of injection period. (b) Flow velocities out of Fault 1 increase until the end of the injection period (20 years) and decrease afterwards depending on pressure reduction of the respective scenarios.

Freshwater salinization due to displaced brine only occurs locally around the faults. Spatial brine distribution in the Rupelian basal sands reaches a maximum lateral extent of 6.1 km, if a fault of two kilometres length serves as a conductive pathway (Table 5). When Fault 1 is completely open (Scenario $F_1^{60\text{km}} B_C$), brine spreads 2.4 km in maximum close to the injection area and only 1.5 km at the fault ends. Differences between the scenarios $F_1^{60\text{km}} B_C$ and $F_{1-4}^{193\text{km}} B_C$ are low, and mainly expressed by salt concentrations rather than lateral extension. Saline water, which migrates into the Rupelian basal sands, originates only from the fault. The depth of its origin mainly depends on the fault length: in Scenario $F_1^{2\text{km}} B_C$ brine is displaced into the shallow aquifer from the upper 298 m of the fault in maximum, while in Scenario $F_{1-4}^{193\text{km}} B_C$ saline water rises only 30 m (Table 5).

3.5.2.2 OPEN RESERVOIR BOUNDARIES

If the reservoir boundaries are open, pressure build-up in the Detfurth Formation is considerably lower, while differences corresponding to the fault length still exist. The mean pressure increase within the reservoir is 2.1 bar, if all four faults are open ($F_{1-4}^{193\text{km}} B_O$), and hence only half as high as in the scenario with closed reservoir boundaries ($F_{1-4}^{193\text{km}} B_C$). In contrary to closed boundary

conditions, pressure build-up at the model boundary does not occur. A pressure increase of at least one bar was observed in a maximum distance of 58 km ($F_1^{2km} B_O$) and 50 km ($F_{1-4}^{193km} B_O$), respectively, from the injection well. After the stop of injection, the pressure within the reservoir reduces substantially faster than under the assumption of closed reservoir boundaries (Figure 25b). Hence, the duration of mass flow into the shallow aquifer is shorter for all three scenarios (Figure 26a). Depending on the open fault length, a significant flow into the shallow aquifer occurs only for 31 years ($F_1^{2km} B_O$ and $F_1^{60km} B_O$) to 42 years ($F_{1-4}^{193km} B_O$). In contrast to closed reservoir boundaries, fluid flow into the Rupelian basal sands is maintained for a longer time period, if all four faults are hydraulically conductive compared to a single fault of only two kilometres length.

Due to lower reservoir pressures and the resulting shorter duration of mass flow, the total amount of brine, which is displaced into the shallow aquifer, is reduced in all cases with open reservoir boundaries. As Figure 26b shows, 40 Mt brine reach the Rupelian basal sands when all four faults are open ($F_{1-4}^{193km} B_O$), corresponding to 66 % of displaced mass for the same fault length but closed reservoir boundaries ($F_{1-4}^{193km} B_C$). The displaced mass of brine is reduced by up to 30 % for a short hydraulically conductive fault segment of two kilometres length ($F_1^{2km} B_O$), because a major part of the fluid spreads within the laterally open reservoir (Figure 26b). After the injection-related upward brine migration stops, a slight backward flow out of the shallow aquifer was additionally observed. Decreasing pressure causes about 3.7 Mt dense fluid to flow out of the Rupelian basal sands back into the fault over a time period of 1,500 years (Scenario $F_1^{2km} B_O$).

3.5.3 OVERLYING SECONDARY RESERVOIR

3.5.3.1 CLOSED RESERVOIR BOUNDARIES

An overlying secondary reservoir has a strong impact on pressure build-up within the injection horizon. If all reservoir boundaries are closed, the mean pressure increase within the Detfurth Formation ranges from 15.9 bar ($F_1^{2km} B_C SR_{200mD}$) to 2.9 bar ($F_{1-4}^{193km} B_C SR_{200mD}$) in correspondence to 80 % and 63 % of the pressure increase, respectively, without considering the overlying secondary reservoir (Table 5). After the injection period, reduction of the comparatively lower overpressures takes significantly longer, e.g. the mass flow into the Rupelian basal sands takes place for about 1,050 years ($F_1^{2km} B_C SR_{200mD}$) and 225 years ($F_{1-4}^{193km} B_C SR_{200mD}$), which is more than three times longer compared to the models without a secondary reservoir. Figure 28 illustrates the explanation for this flow retardation: During the injection, fluid is displaced within the Detfurth Formation, and further through the faults into the Muschelkalk Formation (Figure 28a). Due to the successive pressure reduction in both reservoirs, brine is transported out of the respective reservoir afterwards (Figure 28b).

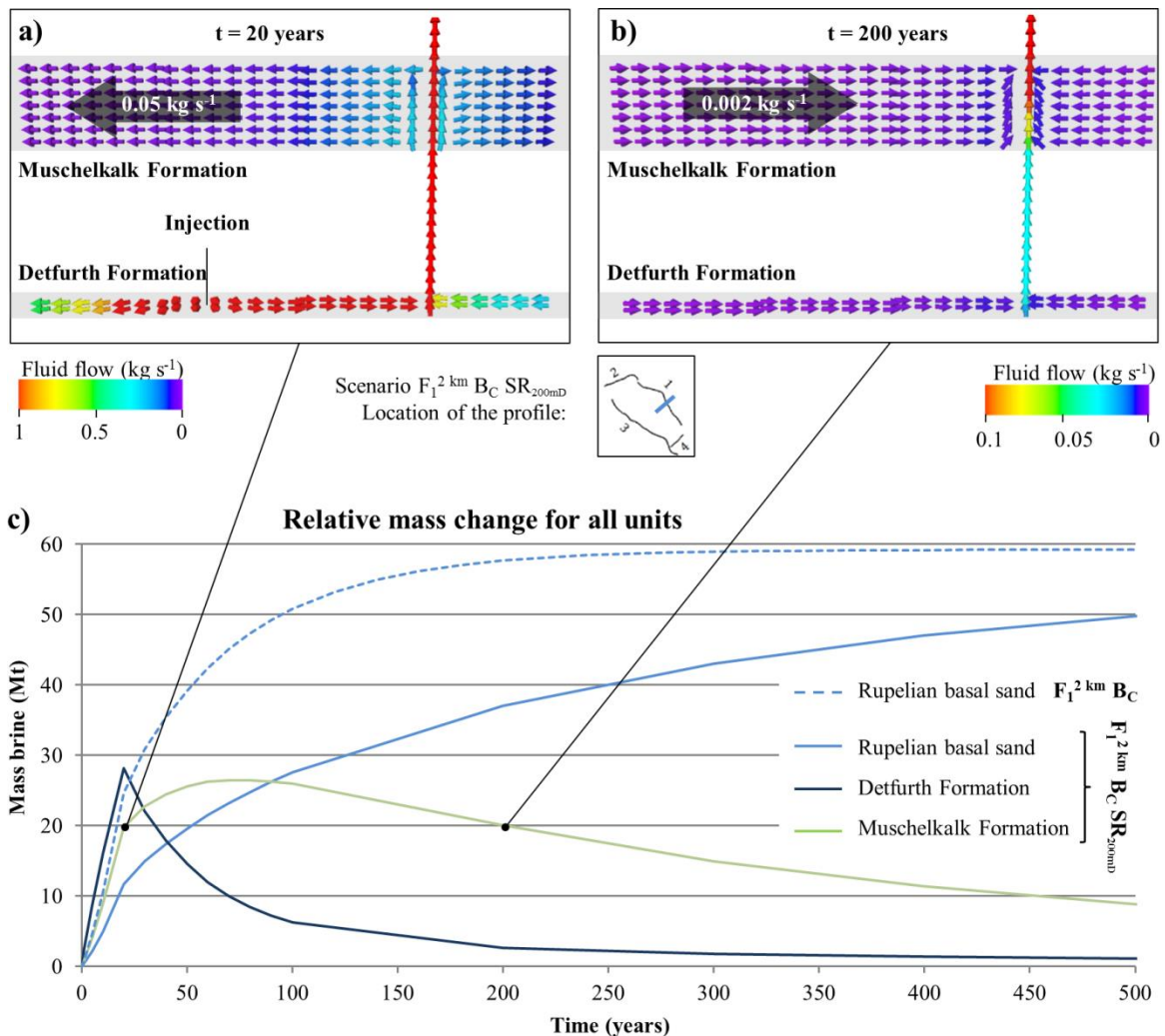


Figure 28: (a) Cross profile normal to Fault 1 shows, that during the injection period the displaced fluid spreads within the Detfurth and the Muschelkalk. (b) Afterwards, brine is transported out of the respective reservoir due to pressure reduction in both reservoirs. (c) Temporal evolution of the relative mass change shows the resulting retardation in fluid flow into the Rupelian basal sands for Scenario $F_1^{2\text{km}} B_C SR_{200\text{mD}}$.

This retardation can be clearly observed in the mass balances, comparing the displaced brine mass into the Rupelian basal sands for the scenarios with and without an overlying secondary reservoir (Figure 28c). However, the overall displaced brine mass into the shallow aquifer is almost identical, when pressure comes to an equilibrium (Figure 29). Nevertheless, for a short open fault of two kilometres ($F_1^{2\text{km}} B_C SR_{200\text{mD}}$) it takes a long time until the pressure conditions prior to injection are re-established, although pressure differences are already low.

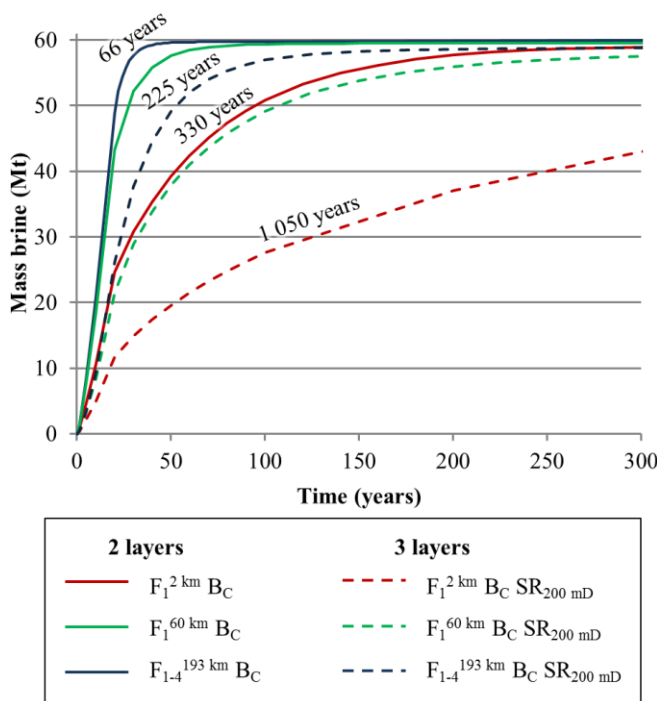


Figure 29: Relative mass change of the Rupelian basal sands illustrates the retardation in fluid flow (black numbers) due to the existence of an overlying reservoir, while the overall displaced brine mass into the shallow aquifer is almost identical, when pressure comes to equilibrium.

Due to lower reservoir pressures, flow velocities are lower as well. This is particularly obvious for Scenario $F_1^{2\text{ km}} B_C SR_{200\text{ mD}}$, where flow velocity out of Fault 1 is halved at the end of the injection period compared to the scenario without the overlying secondary reservoir (Figure 30). However, because the displaced brine mass becomes equal in both scenarios after a certain period of time, the area affected by salinity increase in the Rupelian basal sands is comparable to that observed in the simulations considering only two model layers (Table 5). Because of the delay in mass flow due to the existence of an overlying reservoir, the injection-related pattern occurs damped, and a more even distribution of saltwater in the shallow aquifer was observed. This is especially the case for the scenarios with greater fault length ($F_1^{60\text{ km}} B_C SR_{200\text{ mD}}$ and $F_{1-4}^{193\text{ km}} B_C SR_{200\text{ mD}}$): Salinity and width of the displaced brine normal to the fault are slightly reduced closer to the injection well, while comparatively higher values can be observed at a greater distance to the point of injection.

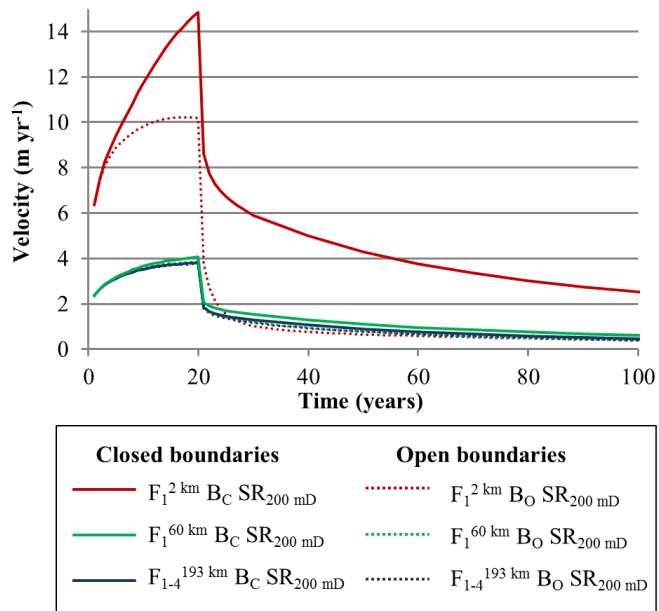


Figure 30: The temporal evolution of the flow velocities out of Fault 1 show a substantial reduction due to lower reservoir pressures for the scenarios considering a secondary overlying reservoir as well as open boundaries.

3.5.3.2 OPEN RESERVOIR BOUNDARIES

Open reservoir boundaries and an overlying secondary reservoir result in the lowest pressure build-up within the Detfurth Formation. The mean pressure increase in the reservoir ranges from 3.2 bar ($F_1^{2\text{ km}} B_O SR_{200\text{ mD}}$) to 1.3 bar ($F_{1-4}^{193\text{ km}} B_O SR_{200\text{ mD}}$), corresponding to 16 % and 28 % of the pressure increase, respectively, without taking into account the overlying secondary reservoir (Table 5). A pressure increase of at least one bar was observed at a maximum distance of 55 km ($F_1^{2\text{ km}} B_O SR_{200\text{ mD}}$) and 40 km ($F_{1-4}^{193\text{ km}} B_O SR_{200\text{ mD}}$) from the injection well, depending on the open fault length. After the injection stop, pressure decreases much faster than in all other scenarios. The overlying secondary reservoir leads to a smaller retardation in fluid flow only, which is not comparable to the observed delay if reservoir boundaries are closed. Duration of mass flow into the shallow aquifer ranges between 31 years ($F_1^{2\text{ km}} B_O SR_{200\text{ mD}}$) and 45 years ($F_{1-4}^{193\text{ km}} B_O SR_{200\text{ mD}}$). A backflow out of the shallow aquifer was observed as well (Figure 31).

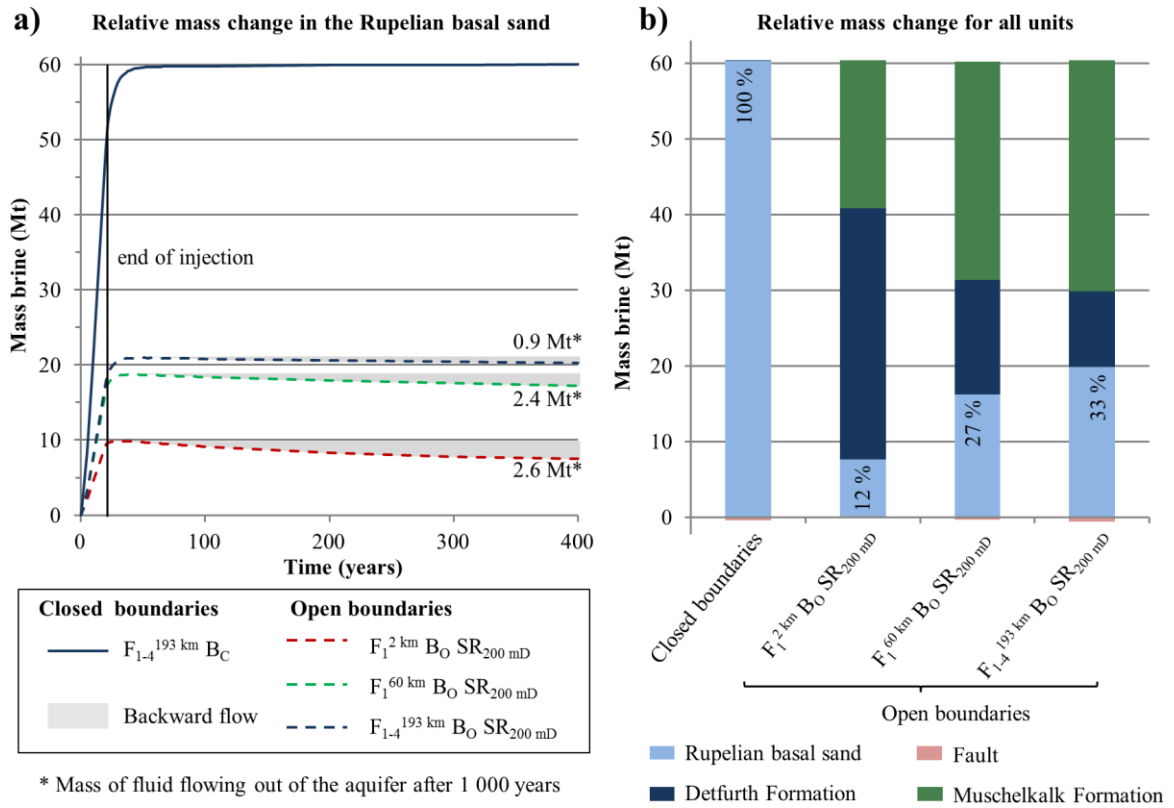


Figure 31: (a) Temporal evolution of the relative mass change of the Rupelian basal sands shows a lower duration of mass flow for open reservoir boundary conditions. Further a slight backward flow out of the aquifer can be observed. (b) Relative mass change for lithological units at 1,000 years (considering the backflow) illustrates, that salinization in the shallow aquifer is substantially reduced, if reservoir boundaries are open, and further an overlying secondary reservoir exists.

The flow velocity out of the two kilometres long fault shows its maximum of 10 m/yr at the end of the injection period. For the scenarios $F_1^{60\text{km}} B_O SR_{200\text{mD}}$ and $F_{1-4}^{193\text{km}} B_O SR_{200\text{mD}}$, flow velocities are only slightly lower, and decrease marginally faster than in the simulations with closed boundaries (Figure 30). The mass of brine displaced upward into the shallow aquifer is further reduced. Taking into account the backflow after 1,000 years, only 7.2 Mt of brine are transported into the Rupelian basal sands for a fault length of two kilometres ($F_1^{2\text{km}} B_O SR_{200\text{mD}}$). This corresponds to 12 % of the mass which reaches the shallow aquifer when reservoir boundaries are closed and no secondary reservoir exists ($F_1^{2\text{km}} B_C$). The major part of the displaced fluid spreads within the laterally open Detfurth Formation. For greater fault lengths, also the mass brine migrating into the Rupelian basal sands is lower: here, only 27 % ($F_1^{60\text{km}} B_O SR_{200\text{mD}}$) and 33 % ($F_{1-4}^{193\text{km}} B_O SR_{200\text{mD}}$) of the injected mass is displaced into the freshwater aquifer, respectively (Figure 31). For these scenarios, a higher amount of brine spreads within the Muschelkalk Formation.

Hence, due to the significantly lower brine displacement into the shallow aquifer, also the lateral brine extension is minor. In the Rupelian basal sands, the salinity increases up to a distance of 2.8 km around the fault with a length of two kilometres ($F_1^{2\text{km}} B_O SR_{200\text{mD}}$). This is less than half the extension compared to the scenario with closed reservoir boundaries and considering only two model layers ($F_1^{2\text{km}} B_C$). Moreover, the brine, which is displaced into the freshwater aquifer, originates from considerably shallower depths: for a fault length of two kilometres

($F_1^{2km} B_O SR_{200mD}$) the brine rises in the extreme from the upper 59 m of the fault. In the case with four open faults, ($F_{1-4}^{193km} B_O SR_{200mD}$) brine mainly originates from the upper 17 m of the faults.

3.5.4 PERMEABILITY DIFFERENCES BETWEEN THE FAULT AND SECONDARY RESERVOIR

Our previous simulations demonstrate that if reservoir boundaries are closed, the permeability of the fault only has a temporal impact on fluid flow only, and the overall displaced brine mass into the freshwater aquifer becomes equal after a certain period. For this case, it is irrelevant if fault permeability is higher, equal or lower compared to the reservoir or aquifer. This is not the case if the reservoir boundaries are open (infinite aquifer).

In Scenario $F_{1-4}^{193km} B_O SR_{200mD}$, the permeability of the Muschelkalk Formation is distinctly higher than that of the fault. The mean reservoir pressure increases by less than half (0.6 bar) compared to the scenario with a Muschelkalk Formation permeability of only 200 mD ($F_{1-4}^{193km} B_O SR_{200mD}$). In addition, the total duration of mass flow into the Rupelian basal sands is lowest with only 23 years compared to all other scenarios. However, in this scenario brine preferentially migrates into the permeable Muschelkalk Formation and not into the shallower aquifer. As illustrated in Figure 32, most of the injected brine is displaced into the overlying secondary reservoir, and only 3.5 Mt remain in the Detfurth Formation.

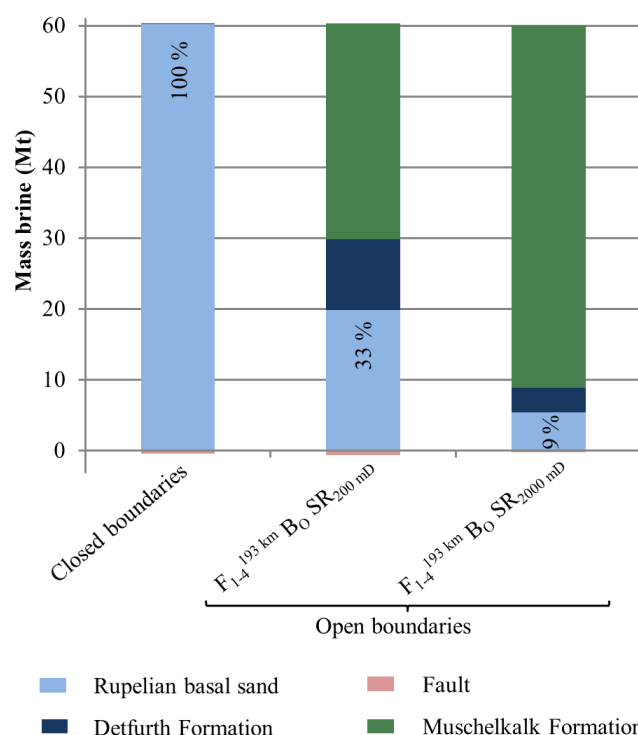


Figure 32: Relative mass change for all lithological units after 1,000 years (considering the backflow) illustrates that if permeability of the fault is lower than of the Muschelkalk Formation ($F_{1-4}^{193km} B_O SR_{200mD}$) brine is preferentially displaced into the overlying secondary reservoir. Consequently, freshwater salinization in the shallow aquifer is lowest compared to all other scenarios.

The mass of saline water transported into the Rupelian basal sands is only 5.5 Mt, corresponding to 9 % of the total injected mass. In consequence, salinization of the Rupelian basal sands is lowest, and the extent of the displaced brine smallest in this scenario compared to all others (Table 5). Moreover, the fluid that is displaced into the shallow aquifer originates solely from the upper 4 m of the faults.

3.6 DISCUSSION

The analysis of all scenarios provides both, general outcomes for a better understanding of the relevant processes and the impact of all investigated parameters as well as site-specific findings. In a previous study, TILLNER ET AL. (2013) demonstrated that pressure build-up in the reservoir is the driving factor in upwards brine migration: Larger pressure build-up leads to stronger brine displacement, and consequently higher salinities in shallow aquifers. Our simulations confirm these observations. Moreover, we have shown that the magnitude of pressure build-up induced by fluid injection and its release strongly depends on the choice of lateral boundary conditions, the effective damage zone volume of faults and the presence of secondary reservoirs. The maximum pressure increase of 19.4 bar in average within the reservoir occurs if the reservoir boundaries are closed, no overlying secondary reservoir exists, and the hydraulically conductive fault segment is short ($F_1^{2km} B_c$). This results in the highest observed flow velocities of 29 m/yr for Fault 1. Consequently, the displaced brine spreads 6.1 km laterally around the fault within the shallow aquifer in the extreme. Moreover, the spatial distribution of pressure build-up leads to an injection-related pattern in fluid flow, resulting in higher salinities within the Rupelian basal sands above fault intervals, which are located closer to the injection well. However, we neglected pore compressibility in our models to maximize pressurization and subsequent brine displacement. Considering pore compressibility, would lead to a slight reduction in injection-related pressure-build up due to higher storage coefficients in the formations, and consequently to less intense brine displacement during the injection period.

All simulations with closed reservoir boundaries that correspond to a spatially restricted reservoir further show that the mass of brine displaced into the shallow aquifer corresponds to the overall injected mass. For that reason, fluid flow persists until the injection-related overpressure within the reservoirs is completely vanished. Hence, only a temporal effect on upward brine migration depending on fault length and the presence of an overlying reservoir was observed in this case. For a fault segment of two kilometres length ($F_1^{2km} B_c$) the flow into the shallow aquifer can last up to five times longer than for the scenario with four open faults ($F_{1-4}^{193km} B_o$). Thereby, the presence of an overlying secondary reservoir results in fluid flow retardation by factor 3.1 to 3.4 in the scenarios $F_1^{2km} B_c SR_{200mD}$ and $F_{1-4}^{193km} B_c SR_{200mD}$, respectively. Open reservoir boundaries represent an aquifer with a quasi-infinite extension and allow lateral pressure dissipation. As a result, substantially lower pressures within the Detfurth Formation and a reduction of shallow aquifer salinization can be observed. Consequently, only 66 % of the brine mass is displaced into the shallow aquifer assuming four open faults ($F_{1-4}^{193km} B_o$) and about 30 % in the two kilometres single fault case ($F_1^{2km} B_o$) in comparison to the corresponding scenarios with closed boundaries. The presence of an overlying secondary reservoir leads to an additional decrease in salinity: 33 % and 12 % of equivalent brine mass

migrates into the shallow aquifer in the scenarios $F_{1-4}^{193km} B_O SR_{200mD}$ and $F_1^{2km} B_O SR_{200mD}$, respectively. These results illustrate the relevance of representing the site-specific geological conditions as close as possible, as previously proposed by e.g. CAVANAGH AND WILDGUST (2011).

As mentioned above, the results of the investigated scenarios emphasize that also the effective volume of the hydraulically conductive length of the fault zones has an important influence on pressure build-up and release in geological underground utilization. Depending on the fault length, also the duration and intensity of the mass flow varies, in turn determining the overall salinization of a shallow aquifer. A short hydraulically conductive fault segment leads to higher reservoir pressures and a wider salinization locally around the fault (F_1^{2km}) than a fault that is open over its entire length (F_{1-4}^{193km}), because pressure dissipation occurs across a smaller area. Based on our definition, that the fault is either permeable (open) or impermeable (closed) for fluid flow, the location of potential salinization is pre-determined. Hence, the open fault length affects both, the location and degree of the occurring salinization. Moreover, these influences correspond not only to fault length, but also to fault width, since porosity was maintained constant during all our simulations. Thus, the effective damage zone volume of hydraulically conductive faults is relevant for the simulation outcome.

TILLNER ET AL. (2013) showed that the permeability of fault zones only has a minor impact and does not influence salinization of shallower aquifers significantly. The authors considered mainly fault permeabilities higher than that of the reservoirs. Our previous simulations have also primarily shown a temporal effect of fault permeability without any significant change in salinization assuming closed reservoir boundaries. Furthermore, our results demonstrate that the relation between fault and reservoir permeability has a crucial impact on salinization of upper aquifers assuming a laterally infinite reservoir extension. In Scenario $F_{1-4}^{193km} B_O SR_{200mD}$, it was shown that fault permeability lower compared to that of the secondary reservoir, determines the preferential brine flow direction. If permeability of the secondary reservoir exceeds that of the fault, the mass of brine migrating into the Rupelian basal sands is only around a quarter of that observed in the opposite case ($F_{1-4}^{193km} B_O SR_{200mD}$).

Simulations taking into account an overlying secondary reservoir result in considerably lower pressures in the storage reservoir. Moreover, a dampening effect on salinization of the shallow aquifer occurs, because fluid is partially displaced into this layer, and thus further brine displacement upward the fault is reduced. Hence, it can be assumed, that the potential salinization of a shallow aquifer is lowered with each aquifer lying in between the reservoir and the shallow aquifer. Similar results were achieved by an analytical approach of NORDBOTTEN ET AL. (2004), investigating fluid leakage through wells in a multi-barrier system with up to 12 aquifers. The authors observed a successive decrease in intensity of fluid upward displacement, caused by loss of fluid into the intermediate aquifer layers, what consequently highly reduces leakage in the shallowest aquifer. BIRKHOLZER ET AL. (2009) also showed, however, without considering a vertical conduit that the amount of fluid displaced into formations above the reservoir, decreases upwards due to the attenuation capacity of the overlying rocks.

For the given geological conditions and the assumed injection rate, the fluid displaced into the shallow aquifer originates solely from the upper part of the fault. Depending on the scenario, brine displaced into the shallow aquifer originates from the upper 4 m ($F_{1-4}^{193km} B_O SR_{200mD}$) to 298 m ($F_1^{2km} B_C$) of the part of Fault 1 lying close to the injection, while the depth of brine origin

is substantially reduced up to less than 1 m at fault edges. Consequently, the initial distribution of salinity within the fault is crucial for the assessment of shallow aquifer salinization. Our simulations with a fault fully saturated with brine correspond to an end member resulting in a maximum freshwater salinization. In this case, a small conductive fault segment would lead to higher salinities and a greater lateral propagation of the saltwater, while faults with a great effective damage zone volume lead to a more distributed salinization but lower spatial widths of the saltwater distribution. If, however, a gradient in salinity exists or the salt-freshwater interface lies below the depth, from which brine is displaced into the shallow aquifer, freshwater salinization is considerably reduced or might not occur. Nevertheless, if the displaced brine reaches the shallow groundwater system it spreads preferentially at the aquifer base, as indicated by considerably higher salinities at the lower element layer in the Rupelian basal sands. These results are in agreement with the findings of OLDENBURG AND RINALDI (2011).

Our simulation results also show that the duration of brine displacement into the shallow aquifer is not limited to the injection period. Even in the scenario assuming open reservoir boundaries and four hydraulically conductive faults ($F_{1-4}^{193km} B_o$), both supporting a fast pressure reduction, brine displacement into the shallow aquifer persists for more than twice the injection period. This illustrates the relevance of considering also the post-injection phase in salinization assessments, since neglecting the ongoing fluid flow processes could lead to an underestimation of the potential freshwater salinization. Moreover, it is important to recognize further post-injection processes, as the observed density-driven flow out of the shallow aquifer back into the faults occurring due to the increased weight of the water column.

Finally, we can complement our general findings with site-specific insights: For the study area, the presence of overlying reservoirs, represented by the Hardegsen, Muschelkalk and Stuttgart formations, as well as the initial gradient in salinity are known. This gradient reduces the potential salinization, because the fluids displaced into the Rupelian basal sands would be of essentially lower salinity than assumed in our simulations. Based on these results, it can be concluded that for a large effective damage zone volume (as in Scenario F_{1-4}^{193km}), shallow aquifer salinization is estimated as low, even if fluid is displaced over extensive areas into the Rupelian basal sands, because the origin depth of these fluids lies in maximum only a few decimetres below the shallow aquifer. At the same time, local and very permeable segments of the fault (as in Scenario F_1^{2km}) affect a higher vertical distance by upward brine migration, resulting in a higher potential for possible freshwater salinization. Furthermore, according to the present study, we are convinced that the three interlayered reservoirs would dampen brine displacement into the shallow aquifers, because fluids would be partly displaced into these layers instead of further migrating upwards.

3.7 SUMMARY AND CONCLUSIONS

In the present study, a regional scale 3D model ($100 \text{ km} \times 100 \text{ km} \times 1.34 \text{ km}$) of the prospective storage site Beeskow in the Northeast German Basin was implemented to investigate a potential salinization of potable groundwater resources due to upward brine migration through hydraulically conductive fault zones. For that purpose, 13 scenarios were examined to assess the impact of fault lengths between 2 km and 193 km in the vicinity and around the injection site. Further, the effects of an overlying secondary reservoir as well as the geological boundary conditions on the salinization of a shallow aquifer were evaluated.

We have shown that pressure build-up and its development over time within the reservoir determine the intensity and duration of fluid flow through the faults, and thereby the salinization of shallower aquifers. Thereby, the total mass of brine displaced into the uppermost aquifer essentially depends on the chosen geological boundary conditions: if reservoir boundaries are closed, representing a spatially restricted reservoir, the fluids migrating into the shallow aquifer correspond to the overall injected fluid mass (assuming zero pore compressibility). Only a temporal effect was observed on the retardation of fluid flow for shorter open fault lengths and the presence of an overlying secondary reservoir. If reservoir boundaries are open, corresponding to an aquifer with quasi-infinite extension, freshwater salinization is considerably reduced. With a secondary reservoir, only 12 % of equivalent brine mass migrates into the shallow aquifer for a hydraulically open fault segment of two kilometres.

The initial salinity distribution and location of the fresh-saltwater interface within the upper part of the fault is of high relevance for risk assessment related to salinization in shallow aquifers. For the considered geological conditions, the fluid displaced into the uppermost aquifer originates in maximum from the upper 4 m to 298 m of the investigated faults. Hence, if the salt-freshwater interface lies below this depth, no salinization is likely to occur, since only freshwater would be displaced into the shallow aquifer. In general, the potential of freshwater salinization is small for greater fault lengths, because the origin depth of the fluids displaced into the shallow aquifer lies a few decimetres below the shallow aquifer in maximum, due to lower pressure build-up. Short and very permeable fault segments may have a higher salinization potential due to a larger vertical distance affected by fluid displacement. Moreover, it can be concluded that aquifers lying in between a deep reservoir and the shallow aquifer, like in a multi-barrier system, further diminish salinization of the shallow aquifer, because saline fluids from the faults are partly displaced into these layers.

The unknown effective damage zone volume of fault zones is the greatest uncertainty in estimating the potential salinization of shallow freshwater resources. Hence, a site-specific assessment of a possible freshwater salinization requires a sensitivity analysis with varying effective damage zone volumes of the present faults. Furthermore, the injection-induced pressure increase generally results in a decrease in effective stresses. In this context, coupled hydro-mechanical simulations support estimating the (re-)activation potential of faults by shear and/or tensile failure as well as fault fill property changes resulting from volumetric strain increments (MAGRI ET AL., 2013; RÖHMANN ET AL., 2013; CAPPA AND RUTQVIST, 2011; CHIN ET AL., 2000). With respect to our simulation results, we conclude that hydraulically conductive fault zones do not necessarily lead to freshwater salinization owing to upward fluid

displacement. This principally depends on the initial salinity distribution, effective volume of the fault damage zone and the geological boundary conditions. We showed that numerical simulations are applicable to obtain site-specific insights on the relevant factors affecting dynamic fluid flow processes. Since every field site is very complex and especially most of the heterogeneities in the subsurface are unknown, we focused here on selected end members to estimate the site-specific bandwidth of the potential salinization. Field explorations should be employed prior to any underground utilization to obtain more accurate data, especially on the effective damage zone volume of present fault zones as well as the initial salinity distribution.

4 FAULT REACTIVATION AND GROUND SURFACE UPLIFT ASSESSMENT AT A PROSPECTIVE GERMAN CO₂ STORAGE SITE

ABSTRACT

The present study assesses potential geomechanical impacts of pore pressure increase induced by CO₂ injection at a prospective CO₂ storage site located in the Middle Bunter sequence in Eastern Germany. A 3D supra-regional-scale structural geological model was implemented in one-way coupled hydro-mechanical simulations to assess caprock and fault integrity. Simulation results show a maximum ground uplift of 0.021 m at the end of CO₂ injection, while shear failure observed at the simulated time steps does not achieve a significant density in the entire model. Consequently, reservoir, caprock and fault integrity are not compromised at any time of CO₂ injection operation.

4.1 INTRODUCTION

A promising option for reducing anthropogenic greenhouse gas emissions into the atmosphere includes the technology of carbon capture and storage (CCS) in deep sedimentary formations acting as geological reservoirs (IPCC, 2005). Geological storage of carbon dioxide (CO₂) in deep saline aquifers offers hereby the greatest potential compared to other options such as storage in depleted hydrocarbon reservoirs or deep unmineable coal seams (MICHAEL ET AL., 2010; IPCC, 2005). Based on the recent scientific research, studies of operating CO₂ injection sites report a significant importance to geomechanics due to changes in pore pressure as a result of the imposed injection pressure (RUTQVIST, 2012). Hence, large-scale pressure build-up impacts on the geomechanical rock and fault behaviour resulting in stress changes, and therefore altering the integrity of reservoir and caprock as well as possibly leading to reactivation of existing faults by shear failure. These geomechanical effects must be carefully assessed in order to determine inherent risks that may pose potential health, security or environmental hazards.

Previous research includes studies as for example the work of RUTQVIST ET AL. 2010 investigating the geomechanical response due to subsurface pressure increase as a result of CO₂ injection within the enhanced gas recovery project at the In Salah storage site, Algeria. Furthermore, that study includes the suggestion that ground deformation can be linked to the volumetric expansion of the CO₂ injection zone due to related pore compressibility (RUTQVIST ET AL., 2010). A related study from 2008 conducts a synthetic case about potential tensile and shear failure related to CO₂ injection into a multi-barrier system (RUTQVIST ET AL., 2008). Another study presents a geomechanical assessment as a significant method to observe the impact of pressure disturbance associated with large-scale CO₂ storage which could lead to potential triggering of notable seismic events, affecting the geomechanical behaviour of reservoir, caprock and surrounding fault systems, and thereby endanger the long-term integrity of a CO₂ storage site

(ZOBACK, 2010). ORLIC (2009) focuses on the possible mechanical impacts of CO₂ injection, and thus stress alteration within the reservoir with regard to seal and well integrity as well as fault stability and concludes that these issues can be addressed by numerical modelling. All these studies show that the use of geomechanical analyses can indicate the suitability of prospective CO₂ storage sites, and thereby support recommendation for overall safe and secure operational constraints.

Here, we present a geomechanical assessment in terms of possible fault and seal integrity and ground surface uplift related to CO₂ injection and associated pore pressure changes. This required a 100 km x 100 km supraregional-scale 3D geological model of a prospective CO₂ storage site which was then implemented in the geomechanical simulator FLAC^{3D} (ITASCA, 2012). We summarise the build-up of the 3D geological model with the Petrel software package (SCHLUMBERGER, 2010A) and the geomechanical model implementation. Concluding, we present and evaluate the results of the geomechanical analysis and potential impacts.

4.2 THE PROSPECTIVE CO₂ STORAGE SITE – LOCATION AND GEOLOGY

In Germany, geological storage of CO₂ received large attention in the past decade which led to the installation of the pilot project in Ketzin, about 25 km west of Berlin which commenced injection of CO₂ in 2008 and is still operating (MARTENS ET AL., 2010). In general, the geology of northern Germany offers the potential to include several storage sites within the sedimentary formations of the North German Basin (NGB), which is part of the Southern Permian Basin (KNOPF ET AL., 2010).

Within the scope of this study, a prospective German CO₂ storage site located in the Northeast German Basin (NEGGB) was investigated. The NEGGB is a sub-basin of the NGB and on account of that presents potential storage horizons for CO₂ injection. The Mesozoic anticline structure Beeskow-Birkholz (in the following only referred to as Beeskow), about 60 km southeast of Berlin in the East of the State of Brandenburg (Figure 33, left), is located within the NEGGB. Because of the location and the main characteristics, Beeskow was selected as a prospective CO₂ storage site (VATTENFALL, 2010; VATTENFALL, 2009).

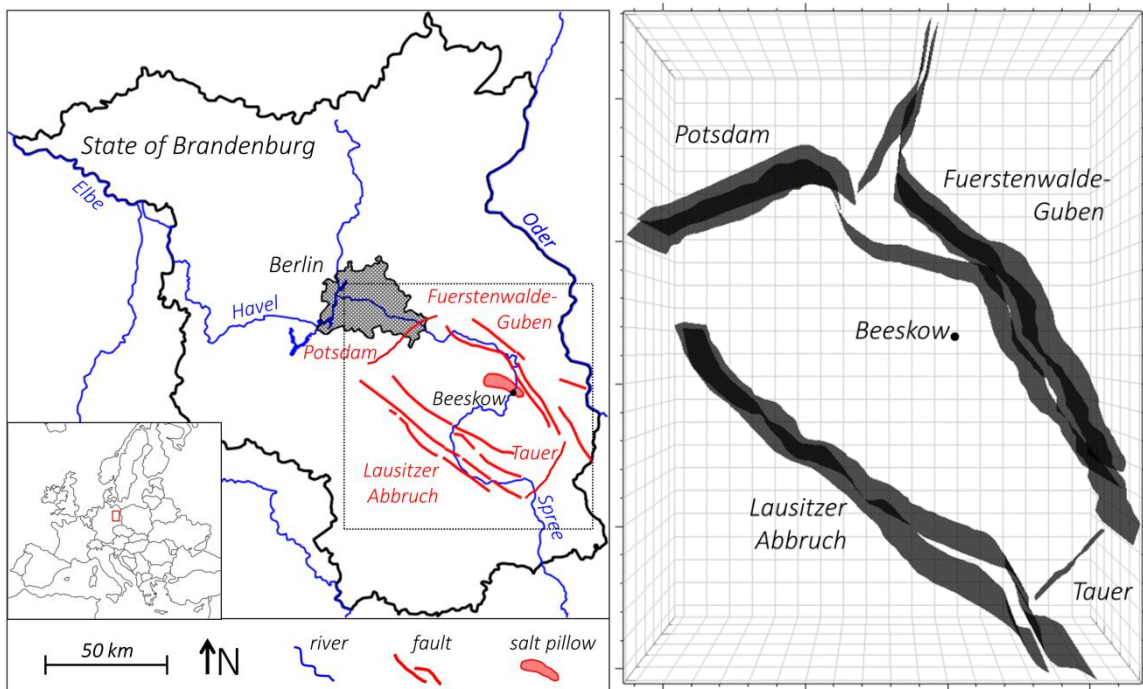


Figure 33: (left) Location of the study area Beeskow-Birkholz indicated by dashed rectangle. Main fault zones are shown as well as the anticline structure that presents the prospective CO₂ storage site (modified after TILLNER ET AL., 2013); (right) All integrated faults displayed in the Petrel software package that build up the fault systems Lausitzer Abbruch, Potsdam, Fuerstenwalde-Guben and Tauer.

The anticline lies above the corresponding Upper Permian (Zechstein) salt pillow and its longitudinal axis is NW-SE oriented with a maximum length and width of about 20 km and 5 km, respectively. The Beeskow salt pillow evolved initially from the regional tectonic pattern during the Mesozoic (starting in the Keuper, Upper Triassic) and subsequent post-depositional salt tectonics and followed basin inversion that started during transition of Lower to Upper Cretaceous (STACKEBRANDT AND MANHENKE, 2004; SCHECK ET AL., 2003). Due to consequential uplift and erosion there is a depositional gap of Cretaceous to Tertiary sediments that indicate that the Beeskow anticline is succeeded from Triassic (Bunter and Keuper) to Jurassic (Lias) to Tertiary deposits, including the Rupelian clay which is the main regional seal (separating deep saline waters from shallow groundwater), to Quaternary deposits (STACKEBRANDT AND MANHENKE, 2004). The regional fault systems generally divide the succession of basin sediments of the NEGB into blocks (BEUTLER AND STACKEBRANDT, 2012). Thereby, the Beeskow anticline lies within the Mittenwalde block that is delineated by the fault systems Fuerstenwalde-Guben (about 5 km east of the anticline, dipping southwest) and Lausitzer Abbruch fault zone (dipping northeast) which are both NW-SE oriented (BEUTLER AND STACKEBRANDT, 2012). In SW-NE orientation the Mittenwalde block is bordered by the continued Potsdam fault zone (dipping southeast) in the North and the Tauer fault zone (dipping northwest) in the South (BEUTLER AND STACKEBRANDT, 2012); (Figure 33, right). All fault systems are constituted mostly of normal faults, except of the Fuerstenwalde-Guben fault zone, which features reverse faults in some parts (BEUTLER AND STACKEBRANDT, 2012).

The prospective storage horizon is the Middle Buntsandstein, which is subdivided (from bottom to top) into the Volpriehausen, Detfurth and Hardegsen sequences. In detail, the Volpriehausen

and the Detfurth sequences represent the prospective storage horizons that each consists of a basal sandstone, constituting the storage formation, that is succeeded by an alternation of sandstone and silt-sandy parts (VATTENFALL, 2010; VATTENFALL, 2009). The Detfurth Formation was selected as prospective storage horizon and has an effective thickness of 23 m and a reservoir top at a depth of about 1,080 m at the chosen CO₂ injection well location (VATTENFALL, 2010; VATTENFALL, 2009). Accordingly, it was also selected for this study as injection formation. Due to public opposition and lack of a national regulation, the industrial storage project was suspended in 2011. Previous studies analysing this area of interest include the work of TILLNER ET AL. (2013) that assessed brine migration through fault zones as a result of CO₂ injection. Analysis of geomechanical aspects such as seal and fault integrity was not yet conducted on a supraregional-scale model. However, in this issue, MAGRI ET AL. (2013) conducted hydro-mechanical simulations over an area of 42 km x 42 km. It was concluded that a larger model is required to rule out boundary effects on the calculated stress field. For this reason, results of pressure distribution based on reservoir simulations on CO₂ injection from TILLNER ET AL. (2013) are integrated into our geomechanical simulations to observe any stress changes and related geomechanical effects.

4.3 PRE-PROCESSING

4.3.1 STRUCTURAL GEOLOGICAL MODEL

The modelled area, which is situated in the East of the State of Brandenburg has an areal extent of 100 km x 100 km. It is approximately centred at the CO₂ storage site Beeskow. The Petrel software package (SCHLUMBERGER, 2010A) was used to build-up the 3D structural geological model. In a first step, depth contour lines of the Middle Bunter, Keuper and Lias were digitised based on the online cartography GeotIS (Geothermal Information System); (SCHULZ ET AL., 2007). From these input data, the major fault systems were also adapted. Based on additional literature data further horizons (topography, Zechstein salt, Zechstein rock, Rotliegend and the basement) were added (STACKEBRANDT AND MANHENKE, 2004; BEER, 2000; SCHECK AND BAYER, 1999). This was performed in order to extend the model, and thereby mitigate boundary effects in the geomechanical simulations. The digitalisation of the stratigraphic contour and major fault lines led to a preliminary model, which was then correlated and adjusted in terms of stratigraphy and depth for each unit. Furthermore, a thickness correction was applied and additional borehole data and profile lines from GeotIS were adopted for corrections.

The final 3D geological model comprises eight layers (Figure 34, left). From bottom to top (at a basal depth of 5,000 m) the basement is succeeded by the Rotliegend, Zechstein rock (transition), Zechstein salt, Middle Bunter (Triassic), Keuper (Triassic), Lias (Jurassic) and Quaternary. In total, there are nine faults in the final structural geological model, which define four regional fault systems. The included fault systems are the Fuerstenwalde-Guben in the East, the Tauer fault in the South, the Lausitzer Abbruch system in the West and the Potsdam fault system in the North (Figure 34, left).

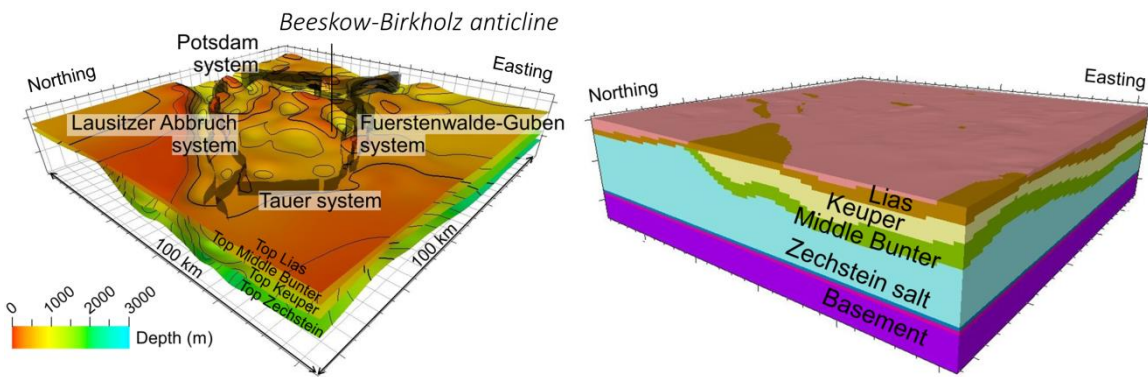


Figure 34: (left) 3D geological structural model of the Beeskow site with geological layers and the major fault zones. Fault zone 1 displays the Fuerstenwalde-Guben, fault zone 2 the Lausitzer Abbruch and fault zone 3 the Potsdam fault system (BEUTLER AND STACKEBRANDT, 2012); (right) 3D model generated in the Petrel software package, which was subsequently exported into FLAC^{3D}.

4.3.2 GRIDDING PROCESS

In order to implement the 3D geological model into the geomechanical simulator FLAC^{3D} it is necessary to discretise the geological model in respect to the general grid convergence criteria of FLAC^{3D}. For this reason, the model was initially gridded in the Petrel software package with a lateral discretisation of 400 m x 400 m and about 130 m in vertical direction. This resulted in a total of 2.5 million elements ($n_x = 250$, $n_y = 250$, $n_z = 40$). The elements were then assigned to zone properties in order to upscale the geological units to the geomechanical grid ensuring maintenance of grid convergence criteria in FLAC^{3D}. The resulting zone model includes all relevant geological information (Figure 34, right). After export of the grid from the Petrel software package, it is converted and implemented to the geomechanical simulator FLAC^{3D} (Figure 35, left).

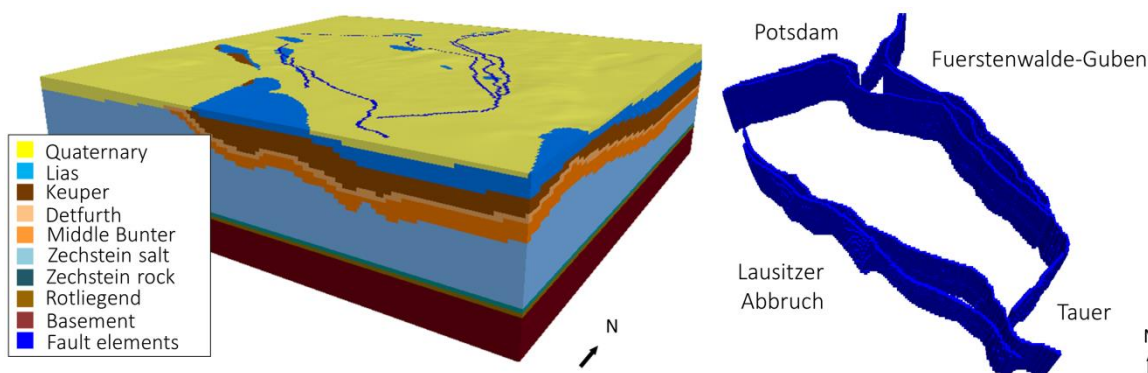


Figure 35: (left) Geomechanical model displayed in FLAC^{3D}; (right) Elements of the mechanical grid that are cut by a fault plane are defined as ubiquitous joints elements.

Additionally, the storage formation (Detfurth Formation) was vertically and horizontally refined resulting in 339,169 additional elements. This refinement was undertaken to account for the CO₂ storage reservoir thickness of about 23 m.

4.3.3 FAULT MODEL

According to our implemented workflow, we proceeded with the fault modelling using the Petrel software package. We started to integrate the fault model in the geological model, but excluded the faults from the gridding process since geometrical gridding of the fault planes was undertaken using the software Rhinoceros 5 (ROBERT MCNEEL & ASSOCIATES, 2012). All faults were then imported as geometry into FLAC^{3D}. In order to integrate the faults into our 3D geomechanical model we used the ubiquitous joints approach. The ubiquitous joints resemble weak zones within the model effective for all elements of the grid cut by a fault (Figure 35, right). The dip angle and dip direction for the ubiquitous joints were assigned to each element cut by a fault according to the values at the respective fault plane location.

4.3.4 GEOMECHANICAL MODEL PARAMETERIZATION

After implementation of the grid to the geomechanical simulator, the resulting geomechanical model was parameterised using the Mohr-Coulomb constitutive law. Mechanical properties that were assigned include Young's modulus (E), Poisson coefficient (ν), friction angle (ϕ), cohesion (τ_0) and tension (T_0) as well as density (ρ) which were taken from literature data (OUELLET ET AL., 2010; MOECK ET AL., 2009; NAGELHOUT AND ROEST, 1997; KOPF, 1965); (Table 6). As for the fault model, the ubiquitous joints were also populated with layer-specific mechanical properties including cohesion, friction and dilation angle (OUELLET ET AL., 2010). Thereby, the faults were modelled as cohesionless to consider a worst-case scenario of possible shear failure. The friction and dilation angles of the ubiquitous joints were assigned after Ouellet et al. (2010), given with 20° for the friction angle and 10° for the dilation angle.

Table 6: Geomechanical properties assigned to the integrated formations of the geomechanical grid (OUELLET ET AL., 2010; MOECK ET AL., 2009; NAGELHOUT AND ROEST, 1997; KOPF, 1965).

Period	Age	Elasticity modulus, E (GPa)	Poisson coefficient, ν (-)	Friction angle, ϕ (°)	Cohesion, τ_0 (MPa)	Tension, T_0 (MPa)	Density, ρ (kg/m ³)
Quaternary		2.6	0.47	29.5	0	0	2,100
Jurassic	Lias	4.0	0.42	25.0	5	5	2,350
Triassic	Keuper	8.5	0.34	27.0	5	5	2,500
	Middle Bunter	27.7	0.26	25.0	5	5	2,453
	Zechstein salt	30.0	0.30	27.0	0	0	2,060
Permian	Zechstein rock	51.8	0.29	30.0	5	5	2,629
	Rotliegend	15.0	0.25	30.0	5	5	2,501
Carboniferous	Basement	40.1	0.19	30.0	5	5	2,698

4.4 GEOMECHANICAL SIMULATIONS

4.4.1 INITIALIZATION

In order to run simulations the geomechanical model was initialised with the assigned mechanical properties and gravitational load applied. Initial pore pressure was applied using a pore pressure gradient, which was consequently adjusted to the adopted initial pore pressure at depth of the reservoir top (a pore pressure of about 10 MPa at 1,080 m depth according to TILLNER ET AL. 2013). In addition, displacements normal to the axial directions were not allowed at the model boundaries except at the model top. The equilibrated model state is used from there as initial stress field for all simulations discussed in the present study.

4.4.2 SIMULATION

A one-way coupling concept was implemented using the spatial distribution of pressure perturbation interpreted from dynamic flow simulations carried out by TILLNER ET AL. (2013), to realize the hydro-mechanical one-way coupling. Thereto, radial pressure distribution was fitted using polynomial functions according to the radii given in Table 7, and subsequently integrated into the geomechanical model. The time frame for the dynamic simulations is 20 years of CO₂ injection. Pressure changes after 10 days and 20 years were considered in the mechanical time steps (Table 7). The maximum pore pressure is reached after 10 days, while the maximum spatial pressure perturbation is encountered after 20 years. Therefore, both time steps were selected for the simulation. Moreover, the simulation was undertaken with a scenario of faults closed for hydraulic flow and an impermeable caprock, limiting pressure perturbation to the area enclosed by the four fault blocks in the storage formation (Figure 33, right).

Table 7: Downhole pressure for selected geomechanical time steps derived from dynamic flow simulations (TILLNER ET AL., 2013).

Time after injection	Downhole pressure (MPa)	Radius of pressure perturbation (m)
Initial	10.0	-
10 days	19.4	3,500
7,300 days (20 years)	17.9	35,000

4.5 RESULTS AND DISCUSSION

The simulation was conducted for an injection period of 20 years. Thereby, a maximum vertical displacement of 0.42 cm (uplift) was observed at the ground surface after 10 days of CO₂ injection. Comparatively, maximum vertical displacement reached 1.2 cm at the top of the Detfurth Formation. Evidentially, vertical displacement increases after the maximum pore pressure is achieved at 10 days of injection resulting in 2.1 cm at ground surface and 2.5 cm at the reservoir top (Figure 36). However, the radius of the pressure perturbation has a considerable greater extent of 35,000 m after 20 years compared to that of 3,500 m after 10

days of injection. The changes in effective stresses (σ_e) show that due to the injection induced pore pressure (p_t) increase the resulting effective principal stresses decrease at the injection depth of about 1,080 m (Figure 37). Consequently, maximum shear stress is reduced by the decrease of the mean stress explaining that shear failure is almost absent in the storage formation and its caprock. Analysis of the stress state of the caprock, reservoir and faults show a scarce occurrence of shear and the absence of tensile failure. Thereby, shear failure in the caprock (Keuper) does only occur at the early stage of injection (maximum pressure increase in the reservoir) with an insignificantly low density of affected elements. No additional failure in the caprock is observed at the last time step (maximum spatial pressure perturbation in the reservoir). Failure within the injection horizon (Detfurth Formation) does not occur in the vicinity of the Beeskow anticline, but in between the adjacent faults (Fuerstenwalde-Guben fault system); (Figure 38, top left and top right). The elements of the faults are also affected by shear failure, whereas its greatest density is mostly apparent below the injection horizon (Figure 38, bottom left and bottom right). Besides, failure is only scattered in the remaining parts of the distributed faults not indicating the occurrence of a consistent slip plane. At the faults close to the injection well at the Beeskow anticline, only few ubiquitous joints elements are affected by shear failure, but failure also occurs within the matrix of these elements. Consequently, fault reactivation cannot be expected at any time of CO_2 injection considering the applied parameterisation.

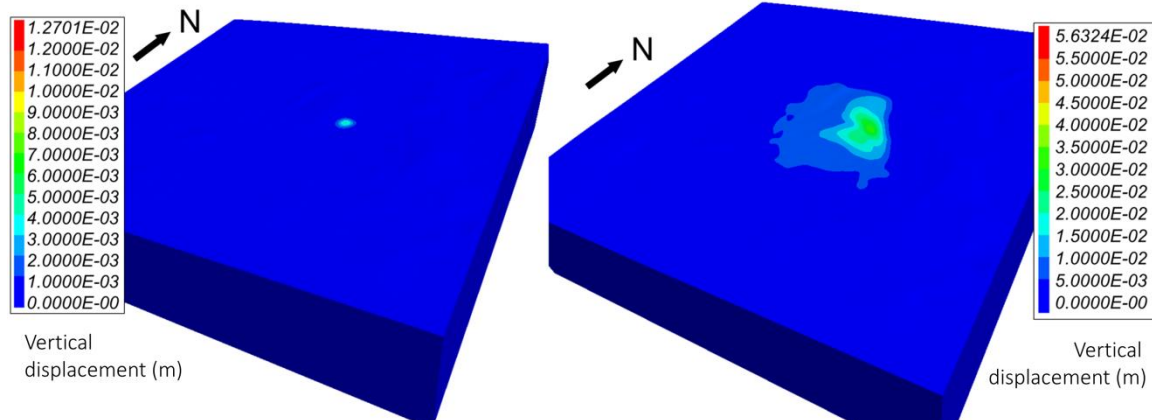


Figure 36: (left) Distribution of vertical displacement after 10 days of CO_2 injection. The greatest vertical displacement at ground surface is at the injection well location; (right) Distribution of vertical displacement after 20 years of CO_2 injection. The greatest vertical displacement at ground surface is at the injection well location (vertical exaggeration: 5).

Within the present study supra-regional geomechanical impacts of CO_2 injection into the Beeskow anticline were investigated with a fixed data set, whereby the simulation results indicate that neither reservoir and caprock nor fault integrity are compromised. This is supported by a regional-scale sensitivity analysis carried out by MAGRI ET AL. (2013), whereas both models show similar displacement patterns and vertical displacements at the top of the Detfurth Formation of about 0.9 cm to 1.2 cm for the maximum pore pressure after 10 days. A comparison for the maximum simulation time of 20 years is not reasonable, since the faults

were assumed to be closed for fluid flow in the present study. Consequently, the calculated vertical displacements are almost twice as high, compared to MAGRI ET AL. (2013). Nevertheless, 3D seismic data for the study area is required for an extensive structural geological assessment. Consequently, we considered the documented main faults penetrating all relevant formations above the Zechstein, whereas assigned fault properties consider a worst-case scenario.

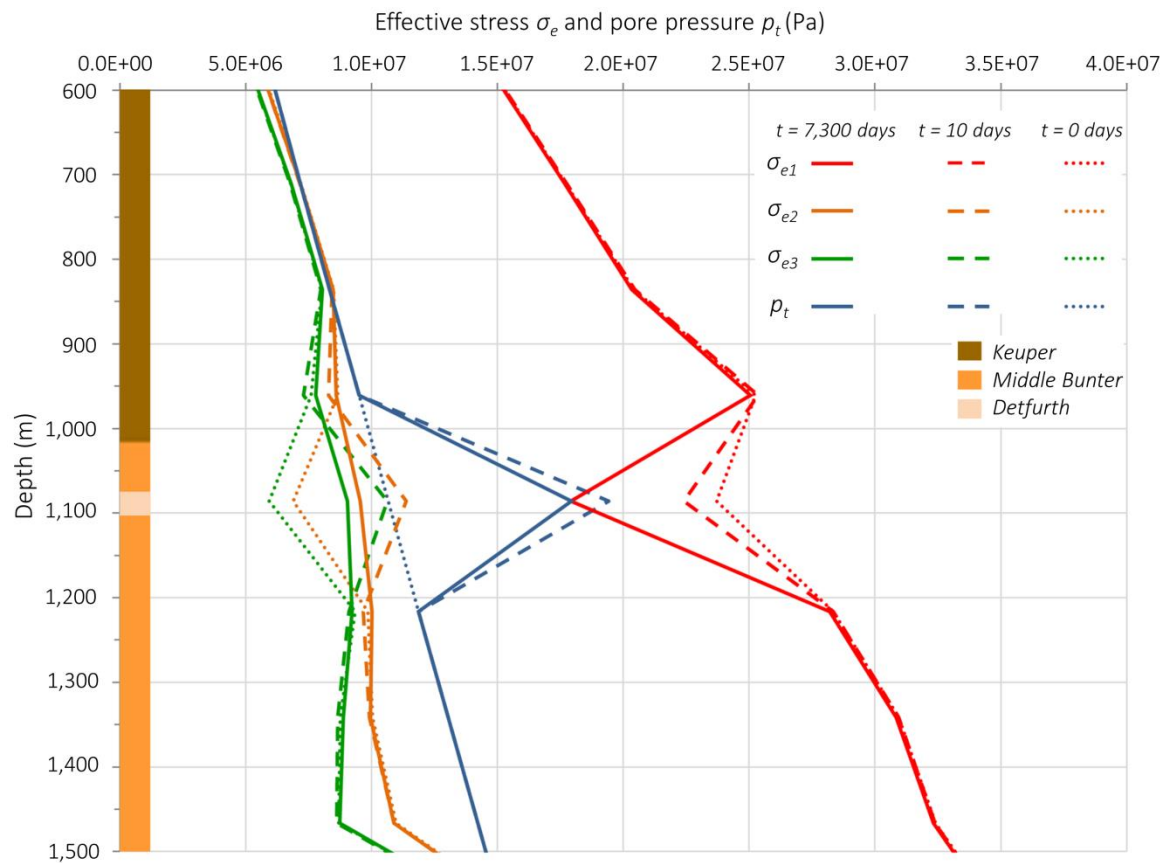


Figure 37: Effective stress (σ_e) and pore pressure changes (p_t) are shown for the time steps 0 days, 10 days and 7,300 days (20 years) plotted against depth.

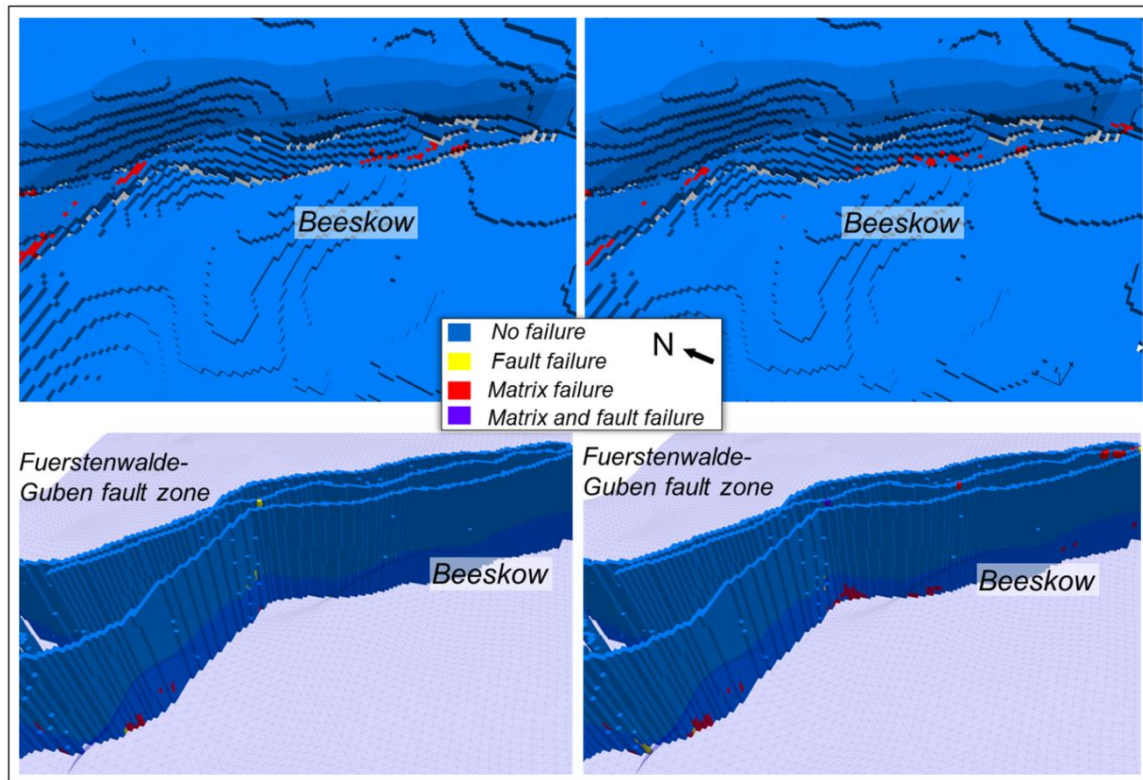


Figure 38: (top left) The state of the injection formation after 10 days; (top right) and 20 years after CO₂ injection. (bottom left) State of the faults with the injection horizon indicated after 10 days; (bottom right) and after 20 years of CO₂ injection (only shear failure is observed; vertical exaggeration is 5).

4.6 CONCLUSIONS

A prospective CO₂ storage site located in the NEGB (Beeskow anticline, which lies in the East of the State of Brandenburg, Germany) was selected for the assessment of potential geomechanical impacts resulting from pore pressure increase. For the purpose of the present study a 100 km x 100 km 3D supra-regional-scale structural geological model was set up integrating available literature data. This 3D geological model comprises eight horizons and includes the storage horizon Middle Bunter (Detfurth Formation). Subsequently, the 3D geological model was transferred to the geomechanical simulator and populated with mechanical properties. Then, a one-way coupling concept was implemented using the results of published dynamic fluid flow simulations. Geomechanical simulations were carried out for 20 years of CO₂ injection. Simulation results show a maximum vertical displacement (uplift) of 0.41 cm at the ground surface after 10 days (maximum pore pressure) and 2.1 cm after 20 years (maximum spatial pore pressure perturbation) of CO₂ injection. Matrix and ubiquitous joints elements shear failure at both simulated time steps does not achieve a significant density in the entire model. Consequently, reservoir, caprock and fault integrity are not considered compromised at any time of CO₂ injection operation. This is also supported by a regional-scale sensitivity analysis (MAGRI ET AL., 2013).

5 COUPLED DYNAMIC FLOW AND GEOMECHANICAL SIMULATIONS FOR AN INTEGRATED ASSESSMENT OF CO₂ STORAGE IMPACTS IN A SALINE AQUIFER

ABSTRACT

Pore pressure variation resulting from geological CO₂ storage may compromise reservoir, caprock and fault integrity. Therefore, we investigate the mechanical impact of industrial-scale CO₂ storage at a prospective Danish site by coupled 3D hydro-mechanical simulations carried out by two independent modelling groups. Even though the two chosen modelling strategies are not identical, simulation results demonstrate that storage integrity is maintained at any time. Vertical displacements are mainly determined by hydraulic fault conductivity influencing spatial pore pressure elevation. The introduced fault zone implementation in the hydro-mechanical model allows for localization of potential leakage pathways for formation fluids along the fault plane.

5.1 INTRODUCTION

Underground storage of the greenhouse gas carbon dioxide (CO₂) is currently seen as a promising strategy to limit the anthropogenic contribution to global climate change. However, effective stress changes resulting from pore pressure elevation generally accompanying CO₂ injection may pose a serious impact on the integrity of faults, reservoir and caprock. Ground surface uplift, reactivation of adjacent faults or caprock fracturing may become potential consequences (E.G. MAGRI ET AL., 2013; RÖHMANN ET AL., 2013; CAPPA AND RUTQVIST, 2011; VIDAL-GILBERT ET AL., 2009; RUTQVIST ET AL., 2008; RUTQVIST ET AL., 2007). In order to investigate how geological CO₂ storage affects the mechanical behaviour of reservoir, caprock and fault zones, coupled dynamic flow and hydro-mechanical simulations for an onshore saline aquifer were undertaken by two different modelling groups. For this purpose, the two dynamic flow simulation codes ECLIPSE (SCHLUMBERGER, 2007) and TOUGH2-MP/ECO2N (ZHANG ET AL., 2008; PRUESS, 2005B) were applied for the multi-phase flow simulations and coupled to the mechanical simulators VISAGE (SCHLUMBERGER, 2010B) and FLAC^{3D} (ITASCA, 2012), respectively. Although potential formation fluid leakage via hydraulically conductive faults at the Vedsted site was assessed previously by dynamic flow simulations (MBIA ET AL., 2014), using the conceptual approach similar to that introduced by TILLNER ET AL. (2013), hydro-mechanical effects were not considered.

5.1.1 STUDY AREA

The Vedsted site, a prospective deep saline onshore CO₂ storage formation, is located in the Norwegian-Danish Basin in Northern Denmark (Figure 39). The Vedsted area is part of the

Fjerritslev Trough, a large graben structure in the Sorgenfrei-Tornquist Zone that developed due to a late Carboniferous to Early Permian rifting phase (NIELSEN, 2003). The structure is bounded by northwest-southeast trending faults and comprises several marine and fluvial sandstone reservoirs of Upper Triassic to Lower Jurassic age, sealed by a multi-barrier system of caprocks consisting of marine Jurassic claystones and Cretaceous chalks (DALHOFF ET AL., 2011).

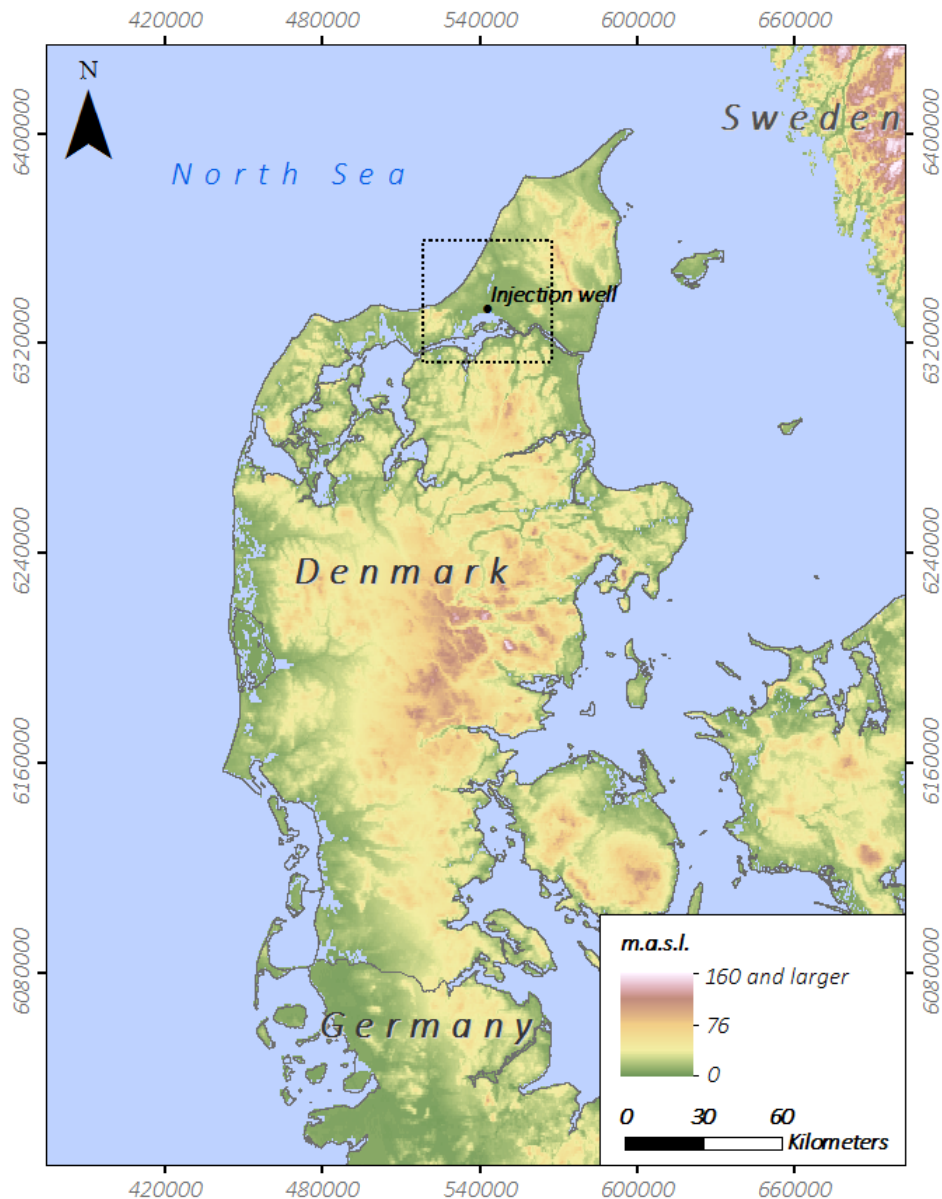


Figure 39: The injection well of the prospective CO₂ storage site is located close to Vedsted in northern Denmark. The dotted rectangle indicates the approximate extension of the structural geological model applied in all simulations. National borders and elevation data were obtained from the DIVA-GIS database (HIJMANS ET AL., 2012). Axes show UTM-coordinates (Spatial Reference: EPSG Projection 32632 - WGS84 / UTM zone 32N).

The marine and fluvial sandstones of the Gassum Formation intercalated with marine and lacustrine mudstones form one potential reservoir suitable for geological CO₂ storage at Vedsted and were chosen as the target horizon for CO₂ injection. The Gassum Formation is located at a

depth between 1,700 m and 2,000 m and characterized by an average thickness of about 290 m, whereas only the upper 64 m and the lower 85 m are sandstone dominated (MBIA ET AL., 2014). The primary seal is the Fjerritslev Formation with a thickness of 530 m (MBIA ET AL., 2014; FRYKMAN ET AL., 2011; FRYKMAN ET AL., 2009).

5.2 COUPLED HYDRO-MECHANICAL SIMULATIONS

In the present modelling study, a one-way coupling procedure was applied, whereby the pore pressure distribution obtained from the two reservoir simulators ECLIPSE and TOUGH2-MP served as a coupling parameter. The two mechanical codes VISAGE and FLAC^{3D} were employed to subsequently calculate strain changes based on effective stress variations as a response to the injection induced pore pressure elevation as previously proposed by e.g. RUTQVIST (2011) and RUTQVIST ET AL. (2002). Open and closed fault scenarios were considered in the numerical simulations.

5.2.1 STRUCTURAL GEOLOGICAL MODEL AND PARAMETERIZATION

The regional-scale 3D model of the Vedsted area implemented by FRYKMAN ET AL. (2011) using the Petrel software package (SCHLUMBERGER, 2012), served as a basis for the coupled hydro-mechanical simulations. The static geological model with a lateral extent of 50 km x 50 km and thickness of about 2.4 km includes five northwest-southeast trending major fault zones in its central part (Figure 40). It was set up and parameterized based on top formation maps and the interpretation of 2D seismic data as well as log and core data from wells drilled in the 1950's within the frame of oil and gas exploration campaigns (BRITZE AND JAPSEN, 1991). The model includes ten different lithological units, from the Post Chalk Group (Tertiary/Quaternary) at the ground surface down to the Skagerrak Formation (Upper Triassic) located below the storage horizon (Gassum Formation).

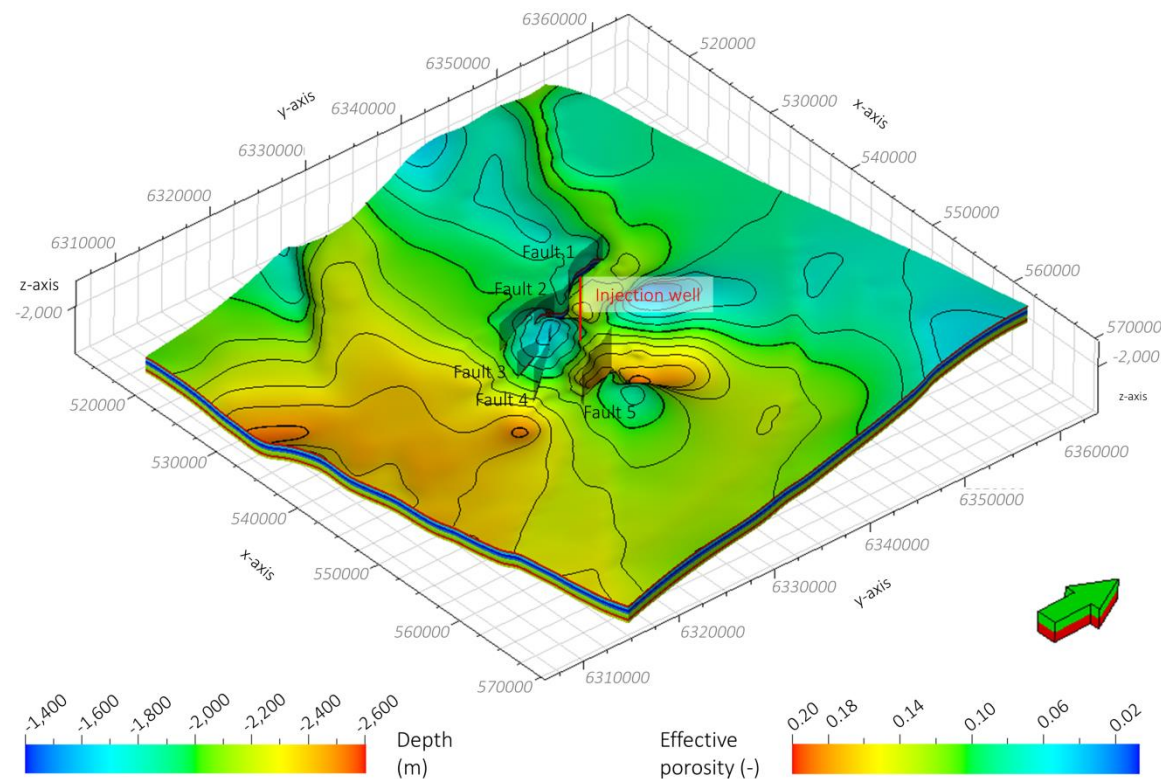


Figure 40: Effective porosity of the Gassum Formation and depth of the formation top. CO₂ injection occurs at the eastern flank of the central anticline structure bounded by five fault zones.

The porosity and permeability distribution of the storage horizon were modelled as homogenous in vertical and horizontal direction, varying between 0 – 0.25 and 0.01 mD – 70 mD, respectively, due to the alternating sand and shale dominated layers within the lithological sequence of the Gassum Formation (MBIA ET AL., 2014; DALHOFF ET AL., 2011; LARSEN ET AL., 2003; NIELSEN, 2003).

All boundaries of the 3D regional-scale dynamic model are characterized by no-flow boundary conditions. However, to simulate an infinite aquifer and to minimize the influence of boundary effects, a pore volume multiplier at the outer lateral boundary elements was applied. The individual simulation runs start from hydrostatic equilibrium assuming an average hydrostatic pressure gradient of 10.3 MPa/km. Hence, at a depth of 1,995 m in the injection well, the pressure is 22.6 MPa considering a brine density of about 1,120 kg/m³ and a reservoir temperature of 66 °C. Temperature is determined by a geothermal gradient of 30 °C/km and constant in the simulations. Rock compressibility amounts to 6.96×10^{-10} 1/Pa in all formations. A maximum capillary entry pressure of 0.1 MPa corresponds to the low-permeability shales representing the primary seal as well as the intra-formational shale dominated layers within the Gassum Formation. Sand dominated layers of the storage horizon were parameterized with a lower entry pressure of 0.01 MPa. During the individual simulation runs 2 Mt CO₂/yr, corresponding to 63.42 kg/s, were injected into the Gassum Formation over a time span of 40 years by using a single injection well located at the eastern flank of the central anticline structure. Both modelling groups developed their individual simulation strategies with differences in grid discretization and parameterization as e.g. caprock permeabilities, fault

implementation and hydraulic fault conductivity, discussed in more detail in the following sections.

5.2.2 GFZ POTSDAM SIMULATION STRATEGY

For the assessment of ground surface uplift and reservoir, caprock and fault integrity by coupled hydro-mechanical simulations, a dynamic reservoir model was implemented based on the structural geological model presented in Section 5.2.1. Subsequently, reservoir flow simulations were performed using the TOUGH2-MP/ECO2N software package to calculate CO₂ injection induced pore pressure changes. In order to minimize the influence of the model boundaries on pressure propagation and stress distribution, the numerical reservoir model was extended in downward and lateral directions. In a next step, the pressure distribution at selected time steps obtained from the dynamic flow simulations was scaled to the extended hydro-mechanical model. Finally, the geomechanical response to the altered pore pressure, and thus effective stress distribution was calculated using the FLAC^{3D} software package.

5.2.2.1 DYNAMIC FLOW SIMULATIONS AND RESULTS

For dynamic flow simulations with TOUGH2-MP/ECO2N, the regional-scale 3D model presented in Section 5.2.1, was discretized into a total number of 720,000 elements ($n_x = 200$, $n_y = 200$, $n_z = 18$) with a constant element size in horizontal direction of 250 m x 250 m. The vertical resolution varies between 25 m and a few hundred meters depending on the different lithological units incorporated. The dynamic flow model comprises nine units from the Post Chalk Group at the ground surface down to the Gassum Formation at a depth of about 1,700 m (top of anticline). During the gridding process, the five vertical fault zones were implemented into the numerical model. Faults were treated as either hydraulically conductive or non-conductive to fluid flow in horizontal direction. Furthermore, a permeability of 0.01 mD was assigned to the caprock (Fjerritslev Formation) and the intra-formational shale layers of the Gassum Formation. It was assumed that the injection well is not completed over the entire storage horizon but only in the upper permeable sandstone dominated part of the storage reservoir. After the 40-year injection period, a ten-year post-injection period was simulated to assess the pore pressure development after site abandonment.

The simulation results show that the bottomhole pressure at the injection increases almost immediately after the injection start by a factor of 1.45 (closed faults) and 1.40 (open faults) up to a maximum of 32.9 MPa and 31.7 MPa at a simulation time of one year and 0.7 years, respectively (Figure 41). From this time on, pressure continuously decreases to 30.6 MPa (closed faults) and 29.8 MPa (open faults) until the end of injection after 40 years. Subsequent to the injection stop, bottomhole pressure drops abruptly and almost reaches initial conditions of 22.6 MPa at the end of the ten-year post-injection period (23.2 MPa, closed faults; 22.9 MPa, open faults). Compared to the bottomhole pressure, wellblock pressure increases less sharply exceeding a maximum of 30.7 MPa after 1 year (closed faults) and 30.1 MPa after 0.7 years. During the ten-year post-injection period, wellblock pressure drops to 22.7 MPa and 22.6 MPa, respectively.

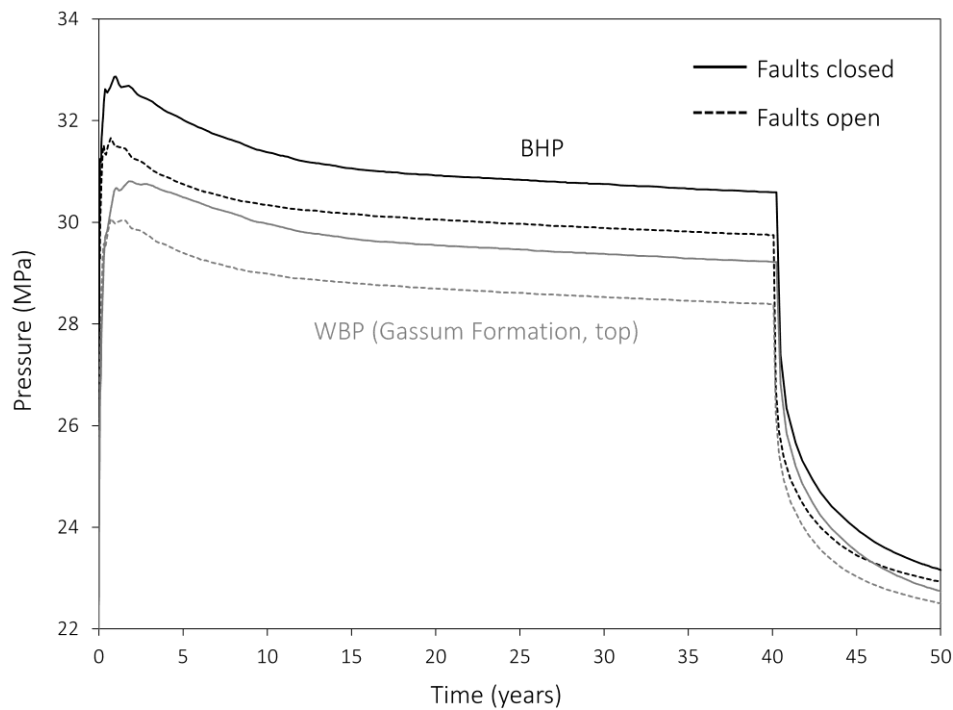


Figure 41: Development of the BHP (bottomhole pressure) and WBP (wellblock pressure) for open and closed faults for an injection period of 40 years and a post-injection period of 10 years.

Figure 41 shows the pressure increase at the top of the Gassum Formation after 40 years of CO₂ injection. According to our expectations, the maximum pressure increase is limited to the injection well vicinity and amounts to 7.2 MPa and 8 MPa for hydraulically open and closed faults, respectively. However, as cross-fault flow is impossible in the closed fault scenario, reservoir compartmentalization forces the pressure to propagate preferentially in north-south direction (Figure 42, right), whereas hydraulically conductive faults allow for unhindered pressure propagation to the top of the anticline and across the faults (Figure 42, left). Pressure increase is below 0.1 MPa at a distance of about 20 km from the injection well and zero at the model boundaries.

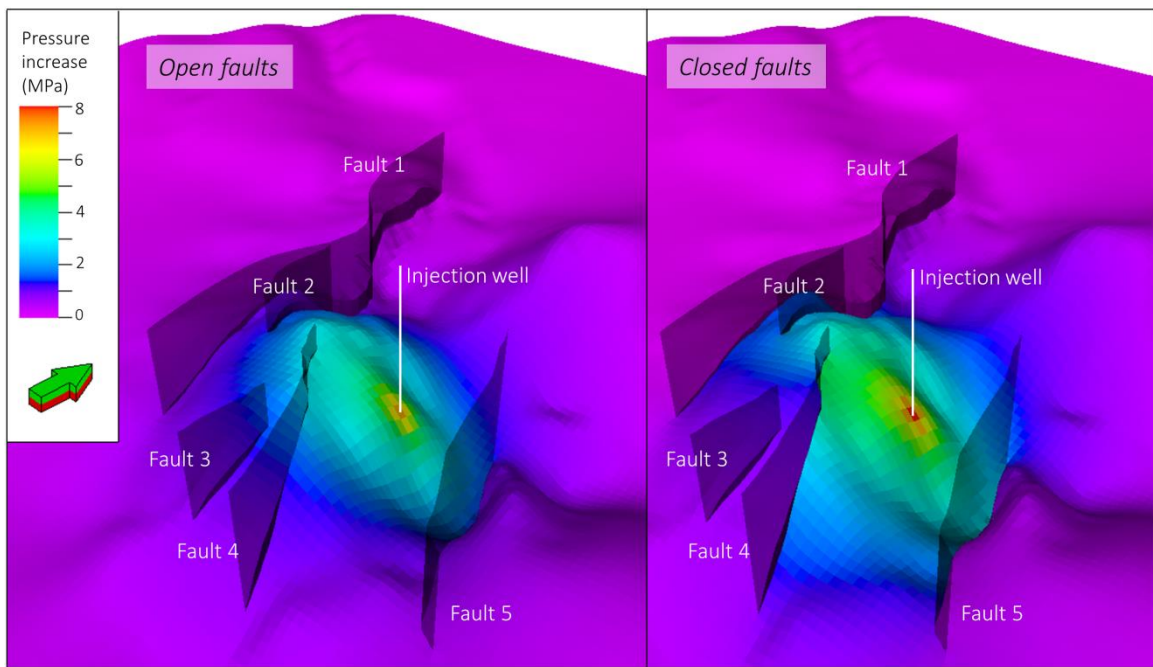


Figure 42: Pore pressure increase at the top of the storage formation for open (left) and closed faults (right) after 40 years.

Figure 43 illustrates the CO₂ extent after a period of 40 years for hydraulically open (left) and closed (right) faults. Due to the lower entry pressure, gaseous CO₂ propagates preferentially within the higher permeable sand layers in both investigated scenarios (open and closed faults). Buoyancy effects force the CO₂-rich phase to migrate upwards to the top of the anticline. The CO₂-rich phase reaches Fault 4 at the structure top after about half the injection period in both cases. After 40 years, the maximum gaseous CO₂ extent is slightly larger assuming hydraulically open faults (5.5 km x 5.7 km) due to the fact that CO₂ can propagate unhindered laterally. Under the assumption of closed faults, the gaseous CO₂ reaches a lateral size of 5.3 km x 5.5 km.

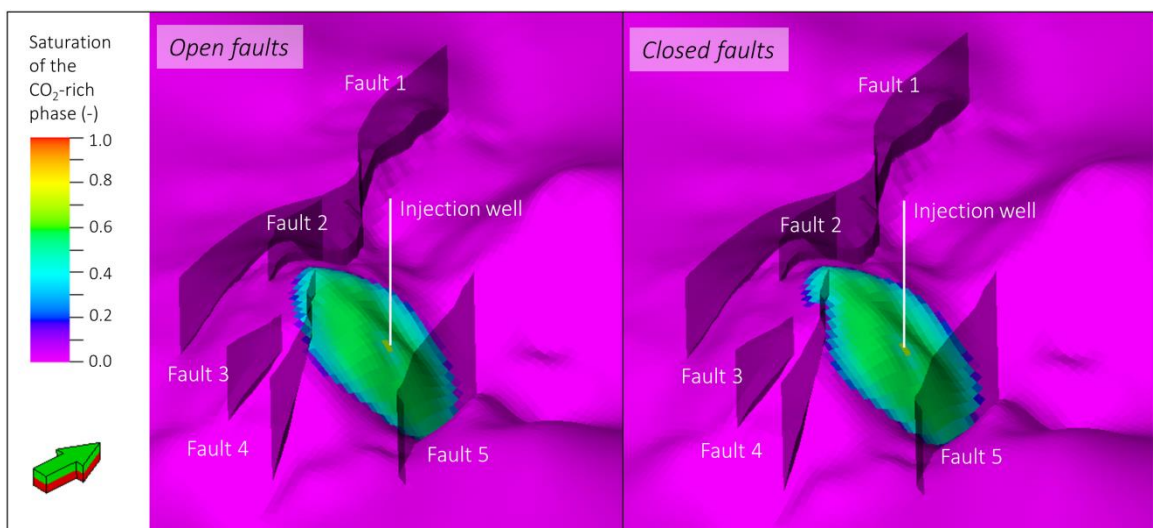


Figure 43: Propagation of the gaseous CO₂ in the upper sand layers of the Gassum Formation after 40 years for open (left) and closed faults (right).

5.2.2.2 GEOMECHANICAL SIMULATIONS AND RESULTS

For hydro-mechanical modelling, the reservoir model with an areal size of 50 km x 50 km was laterally extended to 100 km x 100 km as discussed by KEMPKA ET AL. (2014). In addition to the nine lithological units mentioned above, the hydro-mechanical model comprises the Skagerrak Formation underlying the Gassum storage formation as well as one further basement layer extending downward to a depth of 5,000 m (Figure 44). However, two very thin layers (Boerglum and Flyvbjerg formations) were consolidated into a single unit to maintain the grid quality criteria required by the mechanical simulator. Figure 44 illustrates that the horizontal element size is smallest in the central part of the hydro-mechanical model around the injection well (22 km x 25 km) with 200 m x 200 m and increases towards the model boundaries up to a maximum of 1,600 m x 1,600 m. In total, the model is discretized by 1,640,912 elements ($n_x = 182$, $n_y = 196$, $n_z = 46$), whereby 4,943 elements represent the fault zones using the FLAC^{3D} ubiquitous joints model. Ubiquitous joints are based on a weak plane model introduced in the FLAC^{3D} Mohr-Coulomb plastoelastic model with an orientation that corresponds to the dip angle and direction of the respective fault at the given element location (KEMPKA ET AL., 2014; ITASCA 2012; JIANG ET AL., 2004). The model conversion from the Petrel to the TOUGH2-MP/ECO2N and FLAC^{3D} packages was carried out as discussed by NAKATEN AND KEMPKA (2014).

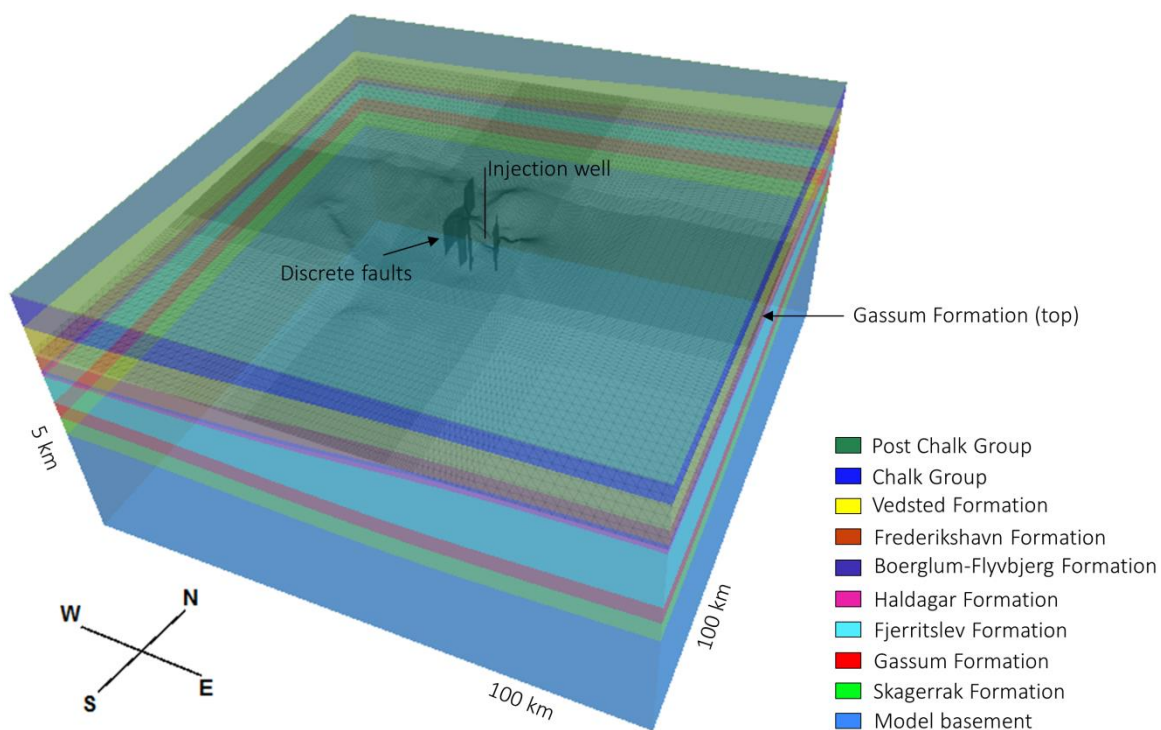


Figure 44: Hydro-mechanical model applied for the hydro-mechanical assessment. Five discrete faults and ten lithological units are implemented. Vertical exaggeration factor is 10.

Table 8 lists the applied parameters for carrying out the hydro-mechanical simulation runs. According to KEMPKA ET AL. (2014), a strike-slip faulting regime ($S_{Hmax} > S_v > S_{hmin}$) with $S_{Hmax} = 1.3 S_v$ was selected as initial stress state at the Vedsted site. The model is initialized with a free top

surface boundary and zero displacement normal to the bottom and lateral boundaries. After a model equilibration considering the given stress regime, pore pressure distribution obtained from the reservoir simulations performed with TOUGH2-MP was upscaled to the hydro-mechanical model. The rock matrix and/or ubiquitous joints may react to stress changes with shear or tensile failure, which is assessed by the Mohr-Coulomb failure criterion at each computation step in the numerical simulation (KEMPKA ET AL., 2014).

Table 8: Mechanical properties derived from KEMPKA ET AL. (2014) (adapted from OUELLET ET AL., 2010; NAGELHOUT AND ROEST, 1997; BELL, 1977) as well as formation depths, densities, pore pressures and vertical stresses. Dilation angle is 0° for all units and 10° for the fault zones.

Lithological unit	Depth (m)	Density (kg/m^3)	S_v (MPa)	P_p (MPa)	Elastic modulus (GPa)	Poisson ratio (-)	Friction angle (°)	Cohesion (MPa)	Tensile limit (MPa)
Post Chalk Group	0	1,900	0.00	0.00	3.50	0.47	35	0.0	0.00
Chalk Group	37	2,112	0.69	0.37	13.2	0.32	30	5.0	2.35
Vedsted Formation	445	2,228	9.14	4.45	9.50	0.21	25	5.0	5.00
Frederikshavn Formation	850	2,186	18.0	8.51	10.0	0.35	25	5.0	5.00
Boerglum-Flyvbjerg Formation	1,075	2,329	22.8	10.8	9.50	0.21	25	5.0	5.00
Haldagar Formation	1,150	2,215	24.5	11.6	19.9	0.35	25	5.0	5.00
Fjerritslev Formation	1,240	2,362	26.5	12.5	19.9	0.21	25	5.0	5.00
Gassum Formation	1,825	2,298	40.0	18.8	19.9	0.35	25	5.0	5.00
Skagerrak Formation	2,138	2,415	47.1	22.2	24.9	0.22	24	5.0	8.30
Model basement	>5,000	2,700			60.0	0.19	30	5.0	5.00
Faults zones							20	0.0	

Figure 45 shows the vertical displacements after 40 years of simulation assuming open faults. The maximum vertical displacement at the Gassum Formation top is 6.1 cm and 21 cm at the ground surface, close to the injection well located at the top of the anticline structure. It is obvious that the calculated vertical displacements appear almost radial symmetric around the injection well. At the ground surface, a region with a radius of 20 km around the injection well is affected by the induced uplift.

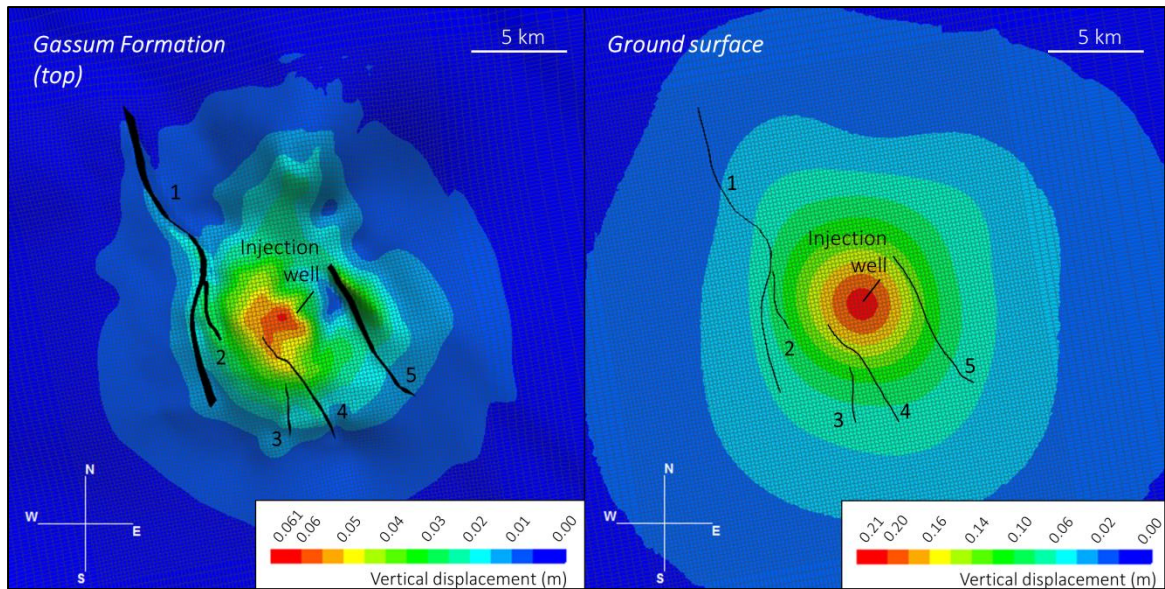


Figure 45: Vertical displacements at the Gassum Formation top (left) and ground surface (right) after 40 years, assuming hydraulically open faults.

The maximum vertical displacement assuming closed faults is 7.9 cm at the reservoir top and 26 cm at the ground surface after 40 years of CO₂ injection (Figure 46). However, due to the fact that the majority of the faults is located west of the injection, vertical displacements do not appear radial symmetric around the injection well, but rather in northern, southern and eastern direction. At the ground surface, vertical displacements are still observed about 18 km from the injection well.

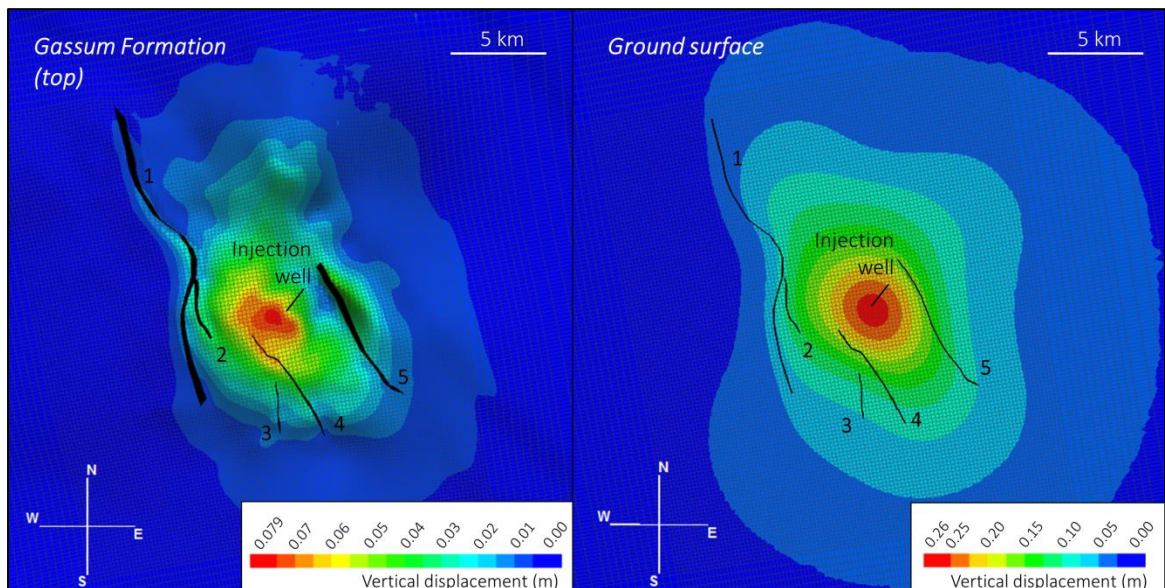


Figure 46: Vertical displacements at the Gassum Formation top (left) and ground surface (right) after 40 years, assuming hydraulically closed faults.

Figure 47 illustrates the slip and dilation tendencies at all fault planes after 40 years of simulation. Neither fault slip, nor dilation as a potential consequence of slip is to be expected during the investigated time span. Both tendencies remained identical to those prior to CO₂ injection and resulting pore pressure elevation.

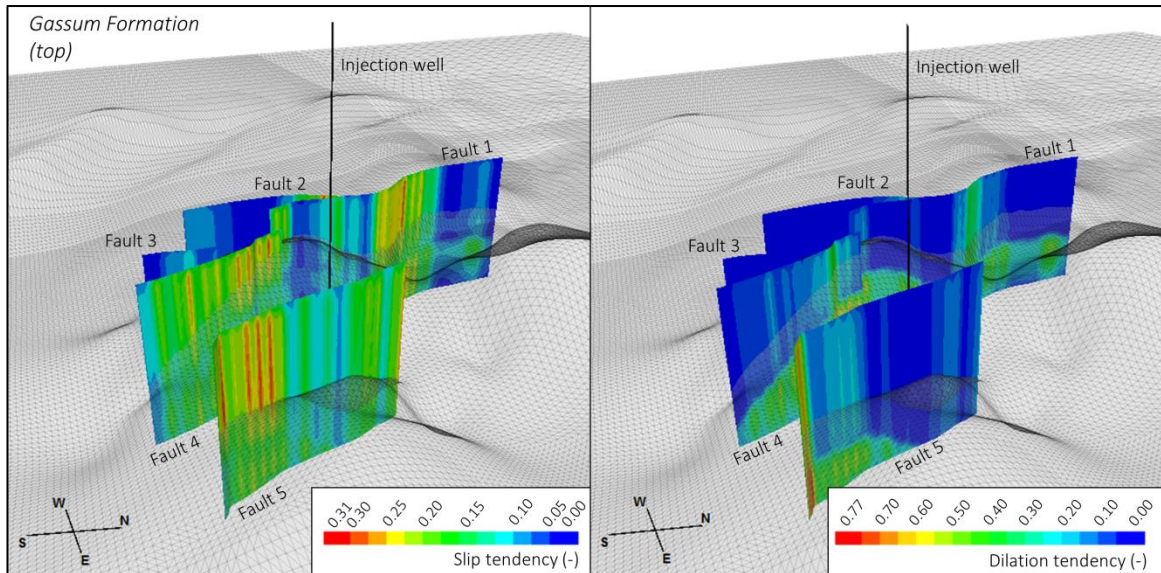


Figure 47: Slip (left) and dilation tendency (right) after 40 years assuming hydraulically open faults. A value of 1 indicates the likely occurrence of slip/dilation, whereas a value of 0 indicates that slip/dilation is unlikely.

5.2.3 IMPERIAL COLLEGE LONDON SIMULATION STRATEGY

Prior to the hydro-mechanical simulations for the assessment of ground surface uplift and storage integrity, a dynamic reservoir model was implemented based on the structural geological model presented in Section 5.2.1. Subsequently, reservoir flow simulations were performed using the commercial code ECLIPSE. For mechanical simulations using the VISAGE software package, the reservoir model was extended downward and laterally as discussed before. Then the augmented reservoir model was imported back into the ECLIPSE simulation model for computation of injection induced pore pressure changes at selected time steps, which were then used as input for the hydro-mechanical simulations.

5.2.3.1 DYNAMIC FLOW SIMULATIONS AND RESULTS

For dynamic reservoir flow simulation the static regional-scale model as presented in Section 5.2.1 with an areal size of 50 km x 50 km x 2.4 km is used. The model includes all overburden layers above the Gassum Formation up to the ground surface and one basement layer. It is discretized by a total number of 1,187,500 regular grid elements ($n_x = 250$, $n_y = 250$; $n_z = 19$), each with an lateral dimension of 200 m x 200 m. In vertical direction, the first ten layers represent the overburden, whereas layers 11 to 18 comprise the Gassum Formation and layer 19 the basement layer.

The overburden and basement layers are assumed almost impermeable with a very low permeability of 0.0001 mD. The simulations were carried out using ECLIPSE 100, a black-oil simulator capable of handling up to four phases, whereby the fluid properties of CO₂ are assigned to the gas phase and brine properties to the oil phase, respectively. It is assumed that the injection well is completed in all layers of the proposed reservoir (Gassum Formation). The five northwest-southeast trending vertical faults (Figure 40) were implemented into the static regional-scale model during the gridding process and treated as hydraulically closed for cross-fault flow in the dynamic reservoir flow simulations. Hydraulically open faults were not taken into account in the present strategy, as the focus was on identifying the mechanical response to the greatest pore pressure increase under the given assumptions. The maximum pore pressure increase can be expected, if faults are closed, and thus introducing a reservoir compartmentalization.

The simulation results show that the bottomhole pressure (BHP) increases almost immediately after the injection start by a factor of 1.6 from the initial pressure of 22.6 MPa up to a maximum of 37.1 MPa (Figure 48).

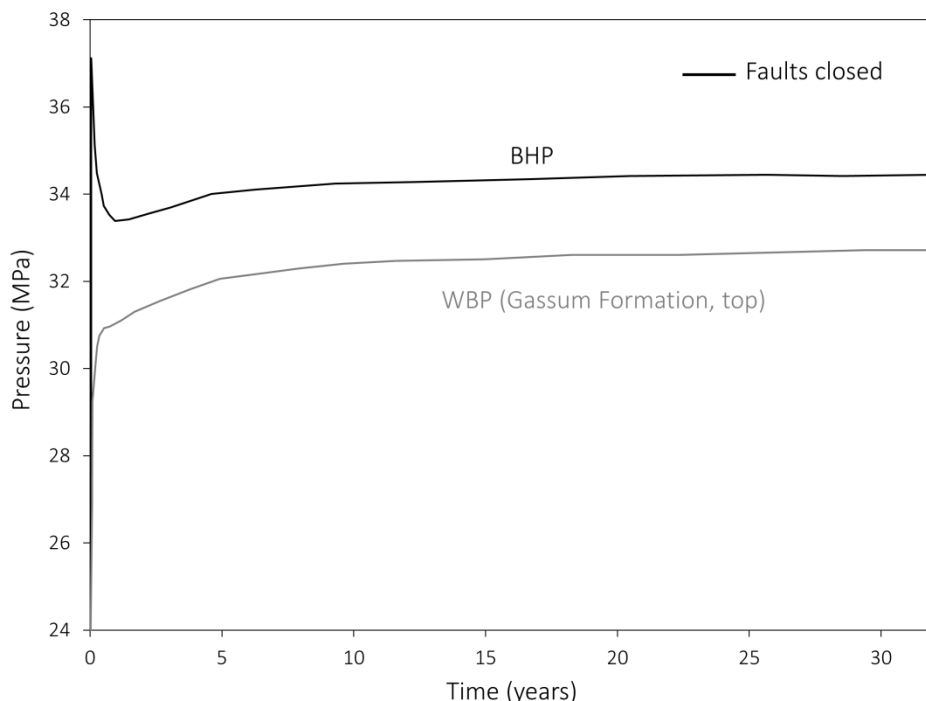


Figure 48: Development of the BHP (bottomhole pressure) and WBP (wellblock pressure) for hydraulically closed faults.

Pressure subsequently decreases down to 33.4 MPa and starts to increase again after 1.5 years up to 34.4 MPa at the end of the simulation after 40 years. The wellblock pressure (WBP) increases less sharply, but on contrary to the bottomhole pressure continuously during the entire injection period and reaching a value of 32.7 MPa after 40 years.

Figure 49 (left) illustrates that the pressure elevation after 40 years is restricted to the near-well area with a maximum of 11.8 MPa at the injection well and zero pressure build-up at the model

boundaries, respectively. As Figure 49 (left) shows, hydraulically closed faults lead to a higher pore pressure increase by about 8 MPa on the eastern side of Fault 3, facing the injection well compared to a pore pressure increase of 4 MPa west of Fault 3.

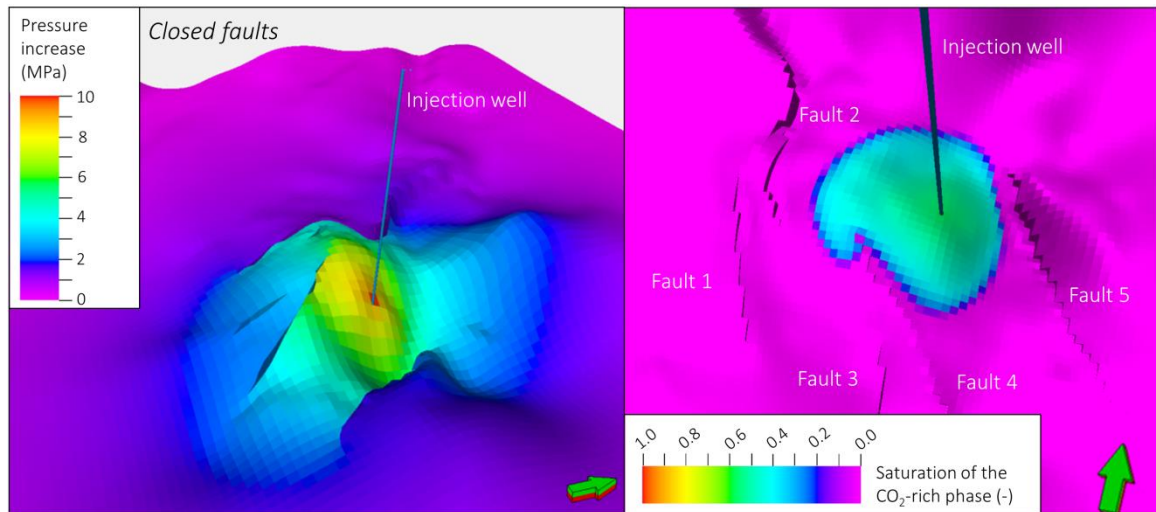


Figure 49: Pore pressure increase in the storage formation (left) and propagation of the CO₂-rich phase in the reservoir (right) after 40 years, assuming hydraulically non-conductive faults.

The CO₂-rich phase migrates preferentially to the anticline top due to buoyancy effects. Figure 36 (right) shows the gaseous CO₂ extent after 40 years. At this time, the CO₂ has already reached the western part of Fault 3 at the anticline top. Nevertheless, compared to the pressure build-up in the storage formation, a much smaller domain is affected by the CO₂ extent.

5.2.3.2 GEOMECHANICAL SIMULATIONS AND RESULTS

For computational reasons, a coarser model than that applied for flow simulations with ECLIPSE including the Gassum Storage Formation, the overburden up to the ground surface as well as one basement layer were introduced into the hydro-mechanical model. Therefore, the regional-scale model as described in Section 5.3.3.1 was reduced to a total number of 234,375 elements ($n_x = 125$, $n_y = 125$, $n_z = 15$), each with a lateral dimension of 400 m x 400 m, by merging different overburden layers. However, the vertical resolution of the storage reservoir (Gassum Formation) and its overlying caprock (Fjerritslev Formation) remained unchanged. The hydro-mechanical model was set up in VISAGE by embedding the coarsened reservoir model in a much larger domain in order to minimize the influence of model boundaries on pressure, and thus on stress changes. The vertical stress (S_v) prior to CO₂ injection was assumed to be determined by overlying rock load and calculated using an average rock density of 2,318 kg/m³ derived from available sonic log measurements. Table 9 lists the rock elastic properties and strength parameters assigned to the different lithological units.

Table 9: Densities and mechanical properties of the lithological units used in the VISAGE based hydro-mechanical model. Properties for the first lithological unit were taken from BELL (1977), while the properties for the remaining units were obtained from GOODMAN (1989).

Lithological unit	Density (kg/m ³)	Elastic modulus GPa)	Poisson ratio (-)	Friction angle (°)	Cohesion BC (UC) (MPa)
Post Chalk Group & Chalk Group	2,318	11.0	0.32	30	0.0 (2.6)
Vedsted Formation	2,318	8.50	0.27	15	0.0 (4.0)
Frederikshavn Formation	2,318	8.50	0.27	15	0.0 (4.0)
Boerglum Formation	2,318	8.50	0.27	15	0.0 (4.0)
Flyvbjerg Formation	2,318	8.50	0.27	15	0.0 (4.0)
Haldagar Formation	2,318	8.50	0.27	15	0.0 (4.0)
Fjerritslev Formation	2,318	8.50	0.27	15	0.0 (4.0)
Gassum Formation	2,318	15.0	0.32	35	0.0 (0.0)
Model basement	2,318	15.0	0.32	35	0.0 (0.0)

BC = Base case; UC = Unfavorable case

Two different scenarios with respect to the magnitude of the maximum (S_{Hmax}) and minimum (S_{hmin}) horizontal stresses were studied. In a base case scenario, the ratio of horizontal stresses to vertical stress is assumed to be equal to one ($S_v = S_{Hmax} = S_{hmin} = 1$). An unfavorable case examines the mechanical response of a strike-slip faulting regime to the CO₂ injection induced pore pressure changes ($S_{Hmax} > S_v > S_{hmin}$) with $S_{Hmax} = 1.2 S_v$ and $S_{hmin} = 0.8 S_v$, which is almost identical to the strike-slip faulting stress regime applied in the GFZ simulation strategy. Potential shear failure assessment was carried out by application of the Mohr-Coulomb failure criterion subsequent to the calculation.

Figure 50 shows that the pressure build-up as described above as well as presented in Figure 48 and 49 (left) would cause a maximum vertical displacement at the top of the Gassum Formation of about 9.4 cm and a ground surface uplift of 11.8 cm under the assumption of an isostatic stress field (base case).

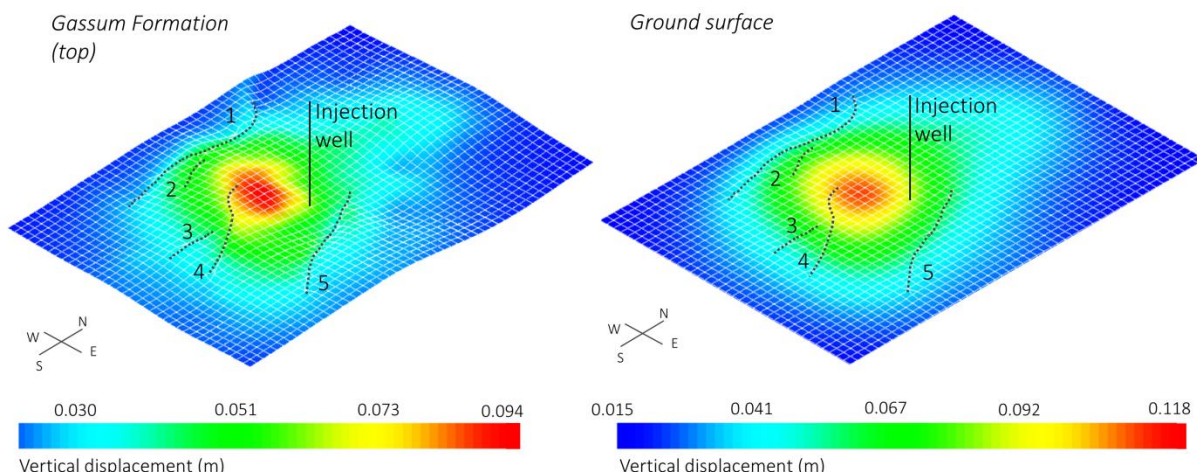


Figure 50: Vertical displacements for the base case scenario after 40 years of simulation.

Figure 51 (base case) and 52 (unfavourable case) show the tendency of shear failure occurrence as defined by the Mohr-Coulomb failure criterion. A value equal or greater than zero indicates that shear failure occurs, whereas a value smaller than zero indicates that shear failure is not to be expected and the rock remains intact. It can be seen from the two figures that the mechanical reservoir (Gassum Formation) and caprock (Fjerritslev Formation) integrity is not compromised after 40 years of CO₂ injection in both cases.

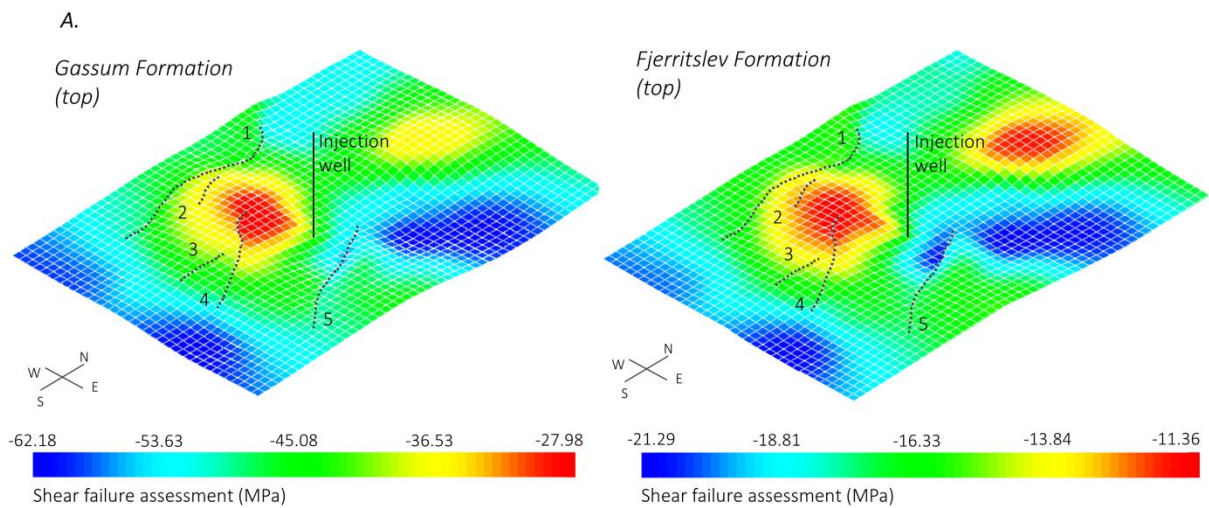


Figure 51: Shear failure assessment (base case) for reservoir (left) and overlying caprock (right) after 40 years.

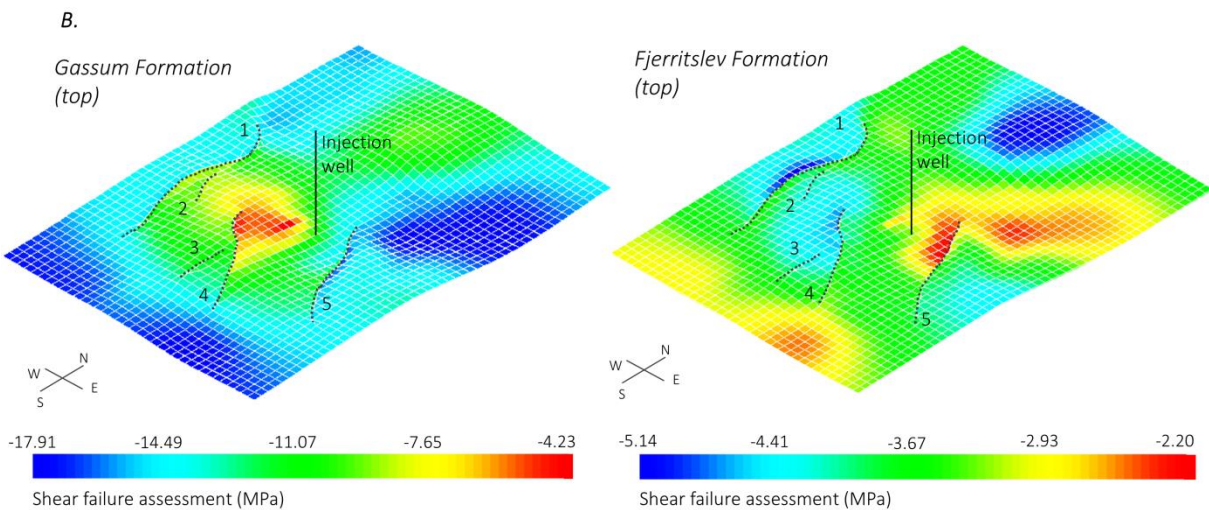


Figure 52: Shear failure assessment (unfavourable case) for reservoir (left) and overlying caprock (right) after 40 years.

However, the safety margin to shear failure is considerably reduced in the unfavourable case (Figure 52), even though the Post Chalk Group and Chalk Group as well as the remaining overburden were parameterized with cohesion values of 2.6 MPa and 4.0 MPa, respectively, whereas in the base case, zero cohesion was assigned to all formations.

5.3 SUMMARY AND DISCUSSION

For the assessment of CO₂ storage impacts at a prospective onshore saline aquifer, coupled dynamic flow and hydro-mechanical simulations were performed by two independent modelling groups. Both modelling groups applied a one-way hydro-mechanical coupling, using the pore pressure distribution from the reservoir simulations as coupling parameter. GFZ performed dynamic flow simulations using the TOUGH2-MP/ECO2N and hydro-mechanical simulations using the FLAC^{3D} software packages, whereas ICL applied the ECLIPSE simulator for fluid flow simulations and the VISAGE software package to calculate the coupled hydro-mechanical response to pore pressure changes.

Different assumptions were made by GFZ and ICL mainly with regard to model parameterization and discretization. The simulation results show that injecting 2 Mt CO₂/yr into an Upper Triassic sandstone reservoir over 40 years results in a maximum pore pressure increase by a factor between 1.45 (GFZ) and 1.6 (ICL), considering hydraulically non-conductive faults. Assuming hydraulically conductive faults allowing for cross-fault flow would reduce the maximum pore pressure increase to a factor of 1.4. The pressure increase in the reservoir after 40 years is mainly limited to the near-well area and declines continuously towards the model boundaries. However, at a distance of at least 20 km from the injection well, pressure increase is still 0.1 MPa, and thus propagates much further than the gaseous CO₂ reaching a maximum extent of 5.7 km x 5.5 km after 40 years. The hydro-mechanical simulation results show that pore pressure elevation leads to maximum vertical displacements of 7.9 cm at the reservoir top and 26.0 cm at the ground surface after 40 years of simulation assuming closed faults (GFZ). In accordance with the maximum pressure increase, maximum vertical displacements occur close to the injection well. The maximum vertical displacement is about 1.8 cm lower at the reservoir top and 5 cm lower at the ground surface, if faults are implemented as hydraulically conductive in horizontal direction. However, open faults allow for an unhindered and more rapid pressure propagation almost radial symmetrical around the injection well. Consequently, a larger area is affected by ground surface uplift but with comparably lower vertical displacements.

ICL calculated a slightly higher vertical displacement at the top of the reservoir of 9.4 cm and a lower ground surface uplift of 11.8 cm after 40 years of simulation considering closed faults. The difference in these results occurs mainly due to varying parameterization of the two hydro-mechanical models. GFZ used a caprock permeability of 0.01 mD, whereas ICL assumed a substantially lower value of 0.0001 mD, resulting in less pressure perturbation in the caprock, and thus higher vertical displacements at the reservoir top. Furthermore, the mean weight of the overburden was defined with 2,190 kg/m³ (GFZ) and 2,318 kg/m³ (ICL), respectively. Therefore, the magnitude of the vertical stress calculated by ICL is higher, inducing a lower vertical uplift of the overburden. In order to be able to localize potential failure, and thus fault slip at pre-defined fault planes, fault zones were implemented into the hydro-mechanical model as ubiquitous joints (GFZ). The simulation results show that neither fault slip, nor dilation is to be expected in the investigated time span, since both tendencies remained unchanged by CO₂ injection.

5.4 CONCLUSIONS

Two modelling groups carried out independent coupled hydro-mechanical simulations to evaluate the mechanical impact at a prospective Danish CO₂ storage site. Despite differing model discretization and parameterization, both modelling groups demonstrated that the mechanical reservoir, caprock and fault integrity is not compromised at any time. Major effective stress changes after 40 years of injection are limited to the injection well vicinity where the highest pressure build-up occurs. Calculated vertical displacements at the reservoir top and ground surface range between 9.4 cm - 26.0 cm depending on horizontal hydraulic fault conductivity and caprock permeability. Furthermore, the presented implementation of fault zones into the hydro-mechanical model allows for a spatial identification of potential zones of failure on the fault plane, and thus potential leakage pathways for formation fluids.

6 DISCUSSION AND CONCLUSION

Long-term underground geological storage of CO₂ in deep saline formations can contribute to the reduction of greenhouse gas emissions into the atmosphere and is therefore considered as a promising measure to prevent anthropogenic global warming and climate change. However, compromised reservoir and/or caprock integrity, reactivation of regional fault zones or large-scale displacement of resident formation brines due to the interaction between hydraulic and mechanical processes are possible adverse effects of industrial-scale CO₂ storage in saline aquifers that need to be explored thoroughly in advance of any field activity. If brine reaches shallower aquifer complexes, freshwater resources can be seriously impaired by salinization.

In the present dissertation, hydraulic and mechanical impacts of industrial-scale CO₂ injection into saline formations were assessed by application of coupled numerical simulations for two prospective storage sites. In the first part of this thesis, the focus was to quantify the degree and bandwidth of potential shallow aquifer salinization via upward brine migration through permeable regional fault zones using a multi-phase flow simulator. With that, factors and geological conditions that increase or diminish the risk of upward brine migration and potential freshwater salinization were identified. For this purpose, two 3D geological models with extents of 1,765 km² and 10,000 km² were implemented. In both models, the fault zones were represented specifically taking into account their complex geometry and curvature. In the regional-scale model, two regional fault zones located closest to the injection and consisting of individual faults with a thickness of 20 m each were represented by virtual elements. Thus, discrete faults were integrated in a very detailed manner. The supra-regional model considers all four regional fault zones located in the near- and far-field of the injection, which were integrated by real grid elements cut by the fault planes.

Simulation results show that pressure build-up in the reservoir is the driving force in upward brine migration: Larger reservoir pressures trigger higher upward brine migration rates through the permeable faults, and consequently higher salinities in the shallow aquifers. The magnitude of pressure build-up induced by fluid injection, and its release thereby, strongly depend on the choice of the lateral boundary conditions, the effective hydraulically conductive volume of fault damage zone and the presence of secondary reservoirs as part of a multi-barrier system overlying the storage formation. A spatially restricted reservoir that is implemented by closed model boundaries representing lateral barriers to flow due to e.g. impermeable or low-permeability layers or faults and unfractured bedrocks, causes the highest formation pressure increase, and thus triggers the highest brine migration rates. In all investigated scenarios in which the shallow aquifer is affected by salinization, salinity increases in close proximity to the fault zones only and does not spread over large areas. These observations are in good agreement with the findings of WALTER ET AL. (2012), who conclude that salinization of potable groundwater caused by CO₂ storage occurs most likely locally and not over large areas, if several overlying caprocks are present. Simulation results further demonstrate that in the shallow aquifer, brine spreads preferentially at the aquifer base, as also observed by OLDENBURG AND RINALDI (2011). The authors further point out that, if the dense brine is allowed spreading

laterally in the upper aquifer, upward flux is sustained until a new hydrostatic equilibrium is reached. All simulations in the present thesis assuming closed reservoir boundaries confirm these results. The mass of brine displaced into the shallow aquifer corresponds to the overall injected mass after several tens to hundreds of years, due to sustained fluid flow until the injection-related overpressure within the reservoirs is completely vanished. In this case, a short hydraulically conductive fault length and the presence of secondary reservoirs have only a temporal effect on upward brine migration and lead to fluid flow retardation by a factor of up to 3.4. Laterally open model boundaries representing a storage reservoir with quasi-infinite extension allow pressure dissipation, and thus significantly reduce the risk of shallow aquifer salinization. Contrary to closed lateral boundaries and depending on the hydraulically conductive fault length, here only about 30 % to 66 % of the corresponding brine mass is displaced into the shallow aquifer until a hydrostatic equilibrium has re-established. These findings support the results previously presented by CAVANAGH AND WILDGUST (2011). The authors illustrate the relevance of representing the site-specific geological boundary conditions as close as possible otherwise brine displacement processes might be over- or underestimated. The presence of an overlying secondary reservoir that is hydraulically connected to the faults leads to an additional decrease in shallow aquifer salinization, since the displaced brine also migrates into this reservoir. Again, depending on the hydraulically conductive fault length, only 12 % to 33 % of the brine mass that is displaced into the shallow aquifer when lateral reservoir boundaries are closed and no overlying reservoir exists, reaches the uppermost aquifer in this case. Hence, it can be assumed that the risk of shallow aquifer salinization is considerably reduced with each aquifer lying in between the reservoir and the shallow aquifer. BIRKHOLZER ET AL. (2009) achieved similar results and showed that the amount of fluid displaced into formations above the reservoir, decreases in upward direction due to the attenuation capacity of the overlying rocks. NORDBOTTEN ET AL. (2004) further observed a successive decrease in the intensity of fluid upward displacement through a leaky well, caused by loss of fluid into the intermediate aquifer layers. An aquifer with infinite extension that allows for unhindered lateral pressure propagation is probably a simplification of nature, especially in tectonically influenced systems. The presence of further permeable layers overlying the storage formation, is more likely instead, for instance in a multi-barrier system. Aquifer systems should rather be considered as semi-open/semi-closed, and thus partly bounded by impervious flow barriers that constrain lateral pressure propagation.

Fault permeability has only a minor impact on shallower aquifer salinization. The difference in salinity increase in the shallowest model layer is only little, when varying the fault permeability between 100 mD and 10,000 mD because also the pressure increase in the shallow aquifer is almost identical. When a sufficient pressure gradient exists, faults apparently do not need to be highly permeable to allow upward brine migration. MBIA ET AL. (2014) recently investigated vertical pressure transmission through overlying rocks via permeable faults, at the prospective Danish CO₂ storage site Vedsted. Faults with a permeability ranging from 0.001 mD to 1,000 mD connect the reservoir formation with upper aquifers. For a fault permeability lower than 1.0 mD, no pressure build-up was observed in the shallow aquifer, whereby pressure increase was between 0.3 bar and 5.0 bar for the cases with 1.0 mD to 1,000 mD fault permeability. These investigations support the assumption that even lower fault permeabilities of 1.0 mD or 10 mD might be sufficient to promote upward brine migration. In a spatially restricted reservoir, the simulation results presented in this thesis demonstrate that fault permeability has only a

temporal effect without any significant change in salinization due to the closed model boundaries. Salinity levels of upper aquifers are almost the same, however, delayed in case of less permeable faults. In turn, the relation between the permeability of faults and reservoirs overlying the storage formation is decisive with regard to shallow aquifer salinization, since the preferable brine flow direction depends on it. If the permeability of the secondary reservoir exceeds that of the fault, the mass of brine migrating into the shallowest aquifer is only around a quarter of that observed in the opposite case. Within the frame of this thesis, it is further demonstrated that the effective, hydraulically conductive volume of the fault damage zones has a strong influence on the duration and intensity of upward brine mass flow. In case of only one permeable fault or a short hydraulically conductive fault segment, smaller areas in the upper aquifer are affected by salinization. Nevertheless, a small conductive fault segment leads to higher salinities and a greater lateral propagation of the saltwater in the shallow aquifer, since pressure dissipation occurs over a smaller area, and brine flow rates into the fault are correspondingly higher. Here, the shallow aquifer is affected by salinization up to a maximum lateral distance of about 6 km from the fault core. The presence of multiple permeable faults exposing a large effective damage zone volume, leads to a more distributed and diluted salinization and lower spatial widths of saltwater distribution (maximum lateral distance of 2.4 km from fault core). Thus, the effective damage zone volume of hydraulically conductive faults is essential for the degree and occurrence of shallow aquifer salinization.

Underground utilization and associated injection-induced pressure increase in storage formations and surrounding rocks can significantly increase the potential of upward brine migration through faults, if these expose slip or dilation due to failure in shear or tension or the altered stress state. Hence, the focus in the second part of this thesis was to assess the potential of fault reactivation in the Beeskow-Birkholz study area and to estimate the magnitude of ground surface uplift to determine potential damage of surface infrastructure. Thereto, a supra-regional-scale 3D geological model with an extent of 10,000 km² including four ambient regional fault zones was successfully implemented in one-way coupled hydro-mechanical simulations. The applied one-way coupling procedure considers the time-dependent pore pressure development obtained from the flow simulations as input to a hydro-mechanical simulator. The hydro-mechanical simulator then calculates stress and strain changes based on the applied constitutive law, and then determines resulting rock mass failure from the calculated effective stress changes. A one-way coupling is undertaken without any feedback to the flow simulator, while a two-way coupling integrates porosity and permeability changes derived from stress changes or volumetric strain increments. For coupling evaluation, the one-way coupling was also performed for one equivalent storage site close to Vedsted in Northern Denmark including a benchmark against the results produced by another well-established modelling group. At both sites, fault zones were represented by plasto-elastic constitutive models, using embedded weak planes at the respective fault element locations, oriented in the same direction as the fault plane. This is an adequate approach for the consideration of discrete fault planes in hydro-mechanical models, since the presence of displacements along faults as well as the repeated occurrence of shear zones and local deformation suggests that fault zones are rather weak compared with the host rock matrix (FAULKNER ET AL., 2010; GUDMUNDSSON ET AL., 2010; RUTTER ET AL., 2001; CAINE ET AL., 1996). Furthermore, this implementation allows for a spatial identification of potential zones of failure on the fault plane, and thus the identification of potential leakage

pathways for formation fluids and CO₂. In a first order approach, the pressure distribution at the Beeskow-Birkholz site, which was obtained from the flow simulations, was fitted by polynomial functions and integrated into the hydro-mechanical simulator for selected time steps.

The results of this hydro-mechanical one-way coupling show that the stress state of the caprock, reservoir and faults exhibits only a punctual occurrence of shear (< 1 %) and the complete absence of tensile failure, indicating that a consistent slip plane did not develop. Thus, injection-induced fault reactivation is unlikely in the Beeskow-Birkholz study area, given the applied initial and boundary conditions. Vertical displacements (uplift) at the ground surface and the reservoir top reached 0.41 cm and 1.2 cm at the maximum pore pressure increase located close to the injection well within a radius of 3,500 m after 10 days of simulation. The maximum spatial pore pressure perturbation is achieved at the end of the injection period after 20 years, where calculated uplifts amount to 2.1 cm (ground surface) and 2.5 cm (reservoir top), respectively. Not only displacements are higher after 20 years, in correspondence with the spatial propagation of pore pressure, but also the area affected by ground uplift is hundred times larger than at a simulation time of 10 days. MAGRI ET AL. (2013) carried out a regional-scale sensitivity analysis for the same storage operation, observed similar displacement patterns and vertical displacements after 10 days of simulation. Calculated vertical displacements after 20 years were only half as large. However, MAGRI ET AL. (2013) considered hydraulically conductive faults, so that the calculated pressure increase and effective stress changes were lower.

For the evaluation of the coupling methodology, a one-way coupling was additionally performed for an equivalent storage site located close to the city of Vedsted in Northern Denmark. In contrary to the Beeskow-Birkholz study area, where different models were employed for multi-phase flow and hydro-mechanical simulations, the application of identical models for this process coupling based on identical element coordinates allowed an element-wise implementation of the time-dependent pore pressure distribution from the flow simulator into the hydro-mechanical simulator. Simulation results demonstrate that fault reactivation at the Vedsted site is also unlikely under the tested initial and boundary conditions. The fault slip and dilation tendencies remained below critical values (< 1) at any time during the injection period and thereafter. The slip tendency of a fault is defined as the ratio of shear to normal stress acting on the fault plane, whereby the dilation tendency depends on the fault orientation to the minimum principal stress. Nevertheless, injection at the Vedsted site was simulated for a longer period as in the simulations of the Beeskow-Birkholz site. This leads to higher vertical uplift at ground surface (maximum of 26 cm) and reservoir top (maximum of 7.9 cm). The magnitude of ground surface uplift thereby strongly depends on fault conductivity and caprock permeability. Raising the caprock permeability by two orders of magnitude in the Vedsted simulation model, slightly reduces the uplift at the reservoir top due to the increased pressure propagation into the caprock, however, this almost triples vertical displacements at the ground surface. Hydraulically conductive faults slightly reduce the maximum pore pressure increase, and thereby the maximum vertical displacement by several centimetres at reservoir top and ground surface. However, due to the greater spatial extent of the pressure increase in case of hydraulically permeable faults, the area affected by ground surface uplift is also larger.

In summary, application of numerical models lead to site-specific insights into the fluid flow dynamics in geological CO₂ storage. The proposed and new workflow based on 3D geological

model and discrete fault zone implementation as well as the applied methodology for the accomplishment of one-way coupled simulations was proven appropriate for determining CO₂ storage impacts in faulted geological systems. At the same time, the simulations are a measure to identify the geological conditions with the greatest impact on upward brine migration through permeable fault zones, and provide an initial assessment of the anticipated risks including their extent and significance.

It was shown that the presence of hydraulically conductive faults does not necessarily lead to shallow aquifer salinization, since various other factors influence the occurrence and degree of shallow aquifer salinization at the Beeskow-Birkholz site. In order to assess the potential of shallow aquifer salinization and fault reactivation in the Beeskow-Birkholz study area, the site-specific insights and facts have to be considered: the thickness of several impermeable intermediate caprocks overlying the storage formation varies between 35 m to 320 m. It is probably more reasonable to expect that the permeability of the fault zones does not exceed that of each caprock, than to assume an overall transmissible fault. Moreover, at least three further reservoirs from the Middle Buntsandstein, the Lower Muschelkalk as well as the Middle Keuper are overlying the potential storage formation located in the Middle Buntsandstein and will probably dampen brine displacement into the shallow aquifers. Fluids would partly be displaced into these layers instead of further migrating upwards as demonstrated by the simulations carried out within the scope of this thesis. Simulation results further showed that the degree of shallow aquifer salinization strongly depends on the initial salinity distribution in the faults, since the brine that is displaced into the shallower aquifers originates solely from the upper part of the fault and not from greater depths. Thus, if the salinity gradient is low or the saltwater-freshwater boundary lies below this depth, shallow aquifer salinization is considerably reduced or unlikely to occur.

With respect to the formulated objectives of this thesis and the findings gained thereof, it can be summarized that salinization of shallow aquifers due to CO₂ storage is unlikely to occur over vast areas at the Beeskow-Birkholz site. It might rather develop to a local problem, since local and very permeable segments within the faults affect a higher vertical migration distance for brine, resulting in a higher potential for possible freshwater salinization, although the three interlayered reservoirs as well as at least partly laterally open aquifers significantly reduce the probability of its occurrence. Structural failure was not observed at the respective site, which further minimizes the potential of upper aquifer salinization. However, in a least favourable scenario with maximum reservoir pressures and brine flow rates, fault mass flow was implemented as a boundary condition into a shallow aquifer model including groundwater resources. The maximum salinity increase above the salt-freshwater boundary was calculated to be locally more than 13-times above the limit prescribed in the German Drinking Water Directive (KEMPKA ET AL., 2015).

In order to enable more precise predictions of the spatial effects of upward brine migration on local groundwater resources without using a coupling of deeper reservoir models with shallower aquifer models, supra-regional scale models extending up to the ground surface should be developed and implemented in numerical simulations. However, integrating complex structures such as fault zones, regional discontinuities of formations or topographic variations into large-scale models is computationally very expensive and numerically challenging. For this reason, site-specific investigations on e.g. brine displacement processes as presented in this thesis are

currently very rare. Moreover, considerable uncertainty is associated with the underlying geological models, since e.g. internal structures of fault zones are unknown and difficult to detect. It is therefore important to implement the models as complex as possible to make still reliable and realistic numerical predictions. As demonstrated in this thesis, fault zones can be adequately represented in a model grid without neglecting their complex geometry and curvature. The applied approach allows quantifying the potential spectrum of upward brine migration for the respective site by taking into account a range of parameters and possible fault-end-members. Furthermore, a spatial identification of potential failure zones on the fault is feasible by this method. As shown in this thesis, the injection-induced pressure increase leads to a decrease in effective stresses. In this context, the application of a two-way hydro-mechanical coupling is recommended for future investigation to account also for fault fill permeability and porosity changes resulting from volumetric strain increments, and thus potential alteration of fluid flow behaviour (E.G. ADAMS ET AL., 2014; CAPPÀ AND RUTQVIST, 2011; CHIN ET AL., 2000).

REFERENCES

- Adams, M., Feinendegen, M., Ziegler, M., Kempka, T. (2014): Geomechanical simulation of the injection of CO₂ into saline aquifers with respect to risk assessment. In: Alejano, L., Perucho, A., Olalla, C. (Eds.), Rock Engineering and Rock Mechanics: Structures in and on Rock Masses. Proceedings of EUROCK 2014, ISRM European Regional Symposium, Leiden: CRC Press/Balkema, p. 1305-1310.
- Bachu, S., Bennion, D.B. (2009): Experimental assessment of brine and/or CO₂ leakage through well cements at reservoir conditions. International Journal of Greenhouse Gas Control, 3, p. 494-501.
- Beer, H. (2000): Geologische Übersichtskarte des Landes Brandenburg 1:300 000, Tiefenlinienkarte der Zechsteinoberfläche. Landesamt für Geowissenschaften und Rohstoffe Brandenburg (LGRB) und Landesvermessungsamt Brandenburg (LVA), Kleinmachnow/Potsdam.
- Bell, F.G. (1977): A note on the physical properties of chalk. Engineering Geology, 11 (3), p. 217-225.
- Benson, S.M., Cole, D.R. (2008): CO₂ Sequestration in Deep Sedimentary Formations. Elements, 4 (5), p. 325-331.
- Beutler, G., Stackebrandt, W. (2012): Der Schollenbau des Tafeldeckgebirges von Brandenburg – Vorschlag für eine einheitliche Benennung [The tectonic pattern of the sedimentary cover of Brandenburg – suggestion for a uniform nomenclature]. Brandenburgische Geowissenschaftliche Beiträge, 19 (1), p. 93-109.
- Birkholzer, J.T., Zhou, Q., Tsang, C.-F. (2009): Large-scale impact of CO₂ storage in deep saline aquifers: A sensitivity study on pressure response in stratified systems. International Journal of Greenhouse Gas Control, 3, p. 181-194.
- Birkholzer, J.T., Nicot, J.P., Oldenburg, C.M., Zhou, Q., Kraemer, S., Bandilla, K. (2011): Brine flow up a well caused by pressure perturbation from geologic carbon sequestration: Static and dynamic evaluations. International Journal of Greenhouse Gas Control, 5, p. 850-861.
- Britze, P., Japsen, P. (1991): Geological map of Denmark 1:400,000. The Danish Basin. “Top Zechstein” of the Triassic (two-way traveltimes and depth, thickness and interval velocity). Geological Survey of Denmark Map Series, 31, 4 maps and 4 pp.
- Caine, J.S., Evans, J.P., Forster, C.B. (1996): Fault zone architecture and permeability structure. Geology, 24 (11), p. 1025-1028.
- Cappa, F. (2009): Modelling fluid transfer and slip in a fault zone when integrating heterogeneous hydromechanical characteristics in its internal structure. Geophysical Journal International, 178 (3), p. 1357-1362.

REFERENCES

- Cappa, F., Rutqvist, J. (2011): Modeling of coupled deformation and permeability evolution during fault reactivation induced by deep underground injection of CO₂. International Journal of Greenhouse Gas Control, 5 (2), p. 336-346.
- Cavanagh, A., Wildgust, N. (2011): Pressurization and brine displacement issues for deep saline formation CO₂ storage. Energy Procedia, 4, p. 4814-4821.
- Celia, M.A., Nordbotten, J.M., Court, B., Dobossy, M., Bachu, S. (2011): Field-scale application of a semi-analytical model for estimation of CO₂ and brine leakage along old wells. International Journal of Greenhouse Gas Control, 5, p. 257-269.
- Chabora, E.R., Benson, S.M. (2009): Brine Displacement and Leakage Detection Using Pressure Measurements in Aquifers Overlying CO₂ Storage Reservoirs. Energy Procedia, 1, p. 2405-2412.
- Chester, F.M., Logan, J.M. (1986): Implications for mechanical-properties of brittle faults from observations of the Punchbowl fault zone, California. Pure and Applied Geophysics, 124 (1-2), p. 79-106.
- Chin, L.Y., Raghavan, R., Thomas, L.K., (2000): Fully Coupled Geomechanics and Fluid-Flow Analysis of Wells With Stress-Dependent Permeability. Society of Petroleum Engineers, 5 (1), p. 32-45.
- Dalhoff, F., Klinkby, L., Sørensen, A.T., Bernstone, C., Frykman, P., Andersen, C., Christensen, N.P. (2011): CCS demo Denmark: The Vedsted case. Energy Procedia, 4, p. 4704-4710.
- Faulkner, D.R., Jackson, C.A.L., Lunn, R.J., Schlische, R.W., Shipton, Z.K., Wibberley, C.A.J., Withjack, M.O. (2010): A review of recent developments concerning the structure, mechanics and fluid flow properties of fault zones. Journal of Structural Geology, 32, p. 1557-1575.
- Frykman, P., Bech, N., Sørensen, A.T., Nielsen, L.H., Nielsen, C.M., Kristensen, L., Bidstrup, T. (2009): Geological modeling and dynamic flow analysis as initial site investigation for large-scale CO₂ injection at the Vedsted structure, NW Denmark. Energy Procedia, 1 (1), p. 2975-2982.
- Frykman, P., Nielsen, C.M., Dalhoff, F., Sørensen, A.T., Klinkby, L., Nielsen, L.H. (2011): Geological modelling for site evaluation at the Vedsted structure, NW Denmark. Energy Procedia, 4, p. 4711-4718.
- Gasda, S. E., Nordbotten, J. M., Celia, M. A. (2011): Vertically averaged approaches for CO₂ migration with solubility trapping. Water Resources Research, 47 (5), W05528, 14 pp.
- Goodman, R.E. (1989): Introduction to rock mechanics. 2nd ed. John Wiley and Sons, 562 pp.
- Grandy, J. (1997): Efficient Computation of Volume of Hexahedral Cells. Technical report, Lawrence Livermore National Laboratory, Livermore, California. Online: <http://www.osti.gov/bridge/purl.cover.jsp?purl=/632793-4p2OLa/webviewable/632793.pdf>.
- Greiner, G., Hormann, K. (1998): Efficient clipping of arbitrary polygons. ACM Transactions on Graphics, 17 (2), p. 71-83.
- Grube, A., Wichmann, K., Hahn, J., Nachtigall, K.H. (2000): Geogene Grundwasserversorgung in

- den Poren-Grundwasserleitern Norddeutschlands und ihre Bedeutung für die Wasserwirtschaft. DVGW-Technologiezentrum Wasser (TZW), Band 9, Karlsruhe, 203 pp.
- Gudmundsson, A., Simmenes, T.H., Larsen, B., Philipp, S.L. (2010): Effects of internal structure and local stresses on fracture propagation, deflection, and arrest in fault zones. *Journal of Structural Geology*, 32, p. 1643-1655.
- Hannemann, M., Schirrmeister, W. (1998): Paläohydrogeologische Grundlagen der Entwicklung der Süß-/Salzwassergrenze und der Salzwasseraustritte in Brandenburg [Paleohydrological basics of the development of the boundary of fresh and salt water as well as of the salt water-outlets in Brandenburg]. *Brandenburgische Geowissenschaftliche Beiträge*, 5 (2), p. 61-72.
- Holloway, S. (2005): Underground sequestration of carbon dioxide – a viable greenhouse gas mitigation option. *Energy*, 30, p. 2318-2333.
- Hotzan, G., Voss, T. (2013): Komplexe hydrogeochemisch-genetische Kartierung zur Einschätzung der Salzwassergefährdung pleistozäner und tertiärer Grundwasserleiter im Raum Storkow-Frankfurt (Oder)-Eisenhüttenstadt [Complex hydrogeochemical-genetic mapping for evaluation of the endangerment of pleistocene and tertiary aquifers by saline waters in the region Storkow-Frankfurt (Oder)-Eisenhüttenstadt]. *Brandenburgische Geowissenschaftliche Beiträge*, 20 (1/2), p. 62-82.
- IEAGHG (2010): Pressurization and brine displacement issues for deep saline formation CO₂ storage. Report: 2010/15, 58 pp.
- IPCC (2005): Carbon Dioxide Capture and Storage. In: Metz, B., Davidson, O., de Coninck, H.C., Loos, M., Meyer, L.A. (Eds.), *IPCC Special Report. Prepared by Working Group III of the Intergovernmental Panel on Climate Change*. Cambridge University Press, Cambridge, United Kingdom and New York, NY, USA, 442 pp.
- Jiang, D., Williams, P., Carter, B. (2004): Numerical modeling of the development of kink-bands in anisotropic plastic materials. In: Köhn, D., Malthe-Sørensen, A. (Eds.), *Numerical Modeling of Microstructures. Journal of the Virtual Explorer, Electronic Edition*, 15, Paper No. 4.
- Johnson, J. W., Nitao, J. J., Knauss, K. G. (2004): Reactive Transport Modelling of CO₂ Storage in Saline Aquifers to Elucidate Fundamental Processes, Trapping Mechanisms, and Sequestration Partitioning. In: Baines, S. J., Worden, R. H. (Eds.), *Geologic Storage of Carbon Dioxide. Geological Society Special Publications*, 233, p. 107-128.
- Jourde, H., Flodin, E., Aydin, A., Durlovsky, L., Wen, X. (2002): Computing permeability of fault zones in eolian sandstone from outcrop measurements. *The American Association of Petroleum Geologists Bulletin*, 86 (7), p. 1187-1200.
- Katzung, G., Ehmke, G. (1993): Das Prätertiär in Ostdeutschland: Strukturstockwerke und ihre regionale Gliederung. Verlag Sven von Loga, Köln, 139 pp.
- Kempka, T., Kühn, M. (2013): Numerical simulations of CO₂ arrival times and reservoir pressure coincide with observations from the Ketzin pilot site, Germany. *Environmental Earth Sciences*, 70 (8), p. 3675-3685.

Kempka, T., Nielsen, C. M., Frykman, P., Shi, J.-Q., Bacci, G., Dalhoff, F. (2014 online): Coupled Hydro-Mechanical Simulations of CO₂ Storage Supported by Pressure Management Demonstrate Synergy Benefits from Simultaneous Formation Fluid Extraction. *Oil & Gas Science and Technology*.

Kempka, T., Herd, R., Huenges, E., Endler, R., Jahnke, C., Janetz, S., Jolie, E., Kühn, M., Magri, F., Meinert, P., Moeck, I., Möller, M., Muñoz, G., Ritter, O., Schafrik, W., Schmidt-Hattenberger, C., Tillner, E., Voigt, H.-J., Zimmermann, G. (2015): Joint Research Project Brine: Carbon Dioxide Storage in Eastern Brandenburg: Implications for Synergetic Geothermal Heat Recovery and Conceptualization of an Early Warning System Against Freshwater Salinization. In: Liebscher, A., Münch, U. (Eds.), *Geological Storage of CO₂ – Long Term Security Aspects*. GEOTECHNOLOGIEN Science Report No.22, Advanced Technologies in Earth Sciences, Springer International Publishing, p. 139-166.

Knopf, S., May, F., Mueller, C., Gerling, J.P. (2010): Neuberechnung möglicher Kapazitäten zur CO₂-Speicherung in tiefen Aquifer-Strukturen. *Energiewirtschaftliche Tagesfragen*, 60 (4), p. 76-80.

Kopf, M. (1965): Feldgeologie – Dichtebestimmung, Norddeutsch-Polnisches Becken, Ergebnisbericht. VEB Geophysik Leipzig, Unpublished Report, 47 pp.

Kühn, M., Kempka, T., Jolie, E. (2011): Evaluation of potential pressurization and salinization of freshwater reservoirs by brine migration as a result of geological CO₂ storage. *GeoProc 2011*, Perth, Australia, 6-9 July 2011, Paper No. GP026, p. 1-9.

Larsen, M., Bidstrup, T., Dalhoff, F. (2003): CO₂ storage potential of selected saline aquifers in Denmark. *Danmarks og Grønlands Geologiske Undersøgelse Rapport*, 39, 83 pp.

Lemieux, J.M. (2011): Review: The potential impact of underground geological storage of carbon dioxide in deep saline aquifers on shallow groundwater resources. *Hydrogeology Journal*, 19, p. 757-778.

Leverett, M.C. (1941) Capillary behaviour in porous solids. *Transactions of the AIME* (142): p. 159-172.

MacMinn, C. W., Szulczeński, M. L., Juanes, R. (2011): CO₂ migration in saline aquifers. Part 2. Capillary and solubility trapping. *Journal of Fluid Mechanics*, 688, p. 321-351.

Magri, F., Bayer, U., Jahnke, C., Clausnitzer, V., Diersch, H., Fuhrman, J., Möller, P., Pekdeger, A., Tesmer, M., Voigt, H. (2005): Fluid-dynamics driving saline water in the North East German Basin. *International Journal of Earth Sciences*, 94 (5-6), p. 1056-1069.

Magri, F., Bayer, U., Tesmer, M., Möller, P., Pekdeger, A. (2008): Salinization problems in the NEGB: results from thermohaline simulations. *International Journal of Earth Sciences*, 97 (5), p. 1075-1085.

Magri, F., Tillner, E., Wang, W., Watanabe, N., Zimmermann, G., Kempka, T. (2013): 3D hydro-mechanical scenario analysis to evaluate changes of the recent stress field as a result of geological CO₂ storage. *Energy Procedia*, 40, p. 375-383.

- Martens, S., Kempka, T., Liebscher, A., Lüth, S., Möller, F., Myrttinen, A., et al. (2010): Europe's longest-operating on-shore CO₂ storage site at Ketzin, Germany: a progress report after three years of injection. *Environmental Earth Sciences*, 67 (2), p. 323-334.
- Mbia, E.N., Frykman, P., Nielsen, C.M., Fabricius, I.L., Pickup, G.E., Sørensen, A.T. (2014): Modeling of the pressure propagation due to CO₂ injection and the effect of fault permeability in a case study of the Vedsted structure, Northern Denmark. *International Journal of Greenhouse Gas Control*, 28, p. 1-10.
- Michael, K., Golab, A., Shulakova, V., Ennis-King, J., Allinson, G., Sharma, S., Aiken, T. (2010): Geological storage of CO₂ in saline aquifers – A review of the experience from existing storage operations. *International Journal of Greenhouse Gas Control*, 4 (4), p. 659-667.
- Mitchell, T.M. Faulkner, D.R. (2009): The nature and origin of off-fault damage surrounding strike-slip fault zones with a wide range of displacements: A field study from the Atacama fault zone, northern Chile. *Journal of Structural Geology*, 31 (8), p. 802-816.
- Moeck, I., Schandelmeier, H., Holl, H.-G. (2009): The stress regime in a Rotliegend reservoir of the Northeast German Basin. *International Journal of Earth Sciences*, 98 (7), p. 1643-1654.
- Nagelhout, A.C.G., Roest, J.P.A. (1997): Investigating fault slip in a model of an underground gas storage facility. *International Journal of Rock Mechanics and Mining Sciences*, 34 (3-4), Paper No. 212.
- Nakaten, B., Tillner, E., Kempka, T. (2013): Virtual Elements for Representation of Faults, Cracks and Hydraulic Fractures in Dynamic Flow Simulations. *Energy Procedia*, 40, p. 447-453.
- Nakaten, B., Kempka, T. (2014): Workflow for fast and efficient integration of Petrel-based fault models into coupled hydro-mechanical TOUGH2-MP - FLAC3D simulations of CO₂ storage. *Energy Procedia*, 63, p. 3576-3581.
- Nicot, J.P. (2008): Evaluation of large-scale CO₂ storage on fresh-water sections of aquifers: An example from the Texas Gulf Coast Basin. *International Journal of Greenhouse Gas Control*, 2, p. 582-593.
- Nielsen, L.H. (2003): Late Triassic – Jurassic development of the Danish Basin and the Fennoscandian Border Zone, southern Scandinavia. In: Ineson, J.R., Surlyk, F. (Eds.), *The Jurassic of Denmark and Greenland*. Geological Survey of Denmark and Greenland Bulletin, 1, p. 459-526.
- Nordbotten, J.M., Celia, M.A., Bachu, S. (2004): Analytical solutions for leakage rates through abandoned wells. *Water Resources Research*, 40 (4), W04204, 10 pp.
- Oelkers, E.H., Cole, D.R. (2008): Carbon Dioxide Sequestration: A Solution to a Global Problem. *Elements*, 4, p. 305-310.
- Oldenburg, C.M., Rinaldi, A.P. (2011): Buoyancy Effects on Upward Brine Displacement Caused by CO₂ Injection. *Transport in Porous Media*, 87, p. 525-540.

REFERENCES

- Orlic, B. (2009): Some Geomechanical aspects of geological CO₂ sequestration. KSCE Journal of Civil Engineering, 13 (4), p. 225-232.
- Ouellet, A., Bérard, T., Frykman, P., Welsh, P., Minton, J., Pamucku, Y., et al. (2010): Reservoir geomechanics case study of seal integrity under CO₂ storage conditions at Ketzin, Germany. Ninth Annual Conference on Carbon Capture and Sequestration, 10-13 May 2010.
- Person, M., Banerjee, A., Rupp, J., Medina, C., Lichtner, P., Gable, C., Pawar, R., Celia, M., McIntosh, J., Bense, V. (2010): Assessment of basin-scale hydrologic impacts of CO₂ sequestration, Illinois basin. International Journal of Greenhouse Gas Control, 4 (5), p. 840-854.
- Pruess, K., Garcia, J. (2001): Multiphase flow dynamics during CO₂ disposal into saline aquifers. Environmental Geology, 42, p. 282-295.
- Pruess, K. (2005a): Numerical studies of fluid leakage from a geologic disposal reservoir for CO₂ show self-limiting feedback between fluid flow and heat transfer. Geophysical Research Letters, 32 (14), L14404, 4 pp.
- Pruess, K. (2011): Modeling CO₂ leakage scenarios, including transitions between super- and sub-critical conditions, and phase change between liquid and gaseous CO₂. Energy Procedia, 4, p. 3754-3761.
- Röhmann, L., Tillner, E., Magri, F., Kühn, M., Kempka, T. (2013): Fault Reactivation and Ground Surface Uplift Assessment at a Prospective German CO₂ Storage Site. Energy Procedia, 40, p. 437-446.
- Rutter, E.H., Holdsworth, R.E., Knipe, R.J. (2001): The nature and tectonic significance of fault zone weakening: an introduction. Geological Society Special Publications, 186, p. 1-11.
- Rutqvist, J., Tsang, C.-F. (2001): A study of caprock hydromechanical changes associated with CO₂-injection into a brine formation. Environmental Geology, 42, p. 296-305.
- Rutqvist, J., Wu, Y.-S., Tsang, C.-F., Bodvarsson, G. (2002): A modeling approach for analysis of coupled multiphase fluid flow, heat transfer, and deformation in fractured porous rock. International Journal of Rock Mechanics and Mining Sciences, 39 (4), p. 429-442.
- Rutqvist, J., Birkholzer, J., Cappa, F., Tsang, C.F. (2007): Estimating maximum sustainable injection pressure during geological sequestration of CO₂ using coupled fluid flow and geomechanical fault-slip analysis. Energy Conversion and Management, 48, p. 1798-1807.
- Rutqvist, J., Birkholzer, J.T., Tsang, C.-F. (2008): Coupled reservoir-geomechanical analysis of potential for tensile and shear failure associated with CO₂ injection in multilayered reservoir-caprock systems. International Journal of Rock Mechanics and Mining Sciences, 45, p. 132-143.
- Rutqvist, J., Vasco, D.W., Myer, L. (2010): Coupled Reservoir-Geomechanical Analysis of CO₂ Injection at In Salah, Algeria. Energy Procedia, 1(1), p. 1847-1854.
- Rutqvist, J. (2011): Status of the TOUGH-FLAC simulator and recent applications related to coupled fluid flow and crustal deformations. Computational Geosciences, 37 (6), p. 739-750.

- Rutqvist, J. (2012): The geomechanics of CO₂ storage in deep sedimentary formations. *Geotechnical and Geological Engineering*, 30 (3), p. 525-551.
- Savage, H.M., Brodsky, E.E. (2011): Collateral damage: Evolution with displacement of fracture distribution and secondary fault strands in fault damage zones. *Journal of Geophysical Research: Solid Earth*, 116 (B3), 14 pp.
- Scheck, M., Bayer, U. (1999): Evolution of the Northeast German Basin - inferences from a 3D structural model and subsidence analysis. *Tectonophysics*, 313, p. 145-169.
- Scheck, M., Bayer, B., Lewerenz, B. (2003): Salt movements in the Northeast German Basin and its relation to major post-Permian tectonic phases – results from 3D structural modelling, backstripping and reflection seismic data. *Tectonophysics*, 361, p. 277-299.
- Schulz, R., Agemar, T., Alten, A.-J., Kühne, K., Maul, A.-A., Pester, S., Wirth, W. (2007): Aufbau eines geothermischen Informationssystems für Deutschland [Development of an Internet Based Geothermal Information System for Germany]. *Erdöl Erdgas Kohle*, 123 (2), p. 76-81.
- Sedlacek, R. (1999): Untertage Erdgasspeicherung in Europa [Underground Gas Storage in Europe]. *Erdöl Erdgas Kohle*, 115 (11), p. 537-540.
- Shipton, Z., Soden, A., Kirkpatrick, J., Bright, A., Lunn, R. (2006): How Thick is a Fault? Fault Displacement-Thickness Scaling Revisited. In: Abercrombie, R., McGarr, A., Di Toro, G., Kanamori, H. (Eds.), *Earthquakes: Radiated Energy and the Physics of Faulting*. American Geophysical Union, Washington DC, p. 193-198.
- Span, R., Wagner, W. (1996): A New Equation of State for Carbon Dioxide Covering the Fluid Region from the Triple-Point Temperature to 1100 K at Pressures up to 800 MPa. *Journal of Physical Chemical Reference Data*, 25 (6), p. 1509-1596.
- Stackebrandt, W. (1998): Grundzüge des geologischen Baus von Brandenburg [Outline of the geological setting of Brandenburg]. *Brandenburgische Geowissenschaftliche Beiträge*, 5 (2), p. 3-7.
- Stackebrandt, W., Manhenke, V., Eds. (2004): *Atlas zur Geologie von Brandenburg*. 1:1 000 000. Landesamt für Geowissenschaften und Rohstoffe Brandenburg (LGRB), 146 pp.
- Tesch, J., Burmann, G., Schwamm, G., Nillert, P. (1987): Hydrogeologischer Ergebnisbericht mit Grundwasservorratsberechnung, Vorerkundung Fürstenwalde. VEB Hydrogeologie Nordhausen, BT Berlin, Berlin, p. 1-309 (unpublished).
- Tesmer, M., Möller, P., Wieland, S., Jahnke, C., Voigt, H., Pekdeger, A. (2007): Deep reaching fluid flow in the North East German Basin: origin and processes of groundwater salinization. *Hydrogeology Journal*, 15, p. 1291-1306.
- Tillner, E., Kempka, T., Nakaten, B., Kühn, M. (2013): Brine migration through fault zones: 3D numerical simulations for a prospective CO₂ storage site in Northeast Germany. *International Journal of Greenhouse Gas Control*, 19, p. 689-703.

REFERENCES

- Van Genuchten, M.T. (1980): A closed-form Equation for Predicting the Hydraulic Conductivity of unsaturated Soils. *Soil Science Society of America Journal*, 44, p. 892-898.
- Vattenfall Europe Technology Research GmbH (2009): Antrag auf Erteilung einer Erlaubnis zur Aufsuchung bergfreier Bodenschätz zu gewerblichen Zwecken. Online: http://www.lbgr.brandenburg.de/media_fast/4055/Antrag%20_Aufsuchung%20bergfreier%20Bodensch%C3%A4tz_Bkh_20090306.15564291.pdf, 12 pp., last access: 18 December 2014.
- Vattenfall Europe Technology Research GmbH (2010): Hauptbetriebsplan – Aufsuchungsarbeiten in Bezug auf den bergfreien Bodenschatz Sole im Erlaubnisfeld Birkholz-Beeskow. Online: http://www.lbgr.brandenburg.de/media_fast/4055/Bkh_HBP_Finale.pdf, 28 pp. last access: 18 December 2014.
- Vermilye, J.M., Scholz, C.H. (1998): The process zone: a microstructural view of fault growth. *Journal of Geophysical Research – Solid Earth*, 103 (B6), p. 12223-12237.
- Vidal-Gilbert, S., Nauroy, J.F., Brosse, E. (2009): 3D geomechanical modelling for CO₂ geologic storage in the Dogger carbonates of the Paris Basin. *International Journal of Greenhouse Gas Control*, 3, p. 288-299.
- Victor, D. G., Zhou, D., Ahmed, E. H. M., Dadhich, P. K., Olivier, J. G. J., Rogner, H-H., Sheikho, K., Yamaguchi, M. (2014): Introductory Chapter. In: Edenhofer, O., Pichs-Madruga, R., Sokona, Y., Farahani, E., Kadner, S., Seyboth, K., Adler, A., Baum, I., Brunner, S., Eickemeier, P., Kriemann, B., Savolainen, J., Schlömer, S., von Stechow, C., Zwickel, T., Minx, J.C. (Eds.), *Climate Change 2014: Mitigation of Climate Change. Contribution of Working Group III to the Fifth Assessment Report of the Intergovernmental Panel on Climate Change*. Cambridge University Press, Cambridge, United Kingdom and New York, NY, USA.
- Walter, L., Binning, P.J., Oladyshkin, S., Flemisch, B., Class, H. (2012): Brine migration resulting from CO₂ injection into saline aquifers – An approach to risk estimation including various levels of uncertainty. *International Journal of Greenhouse Gas Control*, 9, p. 495-506.
- Wibberley, C.A.J., Yielding, G., Toro, G. (2008): Recent advances in the understanding of fault zone internal structure: a review. In: Wibberley, C.A.J., Kurz, W., Imber, J., Holdsworth, R.E., Collettini, C. (Eds.), *The Internal Structure of Fault Zones: Implications for Mechanical and Fluid-Flow Properties*. Geological Society Special Publications, 299, p. 5-33.
- Yamamoto, H., Zhang, K., Karasaki, K., Marui, A., Uehara, H., Nishikawa, N. (2009): Numerical investigation concerning the impact of CO₂ geologic storage on regional groundwater flow. *International Journal of Greenhouse Gas Control*, 3 (5), p. 586-599.
- Zhou, Q., Birkholzer, J., Mehnert, E., Lin, Y. and Zhang, K. (2010): Modeling Basin- and Plume-Scale Processes of CO₂ Storage for Full-Scale Deployment. *Ground Water*, 48 (4), p. 494-514.
- Zoback, M.D. (2010): The potential for triggered seismicity associated with geologic sequestration of CO₂ in saline aquifers. American Geophysical Union (AGU) Fall Meeting 2010, EOS Trans. AGU 91 (52), Abstract NH11C-01.

SOFTWARE REFERENCES

Hijmans, R.J., Guarino, L., Mathur, P. (2012): DIVA-GIS Version 7.5. Online: http://www.diva-gis.org/docs/DIVA-GIS_manual_7.pdf.

Itasca (2012): FLAC3D™ – Fast Lagrangian Analysis of Continua in 3 Dimensions. Software Version 5.0. Advanced, Three-Dimensional Continuum Modeling for Geotechnical Analysis of Rock, Soil and Structural Support. Online: <http://www.itascacg.com/sites/itascacg.com/files/ICG13-BRO-FLAC3D-501-101.pdf>.

Pruess, K. (2005b): ECO2N: A TOUGH2 Fluid Property Module for Mixtures of Water, NaCl, and CO₂. Report LBNL-57952, Lawrence Berkeley National Laboratory, Berkeley, California. Online: http://esd.lbl.gov/files/research/projects/tough/documentation/TOUGH2_ECO2N_Users_Guide.pdf.

Robert McNeel & Associates (2012): Rhinoceros 5.0. Online: <https://www.rhino3d.com/>.

Schlumberger (2007): ECLIPSE 100, Schlumberger Information Solutions. Online: <http://www.software.slb.com>.

Schlumberger (2010a): Petrel Seismic-to-Evaluation Software, Version 2010.2.2, Schlumberger Information Solutions. Online: <http://www.software.slb.com>.

Schlumberger (2010b): VISAGE™ 2010, Schlumberger Information Solutions. Online: <http://www.software.slb.com>.

Schlumberger (2011): Petrel Seismic-to-Evaluation Software, Version 2011.2.7, Schlumberger Information Solutions. Online: <http://www.software.slb.com>.

Schlumberger (2012): Petrel Seismic-to-Evaluation Software, Version 2011.1, Schlumberger Information Solutions. Online: <http://www.software.slb.com>.

Zhang, K., Wu, Y.-S., Pruess, K. (2008): User's Guide for TOUGH2-MP – A Massively Parallel Version of the TOUGH2 Code. Report LBNL-315E, Earth Sciences Division, Lawrence Berkeley National Laboratory, Berkeley, California. Online: http://esd.lbl.gov/files/research/projects/tough/documentation/TOUGH2-MP_Users_Guide.pdf.

APPENDIX: PUBLICATIONS OF THE AUTHOR

1 PAPER (SCI/SCOPUS JOURNALS)

Langer, M., [Tillner, E.](#), Kempka, T., Kühn, M. (2015, submitted): Effective damage zone volume and initial salinity distribution determine intensity of shallow aquifer salinization in geological CO₂ storage. *Hydrology and Earth System Sciences*.

[Tillner, E.](#), Shi, J.-Q., Bacci, G., Nielsen, C. M., Frykman, P., Dalhoff, F., Kempka, T. (2014): Coupled Dynamic Flow and Geomechanical Simulations for an Integrated Assessment of CO₂ Storage Impacts in a Saline Aquifer. *Energy Procedia*, 63, p. 2879-2893.

Kempka, T., Klein, E., De Lucia, M., [Tillner, E.](#), Kühn, M. (2013): Assessment of Long-term CO₂ Trapping Mechanisms at the Ketzin Pilot Site (Germany) by Coupled Numerical Modelling. *Energy Procedia*, 37, p. 5419-5426.

Magri, F., [Tillner, E.](#), Wang, W., Watanabe, N., Zimmermann, G., Kempka, T. (2013): 3D Hydro-mechanical Scenario Analysis to Evaluate Changes of the Recent Stress Field as a Result of Geological CO₂ Storage. *Energy Procedia*, 40, p. 375-383.

Nakaten, B., [Tillner, E.](#), Kempka, T. (2013): Virtual Elements for Representation of Faults, Cracks and Hydraulic Fractures in Dynamic Flow Simulations. *Energy Procedia*, 40, p. 447-453.

Röhmann, L., [Tillner, E.](#), Magri, F., Kühn, M., Kempka, T. (2013): Fault Reactivation and Ground Surface Uplift Assessment at a Prospective German CO₂ Storage Site. *Energy Procedia*, 40, p. 437-446.

[Tillner, E.](#), Kempka, T., Nakaten, B., Kühn, M. (2013): Brine migration through fault zones: 3D numerical simulations for a prospective CO₂ storage site in Northeast Germany. *International Journal of Greenhouse Gas Control*, 19, p. 689-703.

[Tillner, E.](#), Kempka, T., Nakaten, B., Kühn, M. (2013): Geological CO₂ Storage Supports Geothermal Energy Exploitation: 3D Numerical Models Emphasize Feasibility of Synergetic Use. *Energy Procedia*, 37, p. 6604-6616.

2 CHAPTER IN BOOK

Kahnt, R., Kutzke, A., Martin, M., Eckart, M., Schlüter, R., Kempka, T., [Tillner, E.](#), Hildebrand, A., Krooss, B.M., Gensterblum, Y., Adams, M., Feinendegen, M., Klebingat, S., Neukum, C. (2015): "CO2RINA" – CO₂ Storage Risk Integrated Analysis. In: Liebscher, A., Münch, U. (Eds.), *Geological Storage of CO₂ – Long Term Security Aspects*. GEOTECHNOLOGIEN Science Report No.22, Advanced Technologies in Earth Sciences, Springer International Publishing, p. 139-166.

Kempka, T., Herd, R., Huenges, E., Endler, R., Jahnke, C., Janetz, S., Jolie, E., Kühn, M., Magri, F., Meinert, P., Moeck, I., Möller, M., Muñoz, G., Ritter, O., Schafrik, W., Schmidt-Hattenberger, C.,

Tillner, E., Voigt, H.-J., Zimmermann, G. (2015): Joint Research Project Brine: Carbon Dioxide Storage in Eastern Brandenburg: Implications for Synergetic Geothermal Heat Recovery and Conceptualization of an Early Warning System Against Freshwater Salinization. In: Liebscher, A., Münch, U. (Eds.), Geological Storage of CO₂ – Long Term Security Aspects. GEOTECHNOLOGIEN Science Report No.22, Advanced Technologies in Earth Sciences, Springer International Publishing, p. 139-166.

3 CONFERENCE PAPER

Langer, M., Tillner, E., Kempka, T., Kühn, M. (2015): Numerical simulations of saltwater displacement via fault systems due to exploitation of the subsurface, (Geophysical Research Abstracts Vol. 17, EGU2015-12019-2, 2015), General Assembly European Geosciences Union (Vienna, Austria, 2015).

Kempka, T., Tillner, E. (2015): Impact of permeability on vertical ground surface displacements in geological underground utilization, (Geophysical Research Abstracts Vol. 17, EGU2015-12163-1, 2015), General Assembly European Geosciences Union (Vienna, Austria, 2015).

Tillner, E., Kempka, T., Nakaten, B., Kühn, M. (2013): 3D-Simulation der Salzwassermigration über Störungen als Folge einer CO₂-Speicherung in Nordostdeutschland zeigt keine Tendenz zur Trinkwasserversalzung. 19. Tagung für Ingenieurgeologie (Munich, Germany 2013)

Tillner, E., Kempka, T., Shi, J.-Q., Bacci, G., Nielsen, C. M., Frykman, P., Dalhoff, F. (2013): Coupled dynamic flow and geomechanical simulations for an integrated assessment of CO₂ storage impacts in a saline aquifer, (Geophysical Research Abstracts Vol.15, EGU2013-11255, 2013), General Assembly European Geosciences Union (Vienna, Austria 2013).

Magri, F., Tillner, E., Kempka, T., Wang, W., Watanabe, N., Zimmermann, G. (2013): 3D hydro-mechanical scenario analysis to evaluate changes of the recent stress field as a result of geological CO₂ storage, (Geophysical Research Abstracts Vol. 15, EGU2013-2852, 2013), General Assembly European Geosciences Union (Vienna, Austria 2013).

Röhmann, L., Tillner, E., Kempka, T., Magri, F., Kühn, M. (2013): Fault reactivation and ground uplift assessment at a prospective German CO₂ storage site, (Geophysical Research Abstracts Vol. 15, EGU2013-6079, 2013), General Assembly European Geosciences Union (Vienna, Austria 2013).

Nakaten, B., Tillner, E., Kempka, T. (2013): Virtual elements for representation of faults, cracks and hydraulic fracks in dynamic flow simulations, (Geophysical Research Abstracts, Vol. 15, EGU2013-6089, 2013), General Assembly European Geosciences Union (Vienna, Austria 2013).

Tillner, E., Kempka, T., Nakaten, B., Kühn, M. (2013): Potential groundwater salinization due to upward brine migration through fault zones for a prospective CO₂ storage site in Germany. Poster presented at 40th International Congress of the IAH 2013 (Perth, Australia 2013).

Tillner, E., Kempka, T., Nakaten, B., Jolie, E., Kühn, M. (2012): Modeling of brine migration through fault zones as a result of CO₂ injection into a saline aquifer. (Geophysical Research

Abstracts Vol. 14, EGU2012-501-1, 2012), General Assembly European Geosciences Union (Vienna, Austria 2012).

[Tillner, E.](#), Kempka, T., Jolie, E., Kühn, M. (2012): Konkurrierende Nutzung oder Synergie? – Geothermische Energiegewinnung im Rahmen einer geologischen CO₂-Speicherung. FH-DGG Jahrestagung (Dresden, Germany 2012).

Kempka, T., Endler, R., Herd, R., Huenges, E., Jahnke, C., Jolie, E., Janetz, S., Kühn, M., Magri, F., Moeck, I., Möller, M., Muñoz, G., Nakaten, B., Ritter, O., Schafrik, W., Schmidt-Hattenberger, C., Schröder, S., [Tillner, E.](#), Voigt, H.-J., Zimmermann, G. (2012): brine – CO₂ storage in eastern Brandenburg: Implications for geothermal heat provision and conception of a salinization early warning system. Geotechnologien Statusseminar “Geological Storage of CO₂” (Hannover, Germany 2012).

[Tillner, E.](#), Kempka, T., Nakaten, B., Kühn, M. (2012): Numerische Simulationen zur Untersuchung der gleichzeitigen Nutzung eines salinen Grundwasserleiters zur geothermischen Energiegewinnung und geologischen CO₂-Speicherung. GeoHannover, Jahrestagung der DGG (Hannover, Germany 2012).

[Tillner, E.](#), Kempka, T., Jolie, E., Kühn, M. (2012): From competition to synergy – support geothermal exploitation by geological CO₂ storage. The 11th International Conference on Greenhouse Gas Technologies (Kyoto, Japan 2012).

[Tillner, E.](#), Kempka, T., Nakaten, B., Kühn, M. (2012): Regional-scale 3D numerical modelling to assess upward brine migration through permeable faults. Geotechnologien Statusseminar: Geological Storage of CO₂ (Hannover, Germany 2012).

Nakaten, B., [Tillner, E.](#), Kempka, T. (2012): Assessment of fault flow and transport processes using a virtual element concept for description of faults at reservoir scale. GeoHannover, Jahrestagung der DGG (Hannover, Germany 2012).

[Tillner, E.](#), Kempka, T., Nakaten, B., Kühn, M. (2012): Modeling upward brine flow through permeable faults induced by CO₂ injection into a saline aquifer. Internationale GeoEn Konferenz (Potsdam, Germany 2012).

ERKLÄRUNG

Hiermit erkläre ich, Elena Tillner, dass ich als Autorin der vorliegenden Dissertation mit dem Titel: „*Quantifizierung verdrängter Sole aus salzwasserführenden Grundwasserleitern und mechanische Auswirkungen bei der geologischen CO₂-Speicherung*“, die Arbeit selbstständig und ohne unerlaubte Hilfe angefertigt habe.

Ferner versichere ich, keine anderen als die angegebenen Quellen und Hilfsmittel benutzt zu haben. Alle Ausführungen, die anderen Schriften wörtlich oder inhaltlich entnommen wurden, sind als solche kenntlich gemacht.

Die vorliegende Arbeit wurde in keinem anderen Promotionsverfahren angenommen oder abgelehnt.

Ort, Datum

Unterschrift